DCU

Ollscoil Chathair
Bhaile Átha Cliath
Dublin City University

Development and testing of a novel approach to measuring biofouling on sensors and tidal energy materials.

Adrián Delgado Ollero, MSc.

A thesis submitted for the award of PhD

School of Chemical Sciences

Dublin City University

Supervisor(s):

Prof. Fiona Regan

2024

Declaration

I hereby certify that this material, which I now submit for assessment on the programme of study leading to the award of Doctor of Philosophy is entirely my own work, and that I have exercised reasonable care to ensure that the work is original, and does not to the best of my knowledge breach any law of copyright, and has not been taken from the work of others save and to the extent that such work has been cited and acknowledged within the text of my work.

Signed: _____ Adrián Delgado Ollero

Student ID No: 19214715

Date: 1 January 2024

Acknowledgements

I would like to thank my supervisor, Professor Fiona Regan, for her constant support and guidance throughout this process and her confidence in me.

I would also like to thank the entire DCU School of Mechanical Engineering team, in particular PhD candidate Philip Daly and Professor Yan Delauré for their advice and expertise on the NEMMO project, for helping to keep much of this thesis and the projects moving forward, and for their continued effort and dedication.

I am grateful for funding from the DCU Water Institute during the first months of starting the thesis, the European Union's Horizon 2020 Research and Innovation Programme and Project Ireland 2040′s Disruptive Technologies Innovation Fund.

Special thanks to all members of Fiona Regan's research group; Sean Power, Dr. Chloe Richards, Dr. Ciprian Briciu Burghina, Dr Louis Free, Stefanía Scurtu, Dr. Belinda Huerta and Dr. Kristýna Mrštná. I am immensely grateful for the extraordinary opportunity to collaborate with exceptional researchers and cherished friends. These past four years have been a source of tremendous joy, filled with laughter, growth, and unforgettable moments. I extend my heartfelt appreciation to each one of you for making this journey truly remarkable. Your brilliance, camaraderie, and unwavering support have been instrumental in shaping this incredible experience. Thank you for being an integral part of my life and for making our time together so incredibly special.

This work would not have been possible without my partner Andrea Izura and her unwavering support, both personally and professionally. Their belief in me and their willingness to go above and beyond have been the cornerstone of my success. I cherish the moments we shared and the constant encouragement that fueled my determination.

Thank you, Andrea, for being my partner, my confidant, and my biggest cheerleader throughout this incredible journey. Your unwavering support has been the wind beneath my wings, and I am forever grateful for your presence in my life.

Thanks to my family for being there every day supporting me, even from a distance, Higinia Ollero Torres, Alfonso Delgado Ruiz and my brother Alfonso Delgado Ollero.

On the other hand, this would not have been possible without my Irish landlords Paula Heenan and Eileen Galgey who welcomed me in their homes during all this period and gave me very good advice.

I would not like to end my thanks without mentioning my professors and mentors at UAM, Samuel Cirés and Antonio Quesada, without their advice and teachings I would not have been here, and also Víctor Vasconcelos for his advice and recommendations during my master's degree at CIMAR.

Finally, I would like to dedicate these last lines to all the doctors, nurses and people who gave their lives to fight COVID-19.

Table of Contents

List of Abbreviations

Abbreviation	Meaning
EPS	Extracellular polysaccharides
AF	Antifouling
TBT	Tributyltin
SEM	Scanning Electron Microscopy
ANOVA	Analysis of Variance
GF/F	Glass fibre filters
eDNA	environmental DNA
DNA	Deoxyribonucleic Acid
RNA	Ribonucleic Acid
N_2	Nitrogen
AO	Acridine Orange
ITO	Indium Titanium Oxide
RPM	Revolutions Per Minute
Hz	Hertz
e-DNA	extracellular DNA
SR	*Scophthalmus rhombus*
RBA	Raised Bar Array
RCA	Recessed Cavity Array
TWS	Trainable Weka Segmentation
FR	Fouling Rating
API	Antifouling Performance Index
ROV	Remote Operated Vehicle
TEOS	Tetraethyl orthosilicate
QAS	3- (Trimethoxylsilyl) – propyloctadecyldimethyl ammonium chloride
C15	Coating 15
PUD / PUR	Polyurethane
CPU	Central Processing Unit
RAM	Random Access Memory

STP	Training Set of Pixels
ROI	Region of Interest
CFD	Computational Fluid Dynamics
SRB	Sulphate Reducing bacteria
POM-C	High Chemical resistance Polyoxymethylene
POM-H	High density Polyoxymethylene
AF T-B	Antifouling Paint Trilux Black
AF-M-W	Antifouling Paint Micron-Extra White
PMMA	Polymethylmethacrylate
dsDNA	Double-stranded DNA
NGS	Next Generation Sequencing
rRNA	Ribosomal Ribonucleic Acid
STM	Stepper Motor
PETG	Polyethylene terephthalate glycol
OOB	Out of Bag
OH	Hydroxyl group
GW	Gigawatt
mW	milliwatt
EU	European Union
PCR	Polymerase Chain Reaction
PPS	Polyphenylene sulphide
FEP	fluorinated ethylene propylene
ABS	Acrylonitrile Butadiene Styrene
PVC	Polyvinyl chloride
XLPE	Cross-Linked Polyethylene
CR	Chloroprene Rubber
PVDF	Polyvinylidene fluoride
CAD	Computer aided design
NaOH	Sodium hydroxide
HCl	Hydrochloric acid
NaOH	Sodium hydroxide

List of Figures:

List of Tables:

List of Publications

- Delgado, A.; Briciu-Burghina, C.; Regan, F. Antifouling Strategies for Sensors Used in Water Monitoring: Review and Future Perspectives. *Sensors* **2021**, *21*, 389, doi:10.3390/s21020389.

- Delgado, A.; Power, S.; Richards, C.; Daly, P.; Briciu-Burghina, C.; Delauré, Y.; Regan, F. Establishment of an Antifouling Performance Index Derived from the Assessment of Biofouling on Typical Marine Sensor Materials. *Science of The Total Environment* **2023**, 164059, doi:10.1016/j.scitotenv.2023.164059.

- Briciu-Burghina, C.; Power, S.; Delgado, A.; Regan, F. Sensors for Coastal and Ocean Monitoring. https://doi.org/10.1146/annurev-anchem-091922-085746 **2023**, 16, 451–469, doi:10.1146/ANNUREV-ANCHEM-091922-085746.

- Peyvastehnejad, A.; Regan, F.; Richards, C.; Delgado, A.; Daly, P.; Grande, J.; Delauré, Y.M.C. The Impact of Bio-Inspired Micro-Textures on Turbulence and Implications for Bio-Fouling Settlement. Ocean Engineering **2023**, 285, 115223, doi:10.1016/j.oceaning.2023.115223.

- Delgado, A.; Richards, C.; Daly, P.; Power, S.; Briciu-Burghina, C.; Delauré, Y.; Regan, F. Assessment of Biofouling on Typical Marine Sensors Materials. In Proceedings of the OCEANS 2023 - Limerick; IEEE, June 5 2023; pp. 1–8.

- Richards, C.; Ollero, A.D.; Daly, P.; Delauré, Y.; Regan, F. Disruption of Diatom Attachment on Marine Bioinspired Antifouling Materials Based on Brill (Scophthalmus Rhombus). *Science of The Total Environment* **2024**, *912*, 169348, doi:10.1016/j.scitotenv.2023.169348.

Essays and poster presentations

- Grande, J.; Garcia, M.; Carpintero, P.; Delgado, A.; Richards, C.; Regan, F. Making Better Blades for Tidal Energy Generation. *The Journal of Ocean Technology*. 2023, *18*, 1, (Spring).

- *Biofouling studies on marine rated materials and coatings.* In: Environ 2021 - 31st Annual Irish Environmental Researchers Colloquium, 16 - 18 June 2021, Cork/Online.

Awards and conferences

- ESAI Best Poster Presentation at Environ 2021 ESAI Best Poster Presentation at Environ 2021

- Chloe Richards, Adrián Delgado Ollero, Yan Delauré and Fiona Regan, Biomimetic texturing as an effective antifouling solution, Ocean Energy Europe 2021, 8th December, Brussels, Belgium.

- Oceans 2023 Limerick Technical Programme

Abstract

Development and testing of a novel approach to measuring biofouling on sensors and tidal energy materials.

By: Adrian Delgado Ollero

When artificial surfaces are submerged in water, they can experience biofouling, which involves the accumulation of organic matter. The process starts when a clean surface is submerged, and microorganisms such as bacteria diatoms, barnacles and mussels colonize it, forming complex and dynamic microbial communities. These communities are surrounded by a matrix of extracellular polymeric substance (EPS). Currently, biocidal coatings are being utilized to prevent biofilm formation. However, many of these coatings are harmful to the aquatic environment, and their use is now regulated by legislation.

Biofouling has long been considered a limiting factor and is recognised as one of the main obstacles to autonomous environmental monitoring in aquatic environments and tidal energy.

As the demand for infrastructure to be in contact with water increases, the selection of the correct materials depends on the proper selection of the appropriate alloys and composites for the application and service environment. However, the analysis and quantification of biofouling is extremely complex as it is commonly based on biochemical methods like biofilm-extracted DNA analysis to understand the complexity and diversity of biofilms. Using molecular markers such 18S rRNA can help to identify different groups of organisms and thus to know the targets on which to focus prevention strategies on which manufacturers should manage their budgets in order to reduce maintenance cost due to this problem. However, although these molecular techniques are very useful, they are often not cheap and require highly specialised equipment and expertise in biology and bioinformatics.

Therefore, in this work, the use of alternative techniques like image classification based on machine learning on different materials used for sensor manufacturing can help to make biofouling analysis more efficient and cost-effective. In addition to this, particular attention was paid to the examining and analyzing the effectiveness of novel surface topographical features based on Brill fish, (Scophthalmus rhombus), as inspiration to develop an antifouling texture for the first time, but also different materials and coatings on the adhesion of microfouling and macrofouling communities for sensor development and tidal energy applications from a laboratory scale using model organisms (*Amphora coffeaeformis* and *Nitzschia ovalis*) to the field scale with the construction of a floating platform with a turbine to perform environmental biofouling tests in real conditions.

Chapter 1 :

Introduction

1.1 Introduction to Biofouling

Adhesion and growth of micro-organisms at the interface between any non-sterile medium and a solid surface is a widespread phenomenon in most environments on Earth. Solid structures immersed in an non sterile aqueous environment provide a number of benefits to organisms that adhere to it and so are rapidly colonised by micro and macro organisms. The structural rigidity of a solid surface can protect organisms from physical harm, the concentration of nutrient molecules at the interface between aqueous liquid and solid aids growth, the ability to produce protective structures around microorganism leads to thick films of heterogeneous microorganisms that can in turn aid in the adhesion or support macroorganisms such as macroalgae and molluscs [1–5]

The development of disruptive or unwanted biofilms on surfaces is a major problem due to the accumulation of biomass leading to reduced efficiency, contamination, corrosion and failure of engineered components. This process is often undesirable on synthetic materials and surfaces from a technological, health or economic perspective. Therefore, adhesion and undesirable biological growth on surfaces has been termed biofouling [6,7]. The colonisation of solid surfaces by micro and microorganisms, commonly referred to as biofouling is an issue that influence almost all structures submerged in aqueous environments. This problem creates substantial economic losses throughout the majority of marine and freshwater related industries. These losses are generally the result of reduced hydrodynamics creating larger fuel consumption, decreased shipping speeds, more regular cleaning and maintenances of ship and submarine hulls, and biocorrosion reducing the lifespan of marine piping systems, buoys, oil platforms, sea - water cooling systems of power plants and water quality sensors affecting the performance and data quality [8,9]. For example In the context of marine organisms and their relationship to speed, the Reynolds number is crucial because it helps determine the type of flow around an organism moving through water. The behaviour of the flow can significantly affect the drag experienced by the organism.

For marine organisms, such as fish or other swimming animals, the Reynolds number is often used to understand the flow regime around their bodies. There are two main flow regimes:

- **Low Reynolds Numbers (Re < 2000):** In this regime, flow is generally laminar. Viscous forces dominate, and the fluid flows smoothly with well-defined streamlines. At low Reynolds numbers, changes in speed have a relatively small impact on the flow pattern.

- **High Reynolds Numbers (Re > 4000):** In this regime, flow tends to be turbulent. Inertial forces become more dominant, and the flow becomes more chaotic. Turbulent flow is characterized by eddies and swirls in the fluid. At high Reynolds numbers, changes in speed can significantly impact the drag experienced by the organism.

For marine organisms, their swimming speed can influence the Reynolds number, and the Reynolds number, in turn, affects the drag forces acting on the organism. Efficient swimmers often operate in a range of Reynolds numbers where the transition from laminar to turbulent flow occurs. Evolution has led many marine organisms to adapt to these fluid dynamics for optimal swimming performance.

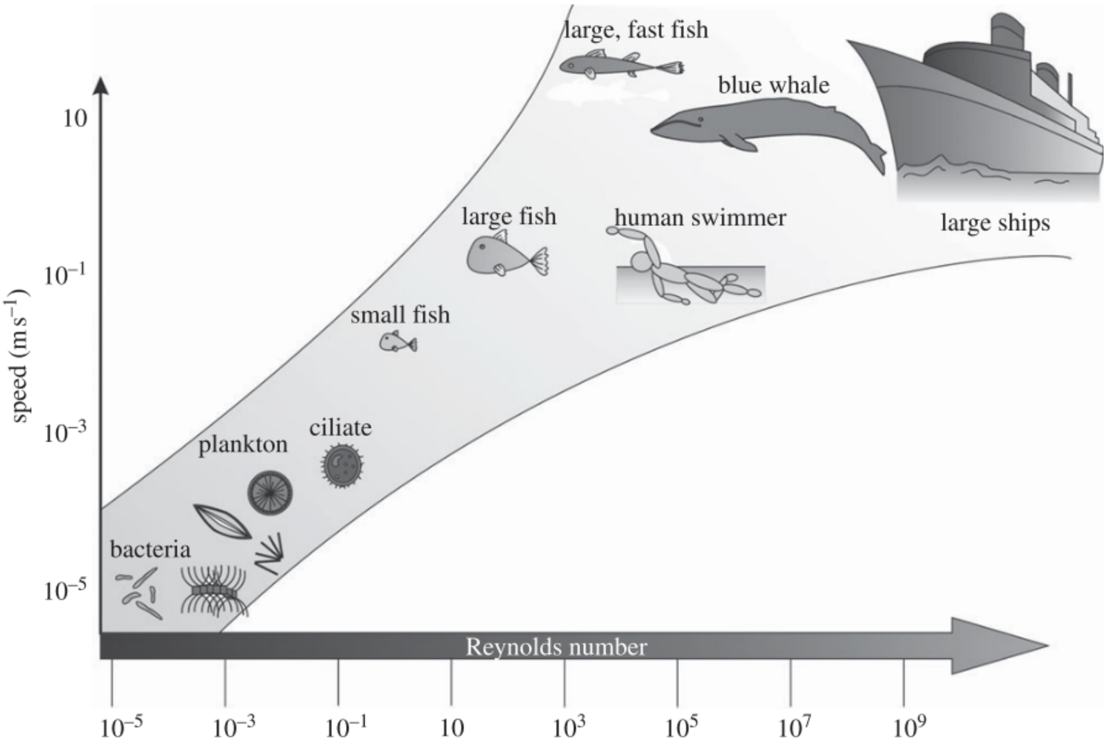

Figure 1: The variation of Reynolds number in marine organisms with respect to speed [10].

1.2 Fouling Overview

Materials immersed in water experience a series of biological and chemical processes, resulting in the formation of complex layers with attached organisms. This biofouling can be divided into microfouling and macrofouling. Microfouling includes the initial events that result in the formation of a biofilm while macrofouling describes the settlement and development of macroscopic species [11,12].

1.2.1 Mechanism of Biofilm Formation/Progression

It has been known since the early works of Zobell and contemporaries that aquatic life is concentrated at the interfaces as for example, benthic-pelagic, littoral-limnetic, oceanic-estuarine, thermocline and halocline interfaces or even air-water interfaces [13,14]. The observations of Zobell and collaborators were noted for the initial insights gained on the mechanisms of microbial fixation on surfaces. For example, important mechanisms that were described by Zobell include reversible attachment such as van der Waals forces or electrostatic forces and irreversible attachment characterised by stronger interactions, including adhesion molecules and specific binding sites were described. They also described biofilm formations where Extracellular Polymeric Substances (EPS) form a protective matrix that helps to anchor the biofilm to the surface and provides structural support to the microbial community. On the other hand, they also describe mechanisms such as Quorum Sensing by which bacteria in biofilms communicate with each other through a cell-density-dependent signalling mechanism. This allows them to coordinate gene expression and behaviour, leading to the formation and maintenance of the biofilm. Their research allowed for the understanding of biofilm formation and the processes that occur when a surface is immersed in an aqueous medium. It is now understood that the process of biofilm formation can be divided into several distinct stages (Figure 2). These stages depend on the length of time the surface has been exposed to the environment, the availability of nutrients and other environmental conditions such as temperature and pH.

The first chemical changes occur as the surface adsorbs the dissolved molecules and ions from the surrounding environment [15,16]. Specifically, the process can be divided into four stages. The first event is the adsorption of organic and inorganic macromolecules immediately after immersion, forming a film that covers the surface. The second event is the settlement of bacteria (microfouling) on the surface followed by a consolidation stage through the production of extracellular polymers, forming a microbial reversible biofilm. Later, a more complex community (macrofouling) develops with the presence of multicellular species, microalgae, secretion of extracellular polymers (acid polysaccharides) and sediments adhering to the surface, producing an irreversible substrate as a polymeric bridge is formed between the cell and the substrate. Finally, the last stage corresponds to the fixation of larger marine invertebrates, such as barnacles, mussels and macroalgae. However, although numerous real-life experiments have been conducted with materials immersed in seawater, no specific fixation pattern can be differentiated for each of the biofouling stages [17]. These stages, unlike the ones mentioned above, do not occur in a completely staggered manner.

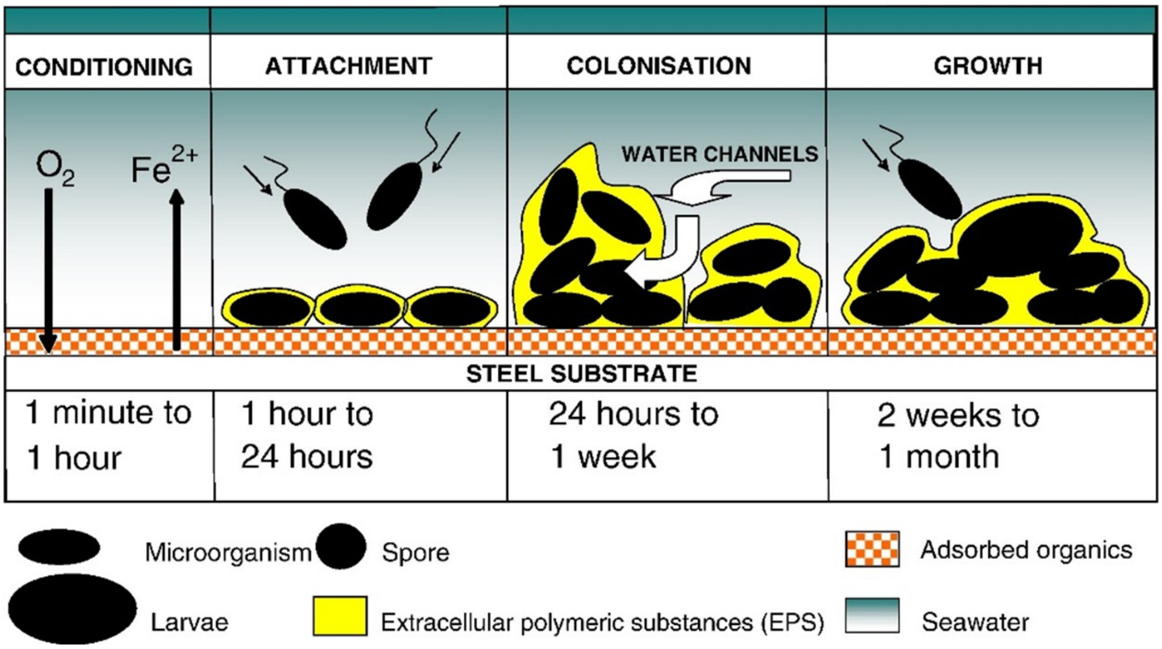

Figure 2: Illustration representing the stages of biofouling formation. Each of the stages shown can occur in the indicated order individually, in parallel or all at the same time [18].

1.2.2 Properties of Biofilms

Bacterial biofilms represent an ancient prokaryotic survival strategy. This is because bacteria achieve significant advantages by providing biofilms for protection from environmental fluctuations in humidity, temperature and pH [19]. The ability to form biofilms does not seem to be restricted to any specific group of microorganisms and it is currently considered that under suitable environmental conditions the vast majority of bacteria, regardless of species, can exist by forming biofilms adhering to surfaces at a solid/liquid interface [19–21]. The biofilm matrix is made up of exopolysaccharides, which constitute its fundamental component, produced by the very microorganisms that make up the matrix. Macromolecules, such as proteins, nucleic acids and various products from the processes of bacterial lysis, are present in smaller quantities. The polysaccharides, nucleic acids and various other proteins are known as extracellular polymeric substances (EPS).

Inorganic components, such as mineral salt crystals, corrosion particles and sediments, can also be found [22]. They can have a neutral charge or polyanionic charge, depending on the type of exopolysaccharide, which would allow them to interact with different antimicrobials so that these can be trapped in the matrix without capacity to act on the bacteria [23].

EPS production is influenced by different environmental factors, such as water quality, temperature, depth and even season or geographical variation.

1.2.2.1 Biofilms composition

Microorganisms primarily exist in aggregates and are commonly classified as sessile, meaning they remain attached to surfaces. This phenomenon is commonly referred to as "biofilm" A biofilm is a sophisticated and intricate structure composed of multiple colonies of microorganisms enveloped by extracellular polymeric substances. It encompasses a diverse array of hundreds and thousands of distinct species and incorporates specialized channels through which nutrients flow and circulate. The biofilm matrix comprises various polymeric compounds, with typical constituents including polysaccharides, proteins, nucleic acids, lipids, humic substances and water [24,25]

Every individual component of the biofilm exerts an influence on its structural integrity and overall lifespan, which is contingent upon the chemical composition and properties inherent in each molecule. However, the growth of biofilms is not driven by covalent C-C bonds between EPS molecules, but rather by weak physicochemical intermolecular interactions [26,27]. These interactions are predominantly facilitated by various types of non-covalent forces, specifically electrostatic interactions, hydrogen bonding, and London forces [28]. These cohesive forces operate within the EPS framework and also between microbial communities, as illustrated in Figure 3.

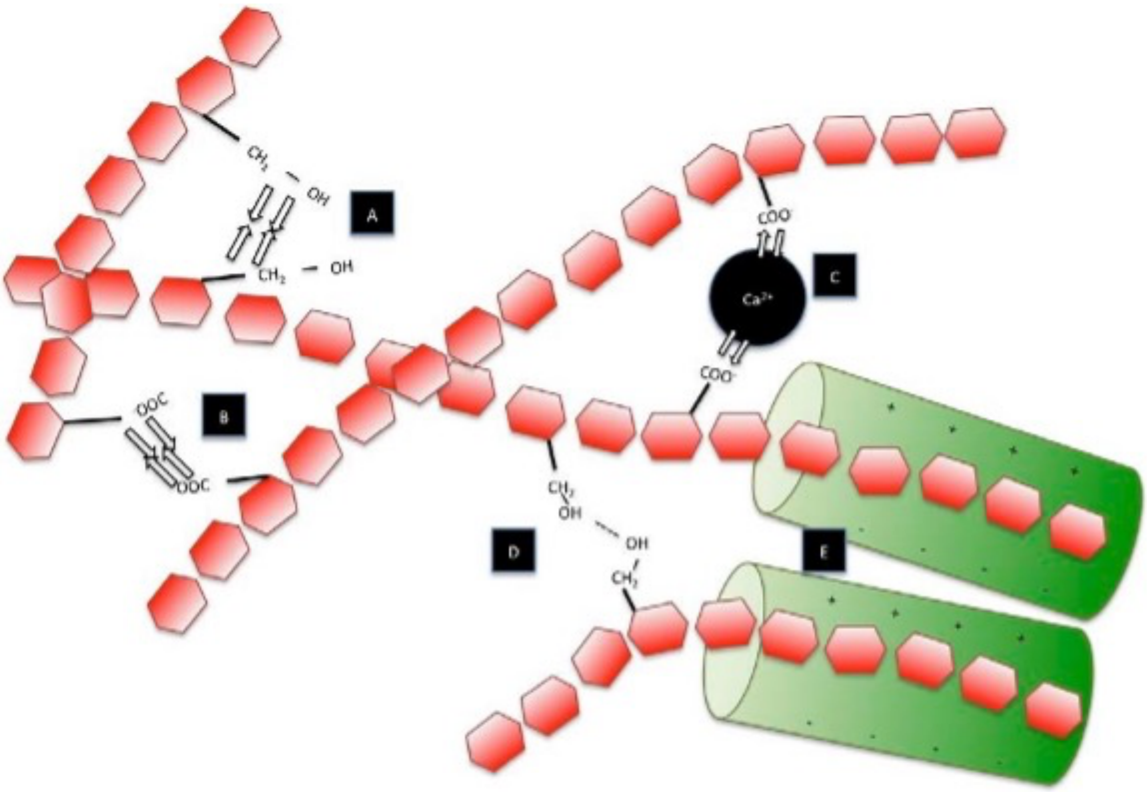

Figure 3: Intermolecular interactions contributing to the biofilm integrity. Five phenomena are illustrated: A = electrostatic interactions, B = repulsive electrostatic interactions between ionic species, C = attractive electrostatic, D = hydrogen bonding and E = electrostatic. Hexagonal shapes denote polysaccharides and protein interactions. (modified from [249])

Three types of weak interactions theoretically exist within a biofilm matrix, giving rise to its integrity and defining its shape:

- **Hydrogen bonding:** Hydrogen bonding primarily occurs between hydroxyl (-OH) groups within a molecule and is particularly abundant in polysaccharides and water molecules. This weak interaction also plays a supportive role in the tertiary structure of proteins. The bonding energy associated with hydrogen bonds typically ranges from 10 to 30 KJ/mol [29]. Polysaccharides that exhibit hydrogen bonding can be influenced by chaotropic agents, such as salt, which disrupt the water molecules surrounding the macromolecule, thus impacting the formation of biofilms [30] Mayer et al. have reported that cleaning formulations do not exhibit significant levels of hydrogen bonding due to the levels present within the biofilm matrix. However, they emphasize that water, which accounts for over 90% of EPS, should not be overlooked in this context

- **Electrostatic effects:** The primary forces at play involve interactions between ions and both permanent and induced dipoles. Ionic interactions are typically strong, and individual cations, such as Ca^{2+}, contribute significantly to the binding energy within the EPS matrix [31]. These divalent cations act as bridges, greatly enhancing the overall binding force of the matrix. Furthermore, positively charged groups from amino acids in proteins or polysaccharides can interact with negatively charged groups, creating instantaneous cohesion forces.

  A study by Chen and Stewart demonstrated the impact of different cations on the viscosity of a biofilm. The addition of sodium, potassium, magnesium, and calcium led to significant decreases in viscosity, while iron cations had a potent effect in increasing the viscosity of the biofilm matrix [31].The binding energy of non-ionic electrostatic interactions typically ranges between 12 and 30 kJ/mol. However, this energy is inherently influenced by the distance between the water concentration and neighboring bonds.

- **London Forces:** The forces described operate throughout the entire molecule, specifically within the biofilm matrix, both internally (intra) and between molecules (intermolecular). Importantly, these forces are not reliant on the specific molecular components. They arise from the spontaneous formation of temporary dipoles, which occur due to fluctuations in the distribution of electrons within the molecule. As a result, neighboring molecules become polarized, leading to attractive dipolar forces. This phenomenon can be understood as oscillating induced-dipole dipole interactions.

  London forces, as they are commonly known, contribute significantly to the binding energy between molecules. Typically, the binding energy associated with a London force falls within the range of 2.5 kJ/mol per carbon in an aliphatic chain. It is crucial to note that these forces are highly sensitive to the distance between molecules, following an inverse relationship represented by $1/r^6$ (where r denotes intermolecular distance). London forces play a significant role in interactions within hydrophobic regions of molecules and between molecules, commonly referred to as "hydrophobic interactions."

However, it is the covalent type bonds that have a significantly higher binding force (250 KJ/mol) than the others mentioned above [29].

1.3 Antifouling solutions and approaches:

The development of effective antifouling solutions is indeed of significant interest across various industries. By implementing and continuously improving antifouling strategies, industries can enhance operational efficiency, extend the lifespan of equipment and structures, reduce environmental impacts an ensure safer and more sustainable operations. Some of the most prominent and widely used antifouling solutions are biocide-based coatings but efforts are also being directed towards more sustainable techniques such as the replication of textures and microtopographies of organisms found in nature which are able to greatly reduce fouling.

1.3.1 Coatings and biocides solutions:

To control this biofouling problem, different antifouling solutions, such as coatings, have been used throughout history. Many of these coatings incorporate biocides, which base their effectiveness on generalised and non-selective toxicity to marine organisms. Many antifouling coatings contain biocides incorporated in a way that they must erode over time in order to be exposed to the environment. This coating erosion process allows the release of the biocide to prevent organisms from attaching (figure 4).

Many of these coatings are in the form of paints similar to enamels, lacquers, sealing varnishes or primers among others [32]. The antifouling elements correspond to ingredients that are incorporated into the coating matrix.

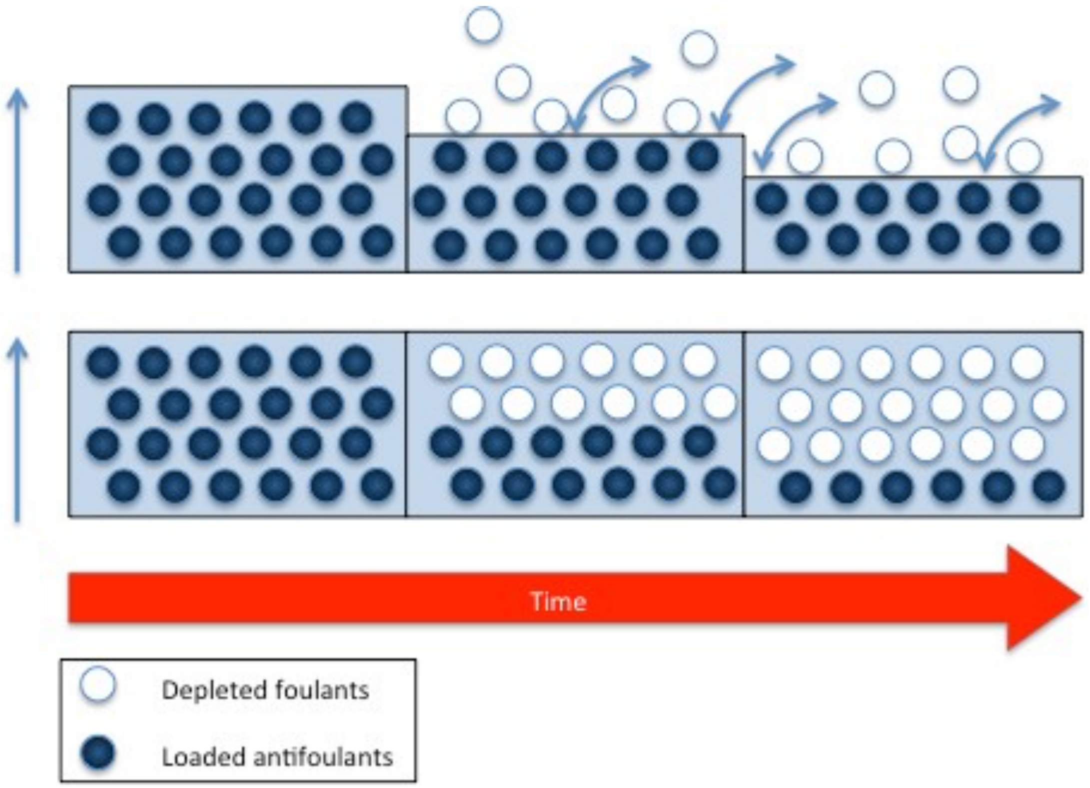

Figure 4: Schematic representation of (top) a soluble matrix biocide release coating and (bottom) an insoluble biocide release coating The blanks represent the increased porosity of some coatings when they release the particles.

However, the impact of these biocides on the environment has led to the creation of legislation to regulate their use [31]. For example, compounds like tributyltin (TBT), included in antifouling coatings was extensively used between the time of its discovery in the 1960s till its phasing out and eventual banning in 2008, its popularity was due to its effectiveness especially when coupled with self-polishing paints. Unfortunately, its widespread use and highly toxic nature highlighted its effect on non-target organisms such as oysters, sea snails. This environmental effect is the issue that has to be taken into account with any biocidal strategy [33]. Therefore, this compound was consequently banned in 2008 by the IMO (International Convention on the Control of Harmful Anti-fouling Systems on Ships, 2008) [34] and the industry fell back on heavy metal and metal oxides such as Zinc, Cobalt, Silver and most commonly Copper. These metals have been used for years to reduce micro fouling but their current extensive use has led to increasing background concentrations in areas of high maritime traffic [34–36].

Due to the increasing environmental scrutiny of copper (Cu^{2+}) and co-biocides, as they are toxic to marine life, bioaccumulation and especially regulatory concerns, there is a renewed interest in the economic impacts of fouling on ships and a greater effort to develop effective non-toxic coatings [37]. Some of these non-toxic examples are biomimetic approaches based on microtopography of animals or surfaces that can be found in nature.

1.3.2 Microtopography and biomimmetic solutions

The biomimetic approach is based on extracting designs from the natural environment, rather than directly copying natural biological function. In a sense, it is inspired by nature rather than imitating it. Biomimetics uses a bottom-up approach and relies on a wealth of resources in nature that have proven to be effective in controlling fouling [38]. Marine organisms have been extensively studied to protect their surfaces from biological fouling [39–43]. Table 1 provides a summary of various marine organisms that have been studied for their surface characteristics and evaluated for their antifouling potential Numerous investigations have shown that the topography of the substrate can influence the settlement of micro-organisms and the subsequent development of biofilms [44–46]. This approach has developed from the knowledge that cells react to nanoscale objects [47].

Table 1: Summary of some bio-inspired microtopographies of marine organisms and their antifouling mechanisms of action [48].

Species	Type of Study	Performance	Visual	Ref
Sea fan: *Pseudopterogorgia acerosa* **Dimension:** Spicules, 2–4 µm	Characterization	**Antifouling effect:** "Release of fouling" at an ideal surface energy range of 20–30 dyn cm^{-1}. **AF mechanism:** Surface chemistry	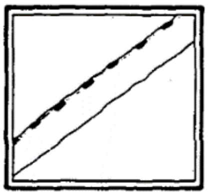	[49]
Brittle star: *Ophiura texturata* **Dimension:** Knobs, 10 µm in diameter	Field	**Antifouling effect:** Deterrent effects on microfoulers. **AF mechanism:** Surface topography	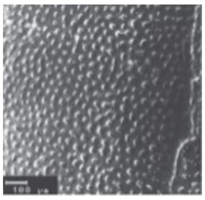	[50]
Sea star: *Linckia laevigata* **Dimension:** Paxillae 100µm (h), 116 µm (d), 17 µm (spacing)	Field	**Antifouling effect:** No effect on the fouling composition, community, and percentage cover during dry season. **AF mechanism:** Surface topography	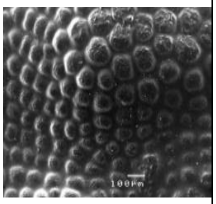	[51]
Sea star: *Fromia indica* **Dimension:** Paxillae 52 µm (h), 172 µm (d), 108 µm (spacing)	Field	**Antifouling effect:** No effect on the fouling composition, community, and percentage cover during dry season. **AF mechanism:** Surface topography (requires a combination of behavioral, mechanical and/or chemical antifouling mechanisms).	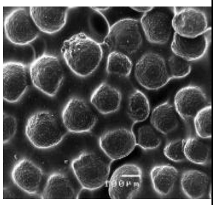	[51]

Brill fish *Scophthalmus rhombus* **Dimension:** Ribs 85 µm (h), 10 µm (d), 10 µm (spacing)	Laboratory and Field	**Antifouling effect:** Reduced coverage and cluster formation observed in the laboratory. Results still unclear in the field **AF mechanism:** Surface topography. Affects microfouling and early biofouling stages by physically limiting the adhesion of microscopic organisms. Attachment Point Theory	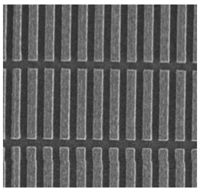	[42]
Shark: Sharklet AF **Dimension:** Ribs, 2 µm, 2 µm, 4–16 µm (width, spacing, length)	Laboratory (Commercialized)	**Antifouling effect:** Reduced spore settlement density by 86 %. *S. aureus* biofilm percentage cover on Sharklet AF covered surface was 7 % compared to 54 % for smooth PDMS control. **AF mechanism:** Attachment Point Theory	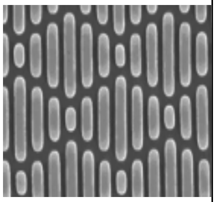	[52–54]
Bivalve: *Mimachlamys nobilis* **Dimension:** Pinholes, few microns	Laboratory	**Antifouling effect:** Topography prone to attachment of *N. closterium* cells. **AF mechanism:** Surface topography	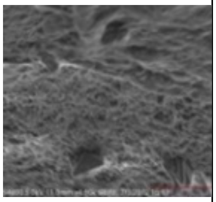	[55]

1.3.3 Nanoparticles

Throughout the ages, the use of nanoparticles went unnoticed due to the limited understanding of its toxicity towards certain organisms. Nanoparticles, which involves manipulating and utilizing matter at the atomic and molecular scale, held great promise [56]. However, its effects remained largely undetected and misunderstood because they operated on such a minuscule level.

For centuries, researchers and scientists were perplexed by the perplexing outcomes observed when certain organisms interacted with nanoparticles [56]. Little did they know, these effects were a result of nanotechnology subtly influencing biological systems in complex ways. For example, in 1856, Faraday showcased his ground-breaking experiment in which he successfully prepared colloidal gold, a discovery he referred to as 'divided metals'. On April 2nd of that year, he documented his achievement, describing the particles he produced as being in 'the divided state of gold'. Remarkably, solutions containing these particles can still be found at the Royal Institution in Mayfair, London.

Fast forward to 1890, when German bacteriologist Robert Koch conducted further research on gold compounds. He demonstrated that these compounds, when incorporated within them, had the ability to inhibit the growth of bacteria. This significant finding earned Koch the Nobel Prize in Medicine in 1905. It is worth noting that the use of gold in medicine is not a recent development, as it has been utilized throughout history for various medical purposes.

Although progress was being made in nanoscience and nanomaterials, it wasn't until recent times that the underlying mechanisms and potential risks associated with nanotechnology began to be understood.

The lack of understanding about the toxicity mode was due to several factors. Firstly, nanoparticles operate at an incredibly tiny scale, with materials manipulated at dimensions smaller than 100 nanometres [57]. This meant that interactions between nanoparticles and organisms occurred at a level that was invisible to the naked eye, making it difficult to perceive their effects. Additionally, the intricate nature of biological systems complicated the assessment of toxicity as the mechanisms through which nanomaterials interacted with organisms were complex and not easily decipherable.

Furthermore, the field of nanoparticles was still in its early stages, and specialized knowledge required to understand its complexities was limited. Scientists and researchers had not yet developed comprehensive frameworks and methodologies to evaluate and analyze the potential risks associated with nanoparticles. Without a solid understanding, the potential hazards of nanoparticles often went undetected or were mistakenly attributed to other factors. However, as scientific knowledge expanded and research in nanotechnology intensified, progress was made in unravelling its mysteries. The development of advanced analytical tools and techniques allowed scientists to delve deeper into the interactions between nanomaterials and organisms, shedding light on their mechanisms of toxicity. With the help of advanced imaging technologies such as electron microscopy and atomic force microscopy, researchers could visualize and study the intricate interactions at the nanoscale.

Additionally, interdisciplinary collaborations between scientific disciplines such as chemistry, biology, physics, and toxicology became more common, facilitating a comprehensive understanding of nanotechnology's impact on living systems. Researchers began to recognize that the physicochemical properties of nanomaterials, such as size, shape, surface chemistry, and stability, played crucial roles in determining their toxicity and biological interactions. In this work we will study the effectiveness of silica nanoparticles embedded in coatings to combat biofouling and their potential application in tidal turbines.

1.4 Biofouling and its problems in the water sensors industry

The requirement for effective antifouling solutions is not limited to the shipping industry and extends to infrastructure for renewable energy, telecommunications and ocean and coastal observations. In the context of ocean monitoring, biofouling has long been considered a limiting factor and is recognised as one of the main obstacles to autonomous environmental monitoring in aquatic environments [58,59]. Much of the equipment currently used to monitor coastal and ocean waters relies on sensors incorporated into various platforms like buoys, subsea moorings and surface and subsurface vehicles [60]. All immersed components, including operational components (membranes, optical windows and electrodes), housings and mooring components are subject to biofouling and prone to irreversible damage (Figure 5 A and B) [61]. For a large percentage of deployed instrumentation, biofouling is the single biggest factor affecting the operation, maintenance and data quality. This is particularly true for coastal and marine deployments. The Alliance for Coastal Technologies has estimated that up to 50% of operational budgets are attributed to biofouling, depending on location and season [62]. Such costs are associated with shorter deployment periods, loss of data due to sensor drift, frequent maintenance requirements and a shorter lifespan of the instrumentation (Figure 5 C). With recent advances in electronics, power management and battery life, and communication, biofouling is the key factor limiting the length of time a water monitoring instrument can stay deployed, particularly in long-term, continuous monitoring applications [62,63]. With a projected increase in operational architectures at the regional and global scales, to provide a backbone for active networking of autonomous platforms and environmental observations, the role of effective antifouling strategies for in situ sensors is paramount. Despite the importance of protection against biofouling for in situ instrumentation, progress towards an ideal operational strategy has been slow. Although many techniques have been developed and tested in the last decade very few of them have been implemented commercially. For example, ultrasonic or electromechanical systems, although effective, cannot be implemented commercially due to high energy requirements that a battery could not supply continuously [8]. In many cases, the strategies used have been developed for the mature shipping industry and applied in their original or altered form to the instrumentation. The most notable developments and advancements have come from industry, with the development of specialised, tailored design solutions.

As biofouling presents technical obstacles and often generates large economic costs and is recognised as one of the major obstacles to autonomous environmental sensing in aquatic environments [18,59,64,65]. Within the oceanographic community, there is a growing demand to acquire more in situ data at various locations and platforms to calibrate environmental models or to operate monitoring of underwater industrial processes. Therefore, there is a need for longer-term in situ instrument deployments. However, longer periods of submergence make oceanographic instrumentation and associated sensors susceptible to higher rates of biofouling. All submerged components such as operational components (membranes, optical windows and electrodes), housings and mooring components are subject to biofouling. Biofouling build-up can inhibit sensor operation, require increased system maintenance and affect the quality of the data generated by the instrument.

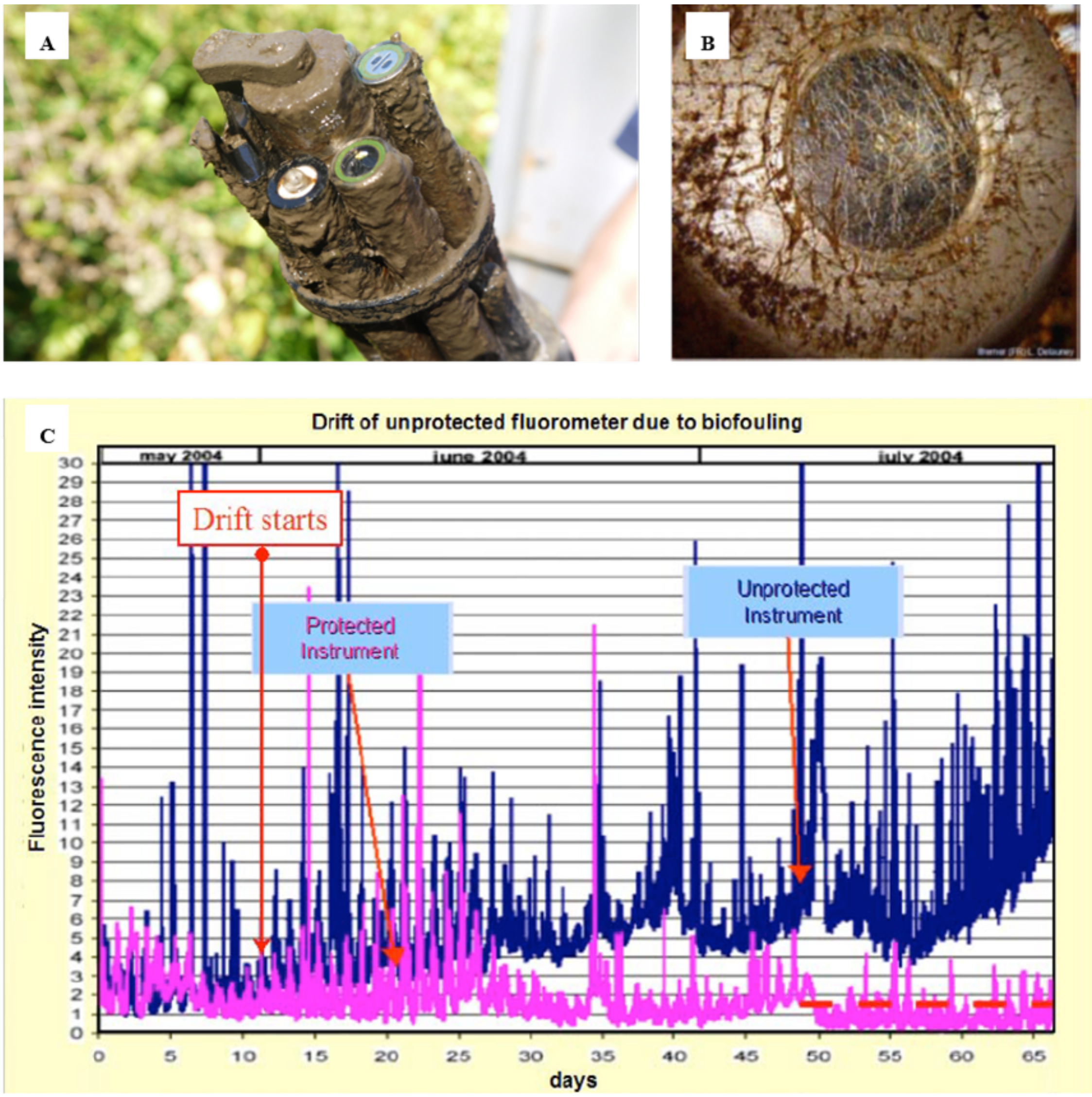

Figure 5: Overview of the biofouling on optical sensors and how this affects measurements over time. (A) EXO-sonde after it had been deployed (reproduced with permission of © 2020 YSI, a Xylem brand [66]); (B) transmissometer after 30–40 days in Throndheim harbour (Norway) during summer; (C) drift of an unprotected fluorometer due to biofouling development on the optics. (Modified from [61])

1.5 Biofouling and its problems in the tidal energy industry

Biofouling is not only a problem for the monitoring of environmental parameters by sensors, it also affects the energy industry such as the tidal industry. One of the objectives in Europe for 2050 is the use of renewable energy sources. Achieving this goal involves harnessing the energy generated by the sea, increasing the energy efficiency of turbines through design improvements and new materials. It is therefore relevant that the EU has set the ambitious target of reaching 100 GW of installed tidal and wave power capacity by 2050 [67]. However, as mentioned above, turbine blades also suffer from the effects of biofouling, which in turn affects efficiency fatigue and loss of energy efficiency due to cavitation problems (Figure 6).

When turbines are operating at full power, they are particularly susceptible to the hydrodynamic process of cavitation [68–70]: as the water rushes past the sharp edges of the blades, it can vary the pressure so much that it immediately changes to a vapour state. The bubbles that form travel to areas of higher pressure and implode, causing structural damage and compromising the lifetime of the structure [71]. Therefore, it is crucial to research and understand the biofouling process in order to develop coatings and materials that can withstand as much as possible any device or structure submerged in the sea for long periods of time and reduce maintenance costs as much as possible.

Figure 6: a: NOVA Innovation turbine covered by biofouling. b: Turbine covered by biofouling after 6 months (Clean Current Tidal Power Demonstration Project).

1.6 Methodologies to assess biofouling

Numerous analytical techniques have been devised to assess the presence of biofouling and its inherent characteristics. The development of materials and coatings to prevent fouling is of vital importance and requires precise techniques that are sometimes very costly and difficult for manufacturers of water quality monitoring sensors or other companies in the marine sector to implement. They often need to use independent laboratories to assess and analyse the quality of materials and components against marine fouling in order to study the performance of coatings. Some of the most commonly used techniques for the assessment of biofouling are listed in this thesis, but in general they can be grouped as follows:

1.6.1 Physical characterisation techniques

Biofilm research focuses on various aspects related to their structure, function and ecology. These range from the initial development of biofilms (the primary adhesion of organic and inorganic molecules together with individual microorganisms adhering to a substrate), to the growth and maturation of the biofilm. Biochemical physiology, complex multicellular interactions based on cell-to-cell signaling, exchange of genetic material, protective and segregating properties of extracellular polysaccharides (EPS), exposure to inorganic and organic contaminants such as biocides, detergents, synthetic surfactants, heavy metals and reactive oxygen species are also studied. In addition, biofilm detachment processes are investigated.

1.6.1.1 Contact Angle

Contact angle measurements provide an indication of the hydrophobicity or hydrophilicity that a surface possesses. The hydrophobicity or hydrophilicity provides insights for microorganism attachment, particularly in the initial fouling stage [72] The free energy can be approximated using contact angle measurements as a function of the surface "wettability", whereby the contact angle is the angle at which the drop of water touches the substrate described by Young's equation (equation 1):

(Eq 1)

$$\gamma_{SG} - \gamma_{SL} - \gamma_{LG} \cos \Theta = 0$$

Surface tension of the solid, liquid and solid-liquid are represented by γ_{SL}, γ_{SG}, and γ_{LG} symbols respectively. The estimation of both wetting and adhesion properties can be achieved by calculating the surface tension resulting from the solid-liquid interface, as shown in Figure 7. Typically, the hydrophobicity of a substrate is determined through the analysis of multiple solvents.

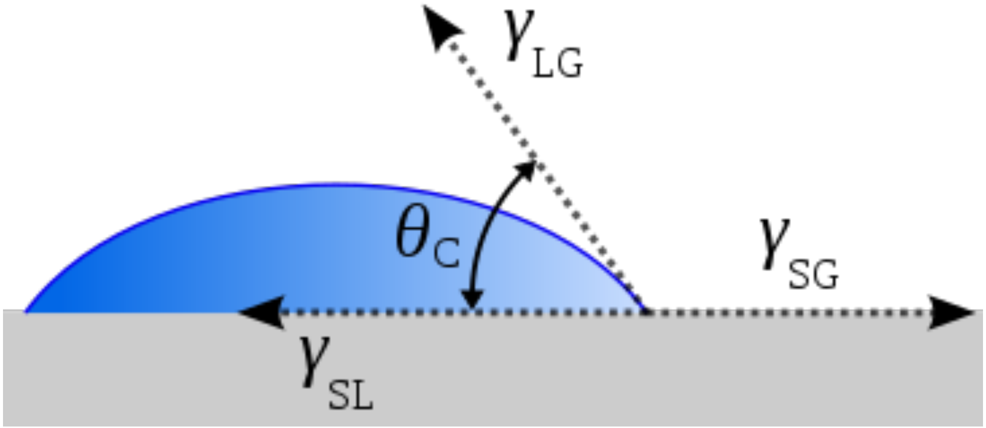

Figure 7: Schematic of a liquid drop on a solid substrate showing the quantities in the Young equation. The contact angle is represented by Θ_c γ_{SG}, γ_{SL} and γ_{LG} correspond to the surface tension of solid, liquid and solid-liquid interfaces.

This method has its set of pros and cons. On the positive side, it is relatively straightforward and allows for the deposition of multiple drops at various locations on a sufficiently large surface, enabling the assessment of heterogeneity. However, one of its drawbacks is that when dealing with smaller sample sizes, it becomes challenging to determine heterogeneity, and it is often assumed [73]. Furthermore, water droplets, being fully submerged, may not accurately reflect the actual environment to which the substrate/material is exposed, as they may be under the influence of other particles such as contaminants that may affect or mask these properties [74]. On the other hand, time-dependent processes also play an important role in the interaction between surfaces and water. A clear example of this are corrosion phenomena in which the properties of the materials are lost or changed causing a change in wettability [75].

1.6.1.2 Calculation of mass or dry weight

The determination of mass is a straightforward process that entails weighing the substrate before and after a study, thereby quantifying any mass increment attributed to surface activity. Typically, the sample is weighed in its dry state to remove water content, which provides insights into the biological and chemical constituents contributing to fouling. This increase in mass is commonly expressed as a percentage of mass increase [76,77].

(Eq 2)

$$M_d \text{ (dry basis)} = \frac{f - i}{i} \text{x}100$$

Where f is the final weight, i is the initial weight, both before and after the drying step or where the weight remained constant. Although dry weighting is a very cheap and easy technique to apply, it is often not possible to establish significant differences between samples due to the minute changes that occur when water evaporates. Therefore, there is a tendency to overestimate or underestimate the changes that are taking place, which means that this technique must be complemented by other techniques such as microscopy like scanning electron microscopy [78,79].

1.6.1.3 Scanning Electron Microscopy

Scanning electron microscopy can be used to investigate the levels of biofouling of a fouled sample on a substrate and remains fundamental for assessing levels of biofouling as well as inspecting materials, nanoparticles and numerous areas of biofouling research [80–84]. For example, Lee and Tsao demonstrated that

SEM could be used to characterize hydrogels with embedded silver nanoparticles, although at low resolution, which did not allow full characterization of the nanoparticles in the composite material [85]. In the field of microbiology, scanning electron microscopy techniques have been used to study the structural composition of microbial constructs attached to substrates [86].

As can be seen, scanning electron microscopy is a viable method for visual enumeration of bacteria adhering to a substrate, as well as providing clear information on the morphology of the bacteria and the surface of the material [87]. However, its limitations are not only that it is time consuming, both in terms of sample preparation and microscope set-up, but also that it is a destructive technique as the sample has to be coated with gold to allow electrons to pass through, which does not allow rapid real-time inspections directly in the field, and only small fields of view can be focused, which does not allow a complete view of the entire surface if it is large.

1.6.1.4 Confocal laser scanning microscopy

Confocal laser scanning microscopy (CLSM) is emerging as a key tool in unravelling the complexities of biofouling. The power of this technique lies in its ability to provide high-resolution, three-dimensional imaging, allowing researchers to dissect the intricate structures and layers of biofilms. Using fluorescent labelling, CLSM allows the visualization of specific components within biofilms, such as bacteria and extracellular polymeric substances (EPS). Live imaging capabilities facilitate the observation of biofilm formation dynamics over time, while optical sectioning and z-stack analysis allow the study of the vertical distribution and architecture of fouling communities. For example, Tow and collaborators used confocal microscopy to monitor biofouling communities under realistic conditions [88]. Quantitative analysis tools help to measure biovolume, biomass and thickness, providing valuable insight into biofouling parameters. In addition, CLSM is proving instrumental in assessing the effectiveness of anti-fouling strategies and can be used to identify microbial species within biofilms using techniques such as fluorescent in situ hybridization (FISH) [89].

1.6.1.5 Fluorescence microscopy:

Fluorescence microscopy is a power tool for assessing biofouling and it offers several advantages over conventional microscopy techniques when studying biofouling. One key advantage is the ability to selectively label and visualize specific components of biofouling, such as bacteria, algae, or extracellular polymeric substances, using fluorescent dyes. For example, we can highlight studies by Ming-Yuan Chen and collaborators in which they use these fluorescence techniques to study EPS [90]. This specificity enables researchers to discriminate between different types of fouling organisms and provides a more detailed and targeted analysis compared to the broader observations provided by conventional microscopy. Furthermore, the technique offers higher sensitivity and resolution, facilitating the detection of low concentrations of fouling agents and the detailed examination of biofilm structures. The use of multiple fluorophores with distinct emission spectra also enables the simultaneous study of various biofouling components within the same sample.

1.6.1 Biologial characterization

In addition to the physical characterization of the materials and their observation are the biological characterizations, the most important for biofouling analysis:

1.6.1.1 Metabarcoding approach

The utilization of molecular markers, such as 18S RNA, has proven valuable in characterizing biofouling on materials and surfaces [91,92]. 18S RNA is a genetic marker commonly found in eukaryotic organisms, including protists and microalgae, which are often key components of biofilm communities.

By targeting and amplifying the 18S RNA gene using molecular techniques like polymerase chain reaction (PCR), researchers can identify and quantify specific eukaryotic species present in biofilms. This approach enables a more comprehensive understanding of the microbial diversity and community structure associated with biofouling.

The analysis of 18S RNA can provide insights into the taxonomic composition of the biofilm, allowing researchers to identify the organisms responsible for fouling. This information is essential for understanding the ecological dynamics and functional roles of different species within the biofilm community. J Azevedo and collaborators have used these techniques to monitor biofouling communities in a Portuguese port in much the same way as explored later in chapter 2 where a morphological and genetic analysis of biofouling communities is combined. [92]

Furthermore, studying the 18S RNA gene can help track the temporal and spatial variation of biofouling communities. By analyzing changes in the abundance and composition of specific eukaryotic species over time, researchers can gain insights into the biofouling process, factors influencing its development, and potential mitigation strategies.

1.6.1.2 Lowry protein assay

The Lowry protein assay is a widely used biochemical technique for the quantification of total protein content in a given sample. It finds application in various fields, including biofouling characterization. Richards and collaborators have successfully employed these techniques for biofouling analysis [93]. The principle behind the Lowry protein assay is based on protein colorimetry. The assay involves a series of chemical reactions that result in the formation of a coloured product proportional to the protein concentration. The colour is developed through the reaction of proteins with a mixture of copper ions (Cu^{2+}) and alkaline reagents, such as sodium carbonate or sodium hydroxide. The reaction leads to the reduction of copper ions, resulting in the formation of a blue-coloured complex. The intensity of the colour is measured using a spectrophotometer at a specific wavelength, typically at 750 nm.

The Lowry assay offers several advantages for biofouling characterization. First, it allows for the quantification of the total protein content in the biofouling sample, providing a comprehensive assessment of the biomass present. Since proteins are the major constituents of cells and extracellular substances, measuring the protein content gives valuable insights into the biofouling community's overall abundance.

Furthermore, the Lowry assay is relatively sensitive and can detect low protein concentrations, making it suitable for analysing biofouling samples, which may contain varying levels of protein content. It also has a broad linear range, allowing for the quantification of a wide range of protein concentrations.

However, it is important to note that the Lowry assay measures total protein content and does not provide information about specific proteins or their functions. Additional techniques, such as gel electrophoresis or mass spectrometry, may be required for detailed protein characterization.

In biofouling characterization, the Lowry protein assay serves as a valuable tool for quantifying the protein content of biofouling samples, however as a disadvantage the technique requires the biofilm to be broken in order to be analysed, which severely limits the temporal studies and/or in situ analysis.

1.6.1.3 Anthrone-sulphuric acid assay

The Anthrone-sulfuric acid assay is another commonly used biochemical technique for the quantification of carbohydrates, particularly polysaccharides, in a given sample. It is widely applied in various fields, including biofouling characterization. Carbohydrates play a significant role in biofouling as they are a major component of extracellular substances and biofilm matrices produced by fouling organisms.

The Anthrone-sulfuric acid assay is based on the reaction between carbohydrates and concentrated sulfuric acid, followed by the addition of Anthrone, a crystalline compound. This reaction results in the formation of a coloured complex, the intensity of which is directly proportional to the carbohydrate concentration in the sample. The colour is measured using a spectrophotometer at a specific wavelength, typically around 620 nm.

1.6.2 Artificial intelligence and image classification algorithms

Characterizing biofouling using artificial intelligence (AI) and image analysis techniques, such as classification and segmentation algorithms, has become an emerging approach in recent years [94,95]. Biofouling analysis can benefit from the application of image segmentation techniques, as they enable the recognition of spatial patterns within biofouling samples. By employing image segmentation algorithms, such as clustering or watershed methods, researchers can identify distinct regions and organisms within the fouling community, facilitating species identification, quantification of coverage, and analysis of spatial patterns. Moreover, image segmentation allows for non-destructive analysis, preserving the integrity of the biofouling samples and enabling repeated measurements and longitudinal studies. This approach offers advantages in terms of efficiency and scalability, as AI-driven algorithms can process large datasets rapidly, providing valuable insights into biofouling dynamics. Some authors have successfully demonstrated the effectiveness of this tool applied to biofouling analysis in a simple and fast way [94,95].

In this thesis a valuable application of an image segmentation technique is demonstrated. These techniques were explored using open-source software such as ImageJ through the Fiji distribution with the Weka Segmentation plugin (University of Waikato, Hamilton, New Zealand) as well as Ilastik software [96,97]. This allowed the creation of a unique database of images of different biofouling classes that could be used to classify in an efficient way the performance of different materials both in the lab and in the field.

1.7 Conclusions

Biofouling poses significant challenges and financial burdens for various industries. Existing strategies for antifouling (AF) are inadequate in providing effective protection against biofouling, particularly in applications such as environmental sensing technologies. Therefore, there is an urgent need for novel and effective AF methods. The development of non-toxic approaches to AF is desirable, but it requires a deeper understanding of the interaction between biofouling organisms and surfaces.

Biofouling assessment and the associated infrastructure maintenance costs represent major challenges for scientists and marine companies developing sensors for water quality monitoring, as well as for the tidal energy industry. In this context, it is crucial to find solutions that are affordable, fast and effective. Fortunately, the use of image classification technologies and machine learning-based algorithms can provide a promising approach in comparison with traditional techniques like DNA analysis, or scanning electron microscope that requires specific equipment, laboratories and expertise.

Image classification techniques and machine learning algorithms make it possible to analyze and process large amounts of data efficiently. In the case of biofouling, these approaches could be used to identify and quantify the presence and degree of fouling in marine infrastructure. By training algorithms with images of known biofouling, a system can be developed that can automatically recognize the presence and type of fouling organisms on surfaces.

The application of these technologies could streamline the biofouling assessment process, enabling early detection of organism build-up and facilitating preventive maintenance on marine sensors and tidal energy systems. In addition, by reducing the need for manual and costly inspections, significant savings in maintenance costs could be achieved.

1.8 Aims and objectives

The aim of this thesis is to continue studying the biofouling process on different materials used in the marine energy industry (tidal energy) and the development of sensors for water quality monitoring in order to select the best materials, coatings and strategies to combat this problem using fast and non-intrusive techniques based on image analysis assisted by machine learning algorithms which allow us to know and accurately quantify the percentage of biofouling covered.

Chapter 2 :

Assessment of biofouling on immersed marine-grade sensor materials using a combined analysis of visual images and biofilm DNA

2.1 Introduction

The presence of natural biofilm growth affects sensors and other infrastructure in the marine environment within a few hours. If left unchecked, this growth can severely affect the integrity and performance of sensor data, as well as have a significant impact on all deployed infrastructure.

Sensors are designed to be submerged at various depths in the water. To function effectively in such environments, these systems need to be constructed using materials that are resistant to chemical and biological corrosion, as well as wear and tear over time. This ensures that the units can continuously provide reliable information.

As the demand for sensors to be in contact with water increases, the selection of the correct materials and antifouling strategies for sensors depends on the proper selection of the appropriate alloys for the application and service environment [8,98]. Table 2 outlines the types of materials that are used in sensing systems currently. The materials listed in the table are a summary of the types and sample applications of sensors. The entire sensor body is exposed to the water and therefore is liable to biofouling. Some manufacturers and researchers address only the measurement portion of the sensor when applying antifouling strategies and others address a whole sensor approach. Figure 1 illustrates a typical optical sensor and materials used, that can be impacted by fouling when immersed in water.

Whether corrosion is caused by varying depth levels, galvanic effects or biological effect, the first priority for good sensor performance over a long period of time is to match the right materials to the service application. Material selection is often affected by system reliability requirements, availability, cost and manufacturing capability.

Table 2: Materials used in the sensor body, connections and sensor head [8,99].

Material	Sample Use of Material in a Sensor	Sensor Type or Application
Metals		
Titanium	Sensor housings	Available in commercial turbidity sensors
Anodised aluminium	Sensor housings	All, freshwater applications
304L Stainless steel	Sensor housings	Specifically, marine applications and corrosive industrial applications
316L Stainless steel	Filtration	Available for particulate matter screening on some conductivity ad temperature sensors
Stainless steel microscreens	Sensor housings	Replacement for SS housings
Copper	Antifouling	Most commercial systems
Plastics		
Polyoxymethylene (Acetal, Delrin ® [100]	Sensor housings	Available on commercial pH, fluorimetry and ORP sensors
Polyphenylene sulphide (PPS) (Ryton ® [101]	Sensor housings	Some pH and ORP sensors
FEP Teflon	Membranes	Dissolved oxygen
Polyurethane	Cables	Most
Acrylonitrile butadiene styrene (ABS)	Sensor housings	Some models; OTT Orpheus Mini
HD polyurethane	Cables	Most
Poly Vinyl Chloride (PVC)	Cables	Most
Cross-Linked Polyethylene (XLPE)	Cables	Most

Chloroprene Rubber (CR)	Cables	Most
Polyurethane (PUR)	Cables	Most
Other Materials		
Epoxy resins	Electronics, housing material	Most
Silicon	Diaphragms	Water level sensors
Sapphire	Optical windows	Turbidity
PVDF membranes	Filtration membranes	Phosphate, combined models
Glass	Optical windows	Turbidity
Fused Silica	Optical windows	Most

In order to deter saltwater corrosion, manufacturers leverage superior materials. An example of this is the use of molybdenum in marine-grade stainless alloys, including 316 stainless steel alloy [28]. This type of material can be found in enclosures for portable power distribution systems designed exclusively for marine locations, industrial lighting products and more. Other types of marine-grade materials include the following: AH36, DH36 and EH36 (carbon steel); grade 5052 and 6061-T6 (aluminium); and C65500 (silicon bronze) [29–31].

Marine-rated devices for use in the marine environment on board ships or in submerged or exposed marine facilities and structures may also be treated with resilient coatings to ensure adequate protection from saltwater corrosion [32,33]. Galvanization is a common method for achieving such features, which involves dipping the material or product in hot zinc [34]. Anodizing is a type of chemical treatment process using an electrolytic acid bath (highly applicable to aluminium). It is designed to strengthen the material by forming a dense and hard oxide layer on the surface. This enhances surface hardness, wear resistance, and adhesion, contributing to improved fatigue strength. The protective oxide layer also bolsters corrosion resistance, preventing degradation and maintaining structural integrity, allowing it to withstand saltwater corrosion.

Advancements in material sciences have led to many manufacturers moving away from PVC and stainless-steel sensors due to the challenges in the operating environment. It has been seen that even materials such as steel can suffer corrosion processes produced by sulphate-reducing bacteria (SRB). These bacteria can produce hydrogen sulphide and acidic metabolites, such as acetic acid. It is suggested that the presence of hydrogen sulphide and acidic metabolites have a significant effect on the cathodic processes attacking these steel surfaces [35]. Therefore, new materials that can withstand salt water and biofouling, for example, polymers or titanium, are being used for sensors because they really increase the durability of the sensor [8,99]. A trend towards the increased use of titanium is noticed among different sensor developers, such as Valeport (Totnes, Devon, UK) or YSI, a Xylem brand (Yellow Springs, OH, USA); others, like Turner Design (San Jose, CA, USA) in their C3 and C6-P models [36,37], use a delrin® (Wilmington, DE, USA) housing, a highly crystalline thermoplastic (acetal resin) whose main advantages are its mechanical resistance and high hardness, ideal for subsea applications. The use of composite materials that combine the benefits provided by different materials can offer a high-performance solution. Such an example is carbon fibre-reinforced methylene polyoxide (POM), which combines the low friction, excellent wear properties and low water absorption of POM with the increase strength, stiffness and toughness provided by carbon fibres [8,94,102]. An example of a custom-made housing, using a combination of reinforced glass fibre with POM, can be found in some specialized manufacturers, such as Develogic Subsea Systems (Ham-burg, Germany) [38].

Sensor manufacturers conduct extensive research on biofouling to select appropriate materials for their sensors. This research involves understanding the behaviour of biofouling and its contributing factors, evaluating material compatibility with fouling organisms, assessing performance under biofouling conditions, conducting laboratory and field tests, considering long-term durability, and collaborating with industry partners.

In the past, the assessment of biofouling organisms relied on morphological identification. However, due to the significant problem that arises as soon as a material or structure is submerged, there is a growing need for earlier and more accurate detection of both microscopic and macroscopic fouling organisms, along with their quantification. In this regard, metabarcoding and image analysis approaches prove to be useful. These techniques allow for the study of organism groups and classification based on morphological features, enabling the naked-eye detection of target species and high-resolution detection of species while simultaneously processing all specimens in a sample.

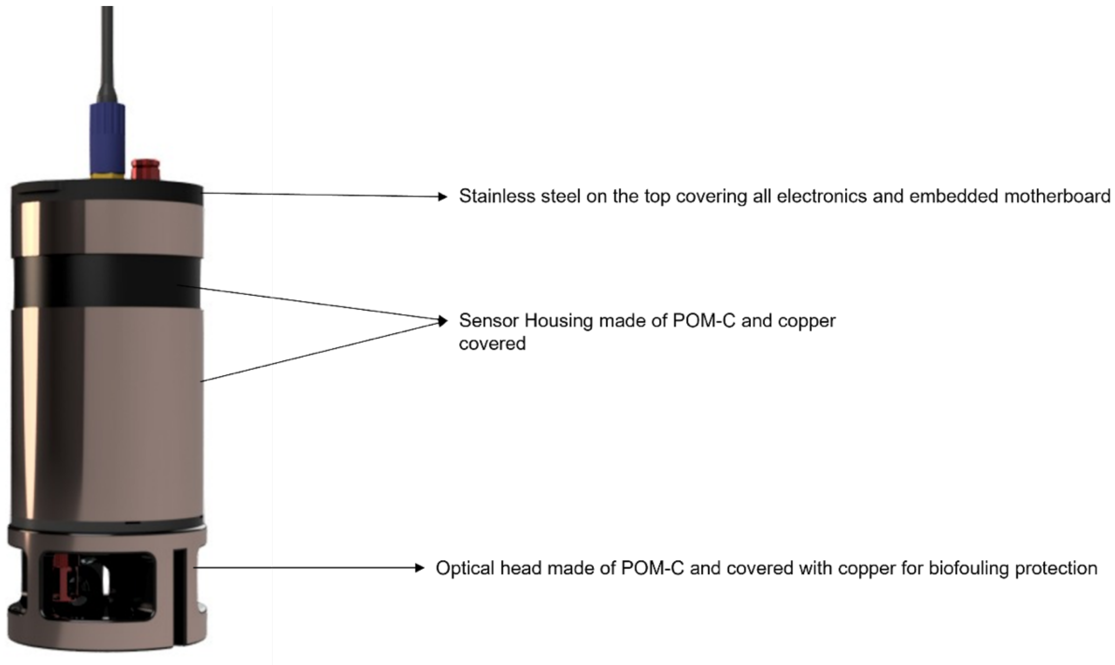

Figure 8: A simplified view of a modular optical sensor and the potential materials used in its individual modules.

2.2 Aims and objectives

In this study the objective is to determine the biofouling related robustness of different materials and coatings used in the construction of sensors deployed in the marine environment. This is done through both image analysis techniques using supervised classification and machine learning, and metabarcoding analysis of the 18S rRNA marker and image analysis.

2.3 Materials and methods

2.3.1 Sampling area

The analysis of biofouling colonization on the submerged panels was carried out in Dublin Bay at Poolbeg Marina 53° 20'39 "N, 6° 13' 03 "W. At Poolbeg Marina an area was selected that was exposed and open to a brackish environment formed by the end of the river Liffey and the sea (Figure 9). This area is frequented by cargo ships and recreational ships, and the Celtic Anglian Water treatment plant is located nearby.

Figure 9: End of the mouth of the River Liffey which forms a brackish environment estuary surrounded by cargo ships and subject to a constant tidal variation. A represents the sampling site at Poolbeg Marina (A), Dublin Bay, Ireland. The arrow represents the movement of waterflow.

2.3.2 Selection of materials

Seven materials used in the construction of water quality monitoring sensors and two antifouling paints used in boat hulls were selected for the study. The materials used were copper, 316L stainless steel, high chemical resistance polyoxymethylene (POM-C), high density polyoxymethylene (POM-H) commonly used in sensor housing, and two commercial antifouling paints Trilux-33 Black (AF T-B) (International, AkzoNobel, Amsterdam, Netherlands) and Micron-Extra White (AF M-W) (International, AkzoNobel Amsterdam Netherlands) coated on 316L- steel panels. In addition, fiberglass composite used in the construction of other structures like tidal turbine blades were also tested. The composite materials tested were designed by INPRE Composites S.L., Spain, from fiberglass and vinyl ester resin with a 200 µm thick coating made from Policor® GEL ISO NPG PA Ral 9003 gelcoat from Polynt with the Luperox® K12 G catalyst from Arkema (Paris; France). The samples included in the study were made and supplied by CANOE technological platform, France. For environmental testing and materials deployment, a triangular prism structure was designed and fabricated from PMMA panels. Test materials were cut in 10x10 cm panels (3 panels for each material) and fixed using nylon screws. To reduce variations due to exposure, sunlight, or water flow replica test panels were mounted on each face of the triangular prism. For protection against impact, the structure was mounted into a robust cylindrical mesh cage (Figure 10 B and C). The mesh cage was moored to a floating pontoon and submerged to 1 m depth throughout the deployment, which is the ideal photic zone for the study of biofouling and communities of photosynthetic benthic organisms.

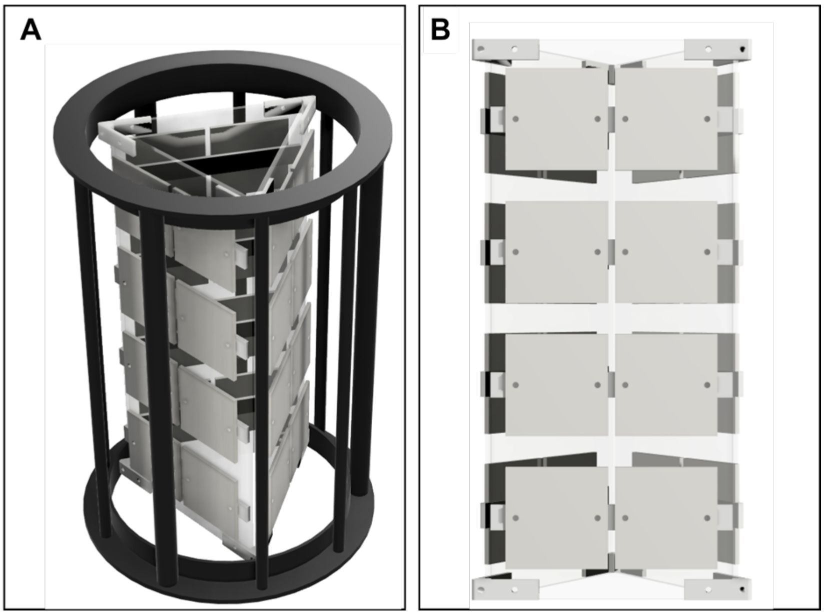

Figure 10: Sampling site and experimental set up employed in this chapter. (A) Render of the sampling cage. (B) PMMA setup with 10x10 cm panels attached.

Table 3: Materials deployed and characteristics

Materials	Application
316L-Stainless Steel	Housing in freshwater sensors, good anticorrosion resistance
Copper	Antifouling guards, mesh for housing and shutters to protect optical head, good mechanical strength and anticorrosion resistance
Polyoxymethylene POM-C	Used in economic sensors, used in sensors housing, non-expensive and easy to use for models and concepts using CNC maching
Polyoxymethylene POM-H	Used in economic sensors, used in sensors housing, non-expensive and easy to use for models and concepts using CNC maching
AF-P Trilux-33 Black	Used in ships hulls to protect against biofouling. Requires water flow to be effective. Ablative paint
AF-P Micron-Extra White	Used in ships hulls to protect against biofouling. Ablative paint
Fiberglass Composite	Used in the manufacture of tidal turbine blades.

2.3.3 Temporal barnacle colonization analysis

To determine biofouling accumulation with time sampling was conducted monthly from March 2020 to March 2021. The panels were permanently submerged during the entire sampling campaign. Upon retrieval of the deployment cage, panels were rinsed with seawater using low-pressure syringes to remove debris and sediments transported by the river. High-resolution photographs (3084x3078 pixel) were taken on-site for each panel using a Canon EOS 2000D with a Canon EF 50mm f/1.8 STM Lens mounted on a tripod. The photos were taken at a distance of about 1.5 meters between the camera and the structure with the materials. The ISO used in the image sensor was pre-set automatically in order for the camera to determine the best light parameters. In the summer months and sunny days, the ISO was set to about 100-200. In the winter and cloudy months, the ISO used by the camera was 400. The number of barnacles per square centimetre every month in triplicate were counted manually and averaged using the open-source software ImageJ with Fiji distribution (Figure 11). The decision to count the number of barnacles on the different materials was taken because a quick and easy method was needed to measure the degree of colonisation of the materials and assess their effectiveness against biofouling, without the need for post-processing of the images or the application of image analysis and/or segmentation.

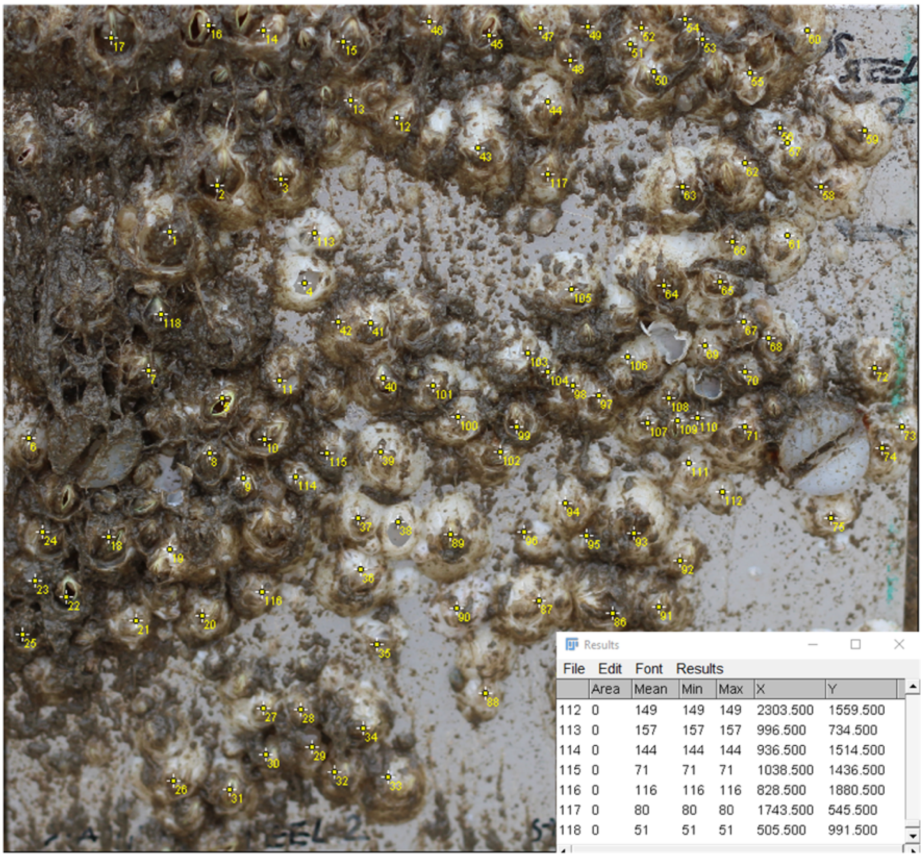

	Area	Mean	Min	Max	X	Y
112	0	149	149	149	2303.500	1559.500
113	0	157	157	157	996.500	734.500
114	0	144	144	144	936.500	1514.500
115	0	71	71	71	1038.500	1436.500
116	0	116	116	116	828.500	1880.500
117	0	80	80	80	1743.500	545.500
118	0	51	51	51	505.500	991.500

Figure 11: Image of the 10 cm x 10 cm stainless steel panel with barnacle count using Fiji distribution (ImageJ).

2.3.4 Supervised classification

A Fiji distribution in ImageJ called Weka Segmentation was used to evaluate the photographs from the triplicate panels exposed after one year of immersion [103]. The photos taken for each panel for this analysis were the same as those taken for the temporal analysis of barnacle colonisation. A Canon EOS 2000D camera with a Canon EF 50mm f/1.8 STM lens was used. Each sample was cleaned with seawater from the site to reduce sediment and dirt. Once the photos were taken, each of them was adjusted for intensity, brightness, and colour saturation prior to analysis.

Weka segmentation plugin uses features such as pixel intensity, edge filters and texture descriptors for modelling. A total of three classes were established (Table 4). Once the classes were established, a random forest classifier with 200 decision trees was used which performs semantic segmentation (see chapter 3)

Table 4: Classes of organisms used in supervised classification applied on the coast of Ireland.

Colour of each class in image analysis	Description of the class
Purple	Background: Clean, unfouled surface. Visually identified with the original colour of the material
Red	Slime: microscopic bacteria, algae and extracellular polymeric substances (EPS). Visually identified as a “brown silt”
Green	Hard biofouling: Barnacles and tube worms.

2.3.5 Biofilm DNA extraction, PCR amplification and hight-throughput sequencing.

Following the one-year immersion, samples in duplicate were scraped, transferred to sterile 50 ml falcon tubes, and stored at -20 °C prior to processing. DNA was subsequently extracted using the DNeasy PowerSoil Kit (Qiagen Hilden, Germany) following manufacturers’ instructions (Figure 12 and Figure 13). DNA extracts were quantified using a Qubit® Fluorometer (Thermo Fisher Scientific; Massachusetts, United States) with double-stranded DNA (dsDNA) high sensitivity assay kit. This kit is designed to accurately and reliably quantify low concentrations of dsDNA samples in a small volume, making it particularly useful for samples with limited amounts of DNA. The assay works by using a fluorescent dye that binds specifically to dsDNA and emits a measurable signal that is detected by the Qubit® Fluorometer. The instrument then calculates the concentration of dsDNA in the sample based on the amount of fluorescence detected, providing accurate and sensitive measurements DNA samples. High-throughput sequencing (NGS) using the Illumina MiSeq System (San Diego, California, United States) was used to sequence the amplified V4 region of the eukaryotic 18S rRNA gene. This would allow the identification and classification of the organisms present in the DNA samples based on the genetic information in 18S ribosomal RNA (rRNA) gene.

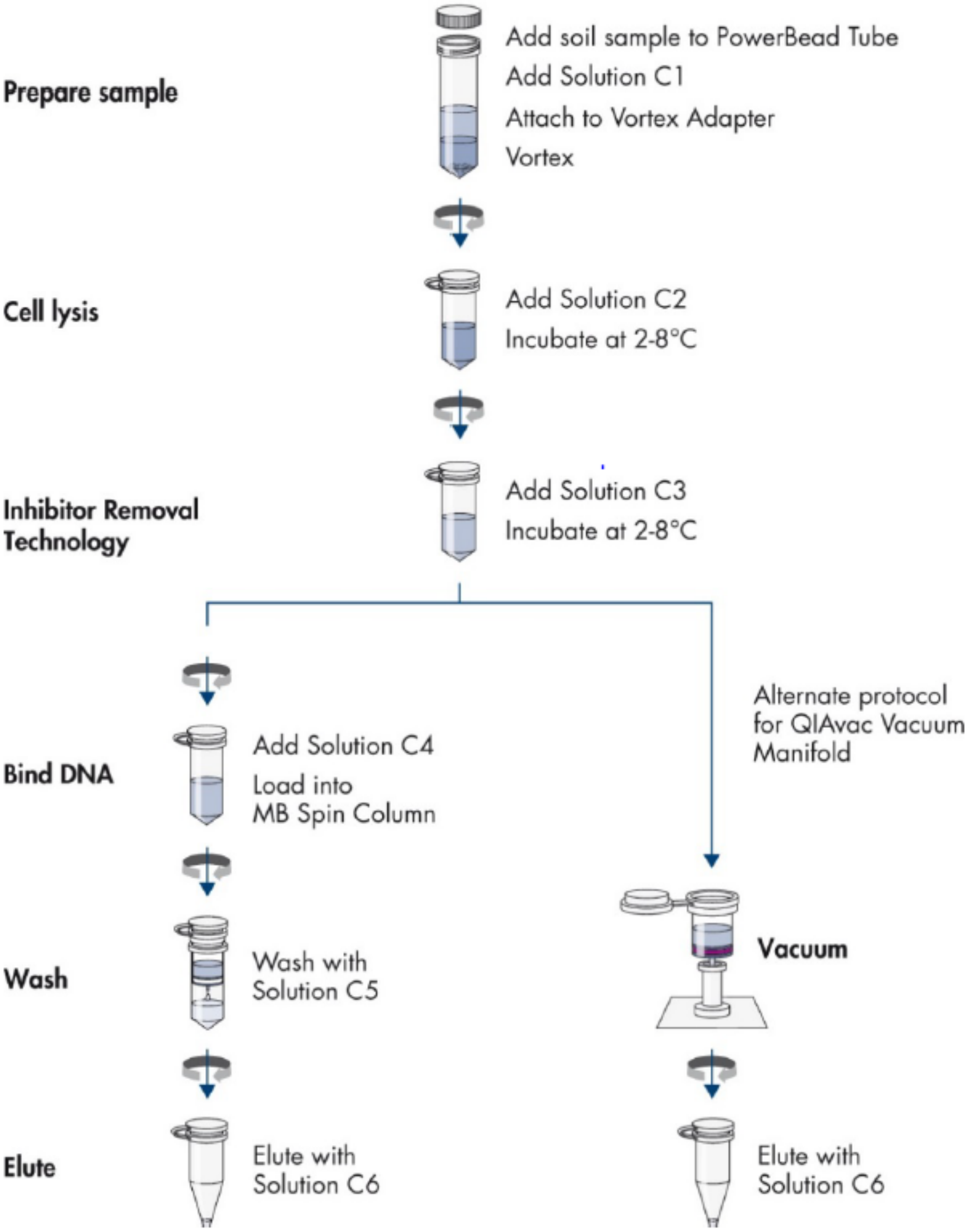

Figure 12: DNeasy PowerSoil Kit for DNA extraction procedure (image source: DNeasy PowerSoil Kit Handbook 05/2017)

The 18S ribosomal RNA (rRNA) gene is a commonly used genetic marker in molecular biology for identifying and classifying eukaryotic organisms. The gene is present in all eukaryotic cells and is highly conserved, meaning that it can be used to study the evolutionary relationships between different organisms.

The V4 region of the 18S rRNA gene is a specific segment of the gene that is commonly targeted for amplification and sequencing in molecular biology research. This region has been shown to be a useful marker for identifying and classifying eukaryotic organisms across a wide range of taxa.

To amplify the V4 region of the eukaryotic 18S rRNA gene, universal primers that are designed to bind specifically to this region of the gene were used. The specific primers used in this study were Uni18SF (5'-AGGGCAAKYCTGGTGCCAGC-3') and Uni18SR (5'-GRCGGTATCTRATCGYCTT-3'), as referenced by a previous publication [104]. These primers are capable of amplifying the V4 region of the 18S rRNA gene in a wide range of eukaryotic organisms (around 300 pb), making them useful for identifying and classifying diverse samples.

Once the V4 region of the 18S rRNA gene is amplified using these primers, it was sequenced using high-throughput sequencing technologies such as the Illumina MiSeq System. Then raw data was processed using Bcl2Fastq conversion software tool from Illumina into text-based sequence (FASTQ).

Then the analysis of the rRNA sequences involved a series of computational steps using a customized bioinformatics pipeline based on the QIIME2 package (v2021.8.0). QIIME2 is a widely used open-source software package for analyzing microbial communities using high-throughput sequencing data.

The first step in the analysis was to import the paired-end reads into the QIIME2 environment and trim them using the q2-cutadapt tool. This tool is designed to identify and remove adapter sequences and low-quality bases from the sequencing reads, which can negatively impact downstream analysis.

Next, the reads were quality filtered, denoised, merged, and chimeras removed using the q2-DADA2 tool. DADA2 is a widely used bioinformatics tool for high-resolution, error-corrected amplicon sequencing data [105]. It uses a model-based approach to remove sequencing errors and resolve closely related sequences to produce high-quality sequence variants, or amplicon sequence variants (ASVs).

Once the ASVs were generated, taxonomic classification was performed using a reference database of known 18S rRNA gene sequences, such as the SILVA database [105]. This allowed the identification of the organisms present in the original DNA samples.

The customized bioinformatics pipeline used in this study was designed to ensure the accurate and reliable analysis of the 18S rRNA gene sequences, from data pre-processing to taxonomic classification.

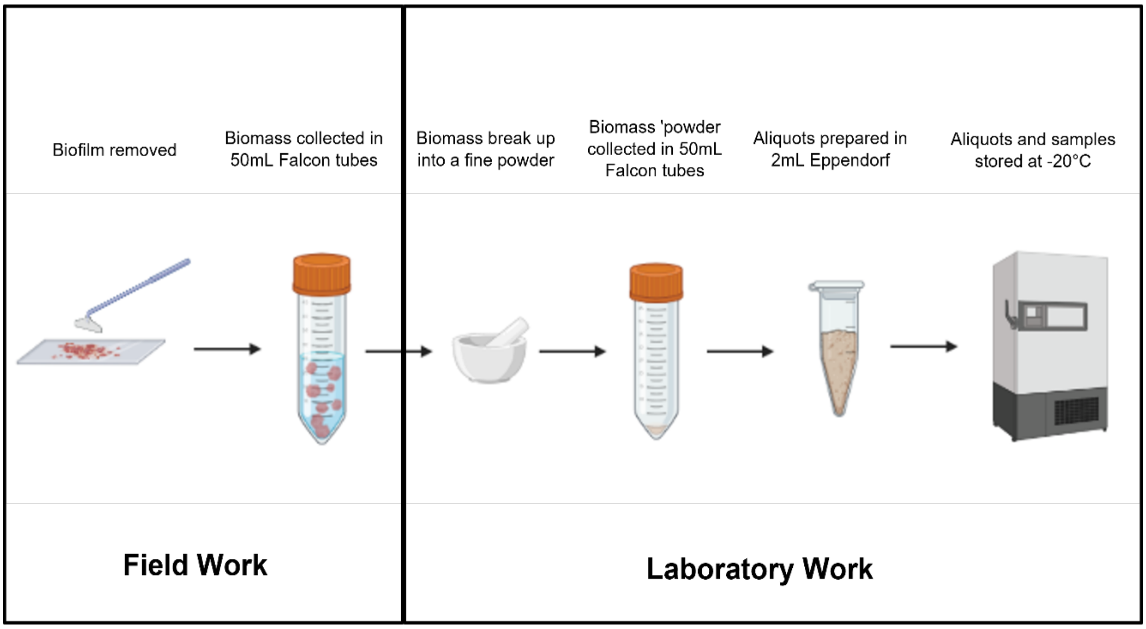

Figure 13: Schematic representation of the DNA extraction process from field sample to laboratory.

2.4 Results and discussion

Image analysis using supervised image classification demonstrates a fast, efficient and above all non-invasive method for measuring biofilm accumulation and progression. Furthermore, this method presents other distinct advantages, including limited sample handling and processing, and the possibility for in-situ application (ie. image collection while the materials are submerged). It has been demonstrated with this technique that it is possible to analyse biofouling accumulation in submerged panels using a Canon EOS 2000 D and 50mm f/1.8 STM lens with appropriate light conditions (Figure 14). It was possible to visualize the differences between the different material samples and above all to transform a qualitative variable into a quantitative variable using this image analysis technique in an accurate way by training the algorithm to recognize pixels.

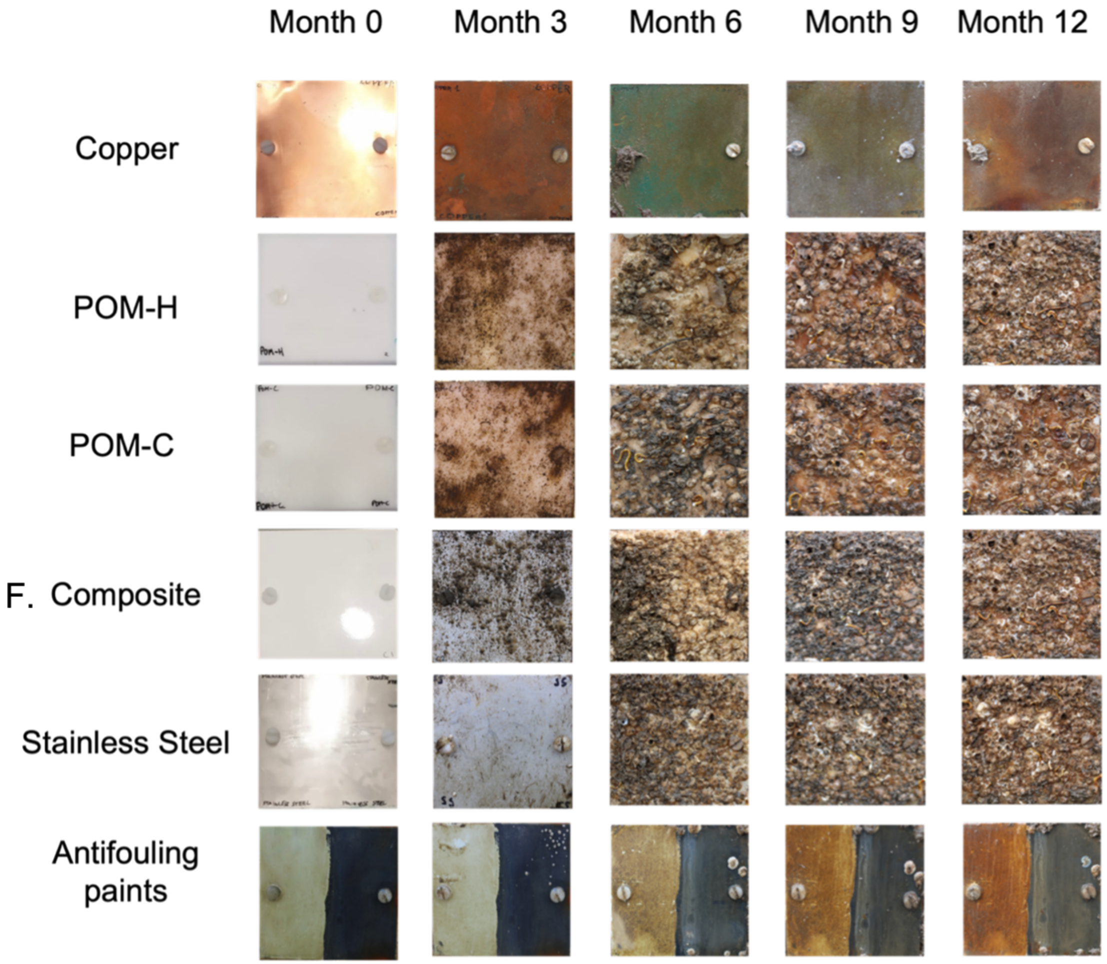

Figure 14: Photographs collected in situ in the field, showing the evolution of biofouling over a period of 1 year on different materials.

2.4.1 Time-based barnacle colonization analysis

An increase in barnacle colonisation was observed in May at the beginning of the summer season after a period of no colonisation from March to April for all the samples (Figure 13). This increase coincides with a rise in water temperature. On the other hand, we observed a decrease in the winter period. Some studies have shown that the temporal variability of biofouling abundance on hard substrates is mainly influenced by the physico-chemical properties of the water, properties of the substrate and the behaviour of the organisms [106–109]. Temperature is one of the key factors that affect these communities, alongside nutrient levels, salinity, and sunlight levels. These studies have shown that biofouling communities tend to increase in biomass and abundance with rising water temperature [110,111].

In terms of antifouling performance, copper panels and Micron-Extra White antifouling paint did not show any colonisation, while Trilux-33 Black antifouling paint showed some colonisation from May onwards and remained stable during the following months (Figure 15). The POM-C and POM-H polymers showed a continued moderate increase in barnacle colonisation starting in May until September, after which a decrease in colonisation was observed. However, 316L-stainless steel and fiberglass composite showed a very rapid barnacle colonisation from May to June. Subsequently, their colonisation rate decreased but remained positive until August in the case of the 316L stainless steel, while for the fiberglass composite, their colonisation rate continued to increase but at a much more moderate rate. Subsequently, during the month of September, a decrease in colonisation was observed for this material, POM-H, POM-C and

316L-Stainless Steel. Towards the end of the summer season, a general stabilisation was observed for all the samples in the study, apart from the fiberglass composite, whose colonisation continued to decrease. A very weak trend of increasing colonisation of Trilux-33 Black antifouling paint was also observed.

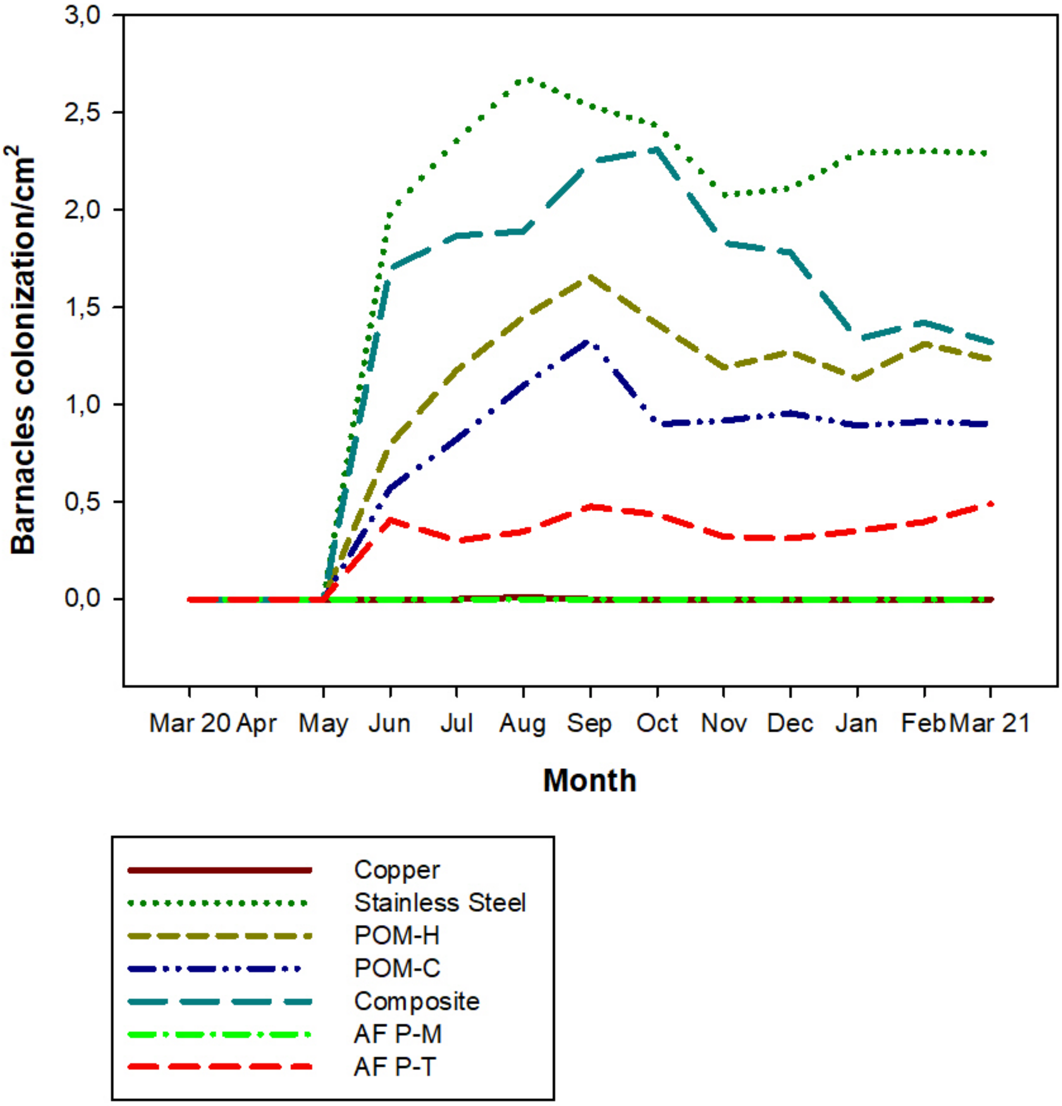

Figure 15: Barnacle's colonization per square centimetre per each 10x10cm panel in 1 year study. This graph shows the count of the number of barnacles using the technique shown in figure 9 with photographs and using Fiji distribution (ImageJ).

2.4.2 Supervised classification

Visual inspection from figure 17 of the heavily fouled panels generated three classes: clean (unfouled surface), hard fouling (macroscopic organisms such as barnacles and tubeworms) and slime (microscopic organisms encompassed within the slime).

A minimum of 50 manual spots for each biofouling type were used to create each class in the library. The accuracy of the resulting segmentation maps was verified by visual comparison with the original photographic images. Each image was calibrated individually by training the algorithm to learn to recognise the clear part of biofouling from the covered part.

The segmentation maps shown in Figure 17, reflect higher antifouling performance of both Trilux-33 Black and Micron-Extra White antifouling paints and copper. Their percentage of uncovered surface area was 94.44 % for copper and 84.78 % and 75.82 % for the antifouling paints Micron-Extra White and Trilux-33 Black respectively. On the other hand, the results on the segmentation maps (Figure 17) showed that the 316L-stainless steel has a certain variety of both hard biofouling and soft biofouling, with a covered surface area of 36.56 %. However, the composite showed a relatively high percentage of hard biofouling covered surface area of about 61 % while the slime was only 3.31 %. Its percentage of uncovered surface was 36.04 %. The POM-H and POM-C samples showed very similar results. In both cases the hard biofouling was high with 63.45 % for POM-H and 51.34 % for POM-C. The slime was quite similar 12.92 % and 13.21 % for POM-H and POM-C respectively as well as the percentage of uncoated surface 23.64 % for POM-H and 35.41 % for POM-C.

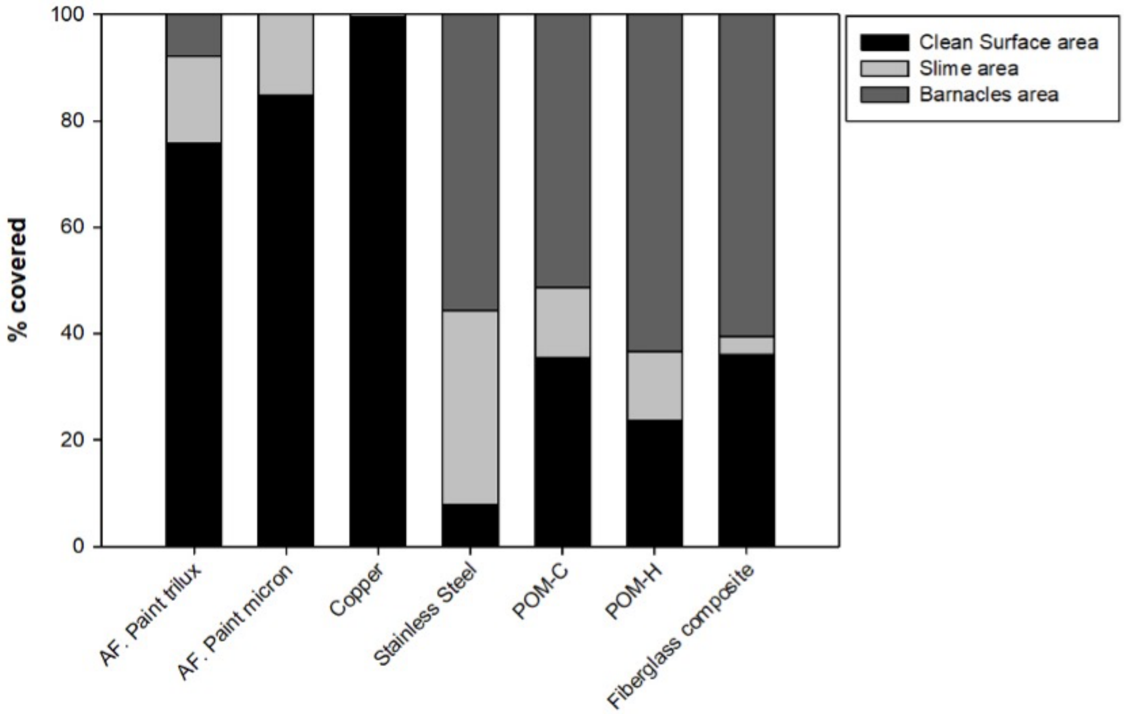

Figure 16: Bar-plot representing the percentage of surface covered by slime, and hard biofouling in each sample. Clean surface area was calculated on the spot where the colour of the material was visually visible and was not covered with any of the other two classes. Each bar was calculated by the analysis of colour from the segmentation map obtained from only one panel.

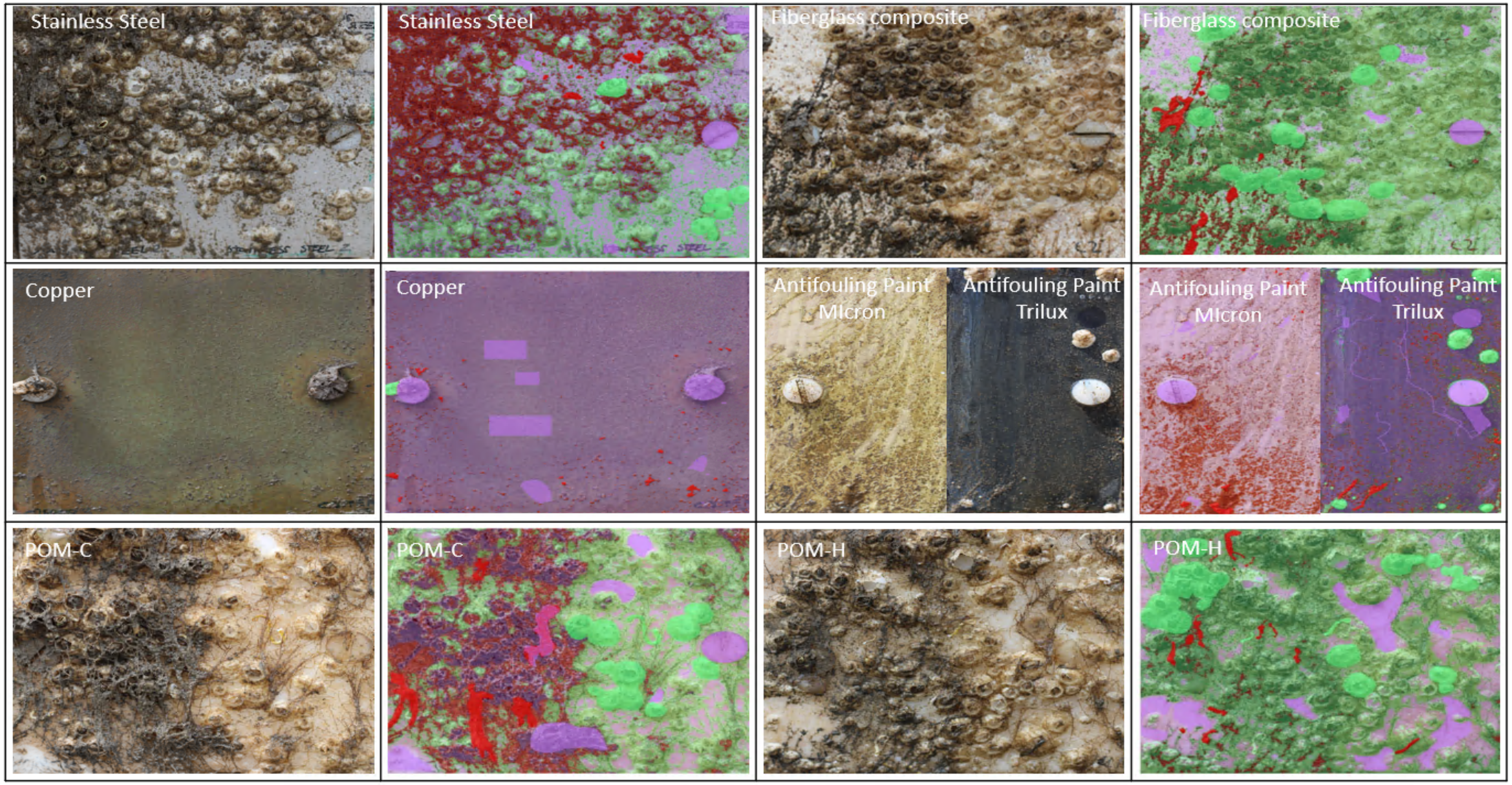

Figure 17: Photograph of one of the triplicates of each sample followed by the probability map obtained by pixel-segmentation. Colour red represents slime class, green represents hard biofouling and purple clean surface. This segmentation map was calculated using Random Forest model with 200 decision trees.

2.4.3 Metabarcoding

The genetic marker used in this metabarcoding approach was the gene region encoding 18S rRNA and was successfully PCR amplified from all samples. High throughput sequencing produced a total number of 1,025,271 raw sequences for 18S rRNA. The total number of OTUs for 18S rRNA, was 143,094. DNA concentration varied from 104 ng/μL to 9.22 ng/μL after extraction using the Qiagen DNeasy PowerSoil Pro Kit.

In total, 47 phyla were identified using the 18S rRNA sequencing approach, with Ciliophora, Nematozoa and Arthropoda representing the most abundant groups (Figure 18 and Table 5). There is a difference in the relative frequency of phyla on the different materials, with antifouling paint Micron-Extra White and Copper having higher abundance for Ciliophora (77.9 % and 88.9 %, respectively) while in the rest of the materials, their abundance was notoriously low compared to the previous ones. Research on the toxicity of trace metals to ciliates is sparce, although some studies carried out on soil communities of ciliates have shown that some strains used were sensitive to trace metals and the growth of ciliate species was often inhibited by the presence of Cu^{2+} [112–115]. However, there is a discrepancy regarding the effects on abundance at high concentrations as authors showed a positive effect on abundance which shows that in general protozoa are very resistant to Cu^{2+} toxicity [116]. The resistance of ciliates to copper can be attributed to the presence of a large number of cytoplasmic granules within the cell. These play an important role in the compartmentalisation of metals, thus increasing their tolerance [117,118].

However, in the next nine most abundant groups the relative abundances increased for all materials except for copper and antifouling paint Micron-Extra

White which were lower. This may be because the bivalent Cu^{2+} present in coatings and paints interferes with enzymes in cell membranes, preventing cell division [119,120] and therefore reducing biofouling [121]. Previous studies using commercial antifouling coatings have reported reduced diversity of fouling communities as a result of the presence of these commercial products on surfaces [122–125]. However, the antifouling paint trilux-33 black showed a higher relative abundance of biofouling communities compared to Micron-Extra White. This could be due to the loss of efficacy of the coating over time, in which the erosion rate of the matrix containing the biocide is too high from the moment the surface is laid out in the water [126]. This gradually decreases the release rate of the toxic particles, causing the degree of protection to decrease [127]. According to the technical documents provided by the manufacturer. Micron Extra White provides the longest lasting protection of up to 3 years as it has a controlled polish that smoothes over time maximising the efficiency of the biocidal effect of the copper. However, the recommended lifetime for Trilux -33 black is 24 months in which the gloss finish is prioritised over its antifouling efficacy [127] which may explain its somewhat lower performance. These paints commonly used on ship hulls have relatively weak biocidal activity in stationary conditions, making them unsuitable for sensors that are moored or stationary in one place and will ultimately suffer from biofouling activity [128]. The reason for the limited suitability of commonly used ship hull coatings with weak biocidal activity for moored or stationary sensors lies in their inability to effectively counteract biofouling in such static conditions. These coatings, designed for ship hulls, rely on movement through water to activate and enhance their biocidal properties, preventing the accumulation of fouling organisms. In stationary or moored scenarios where there is minimal water flow, the biocidal activity of these paints becomes comparatively weak, rendering them ineffective in preventing biofouling [129]. As a result, sensors in static positions are more susceptible to biofouling, potentially compromising their functionality and accuracy over time.

Nematozoa were the most highly abundant phylum on the antifouling paint trilux-33 black (25.75 %), fiberglass composite (27.02 %), 316L stainless steel panels (13.15 %), POM-C (41.07 %) and POM-H (68.96 %). However, some studies have reported that nematodes have previously been shown to be severely impacted by heavy metals [130] which explains the very low levels found in the copper panels (0.89 %). Arthropoda were not detected on antifouling paint Micron-Extra White, POM-C and copper panels. Studies have shown that the use of copper alloy components for marine structural applications is being actively promoted as a viable alternative to TBT-based coatings [131] due to reduced maintenance costs, extended service life, increased reliability and high recyclability [132,133]. However, Arthropoda abundance was remarkably high in the fiberglass composite (47.11 %). and very low in POM-H (0.27 %) and POM-C (0 %) and the antifouling paint trilux-33 black (3.25 %). Md Redzuan Zoolfakar and co-workers showed in studies that materials such fiberglass have high biofouling rates [134]. Low Arthropoda values found in POM-C and POM-H can be explained by the wettability of the surface. The wettability of a surface affects the attachment of organisms to it because they can more easily retain water and allow for the formation of a thin film of water between the surface and the organism [135–140]. This can make it easier for the organism to anchor itself to the surface. Rough hydrophilic surfaces can provide more surface area for attachment and can create microenvironments that are more favourable for settlement. Some studies reported the apparent preference of some fouling organisms like *B. amphitrite* for hydrophilic surfaces [141–143]. Therefore these studies have shown that some cyprids prefer rough hydrophilic surfaces. This is because hydrophilic surfaces provide more surface area for adhesion. Rough surfaces may also create more favourable microenvironments for settlement, such as areas of increased water flow or areas with higher nutrient concentrations . On the other hand, smooth hydrophobic surfaces, may be less attractive for settlement because they provide less surface area for attachment. For example, low-energy surfaces such as poly-(dimethylsiloxane) (PDMS) elastomers are used commercially as release coatings because the fouling organisms adhere weakly and are released under suitable hydrodynamic conditions [144] .However, some authors reported that *B. improvisus* demonstrated an opposite tendency for settling on hydrophobic (low-surface-energy) surfaces [145][146]To understand this we must first understand that there are two main ways in which wettability can act on larval settlement. Firstly, larvae can sense surface chemistry by coming into physical contact with the surface through various parts such as the antennules . Secondly, assuming that unfavourable wettability prevents contact with the surface, the mechanism of action could be explained in terms of physico-chemical forces acting between the surface and the larva. For example, we can highlight electrostatic repulsion [147]. Hydrophilic surfaces have mainly carboxylate groups on the surface. This chemical group has strong negatively charged elements. In addition, any surface that is in contact with water tends to become negatively charged, largely because the cations present in water have a greater tendency to hydrate than anions. Therefore, cations will remain in the aqueous phase, while anions tend to adsorb to surfaces. Therefore, the cyprid larva itself would represent a surface that could become negatively charged by adsorbing anions present in the water, so that there would be electrostatic repulsive forces between the cyprid and the surface preventing surface contact.

However, this explanation does not explain the predisposition of *B. amphitrite* larvae to favour highly wettable substrates, so the differences in substrate wettability preference between congeneric larvae of *B. improvisus* and *B. amphitrite* is probably not a matter of wettability acting on adhesion or adhesive forces, as studies have shown that the temporary adhesion tenacity of *B. amphitrite* cyprids is not a matter of adhesion strength, as studies have shown that the temporary adhesion tenacity of *B. amphitrite* cyprids is not affected by the wettability of the underlying surface [148].

Chlorophyta phylum was higher on the 316L stainless steel (17.79 %) while in the rest of the materials their abundance was similar, being the lowest in copper (0.48 %). In the Apicomplexa phylum the highest abundance was found in stainless steel again (14.52 %) and POM-C (6.74 %). In the rest of the materials, hardly any significant abundance was found.

The high values for 316L stainless steel can be explained by the fact that they do not have any bactericidal properties and biofilms can easily adhere to them [149]. Studies comparing 304 stainless steel, which is very similar to 316L stainless steel, and the same steel treated with copper particles showed a big difference in biofilm formation [150]. This makes stainless steel a useful positive control sample due to its high biomass growth [151].

Tunicates also showed very low levels of relative abundance. They were not found in POM-C and POM-H nor in the fiberglass composite, and the levels in the rest of the materials were very low; antifouling paint Micron- Extra white (1.42 %), and antifouling paint Trilux-33 black (1.17 %) and copper (0.75 %) As for Ascomycota, stainless steel showed the highest levels of relative abundance (14.04 %) followed by POM-C considerably lower (5.67 %), antifouling paint trilux-33 black (4.39 %), POM-H (3.15 %), fiberglass composite (2.28 %), antifouling paint Micron-Extra White (1.59 %) and finally copper (0.56 %). The relative abundance of Cercozoa also showed low levels among all materials with POM-C being the highest (8.97 %) followed by stainless steel (6.01 %) then POM-H (3.75 %), antifouling paint trilux-33 black (2.87 %), fiberglass composite (1.64%) and finally copper (0.43 %).

Comparing the results shown in percentage surface area covered within the supervised classification show a very high similarity to the metabarcoding results as well as the temporal barnacle colonization analysis. Copper and the two antifouling paints showed both the lowest relative abundances percentage, the lowest percentage surface area covered and lowest barnacle colonization per square centimetre, while 316L stainless steel and fiberglass composite were the most diverse which is also shown in the manual barnacle count per square centimetre analysis. However, it is worth noting that the technique of manually counting barnacles per square centimetre was especially complicated when the panels began to be completely covered, causing an underestimation of the colonization percentage over the months.

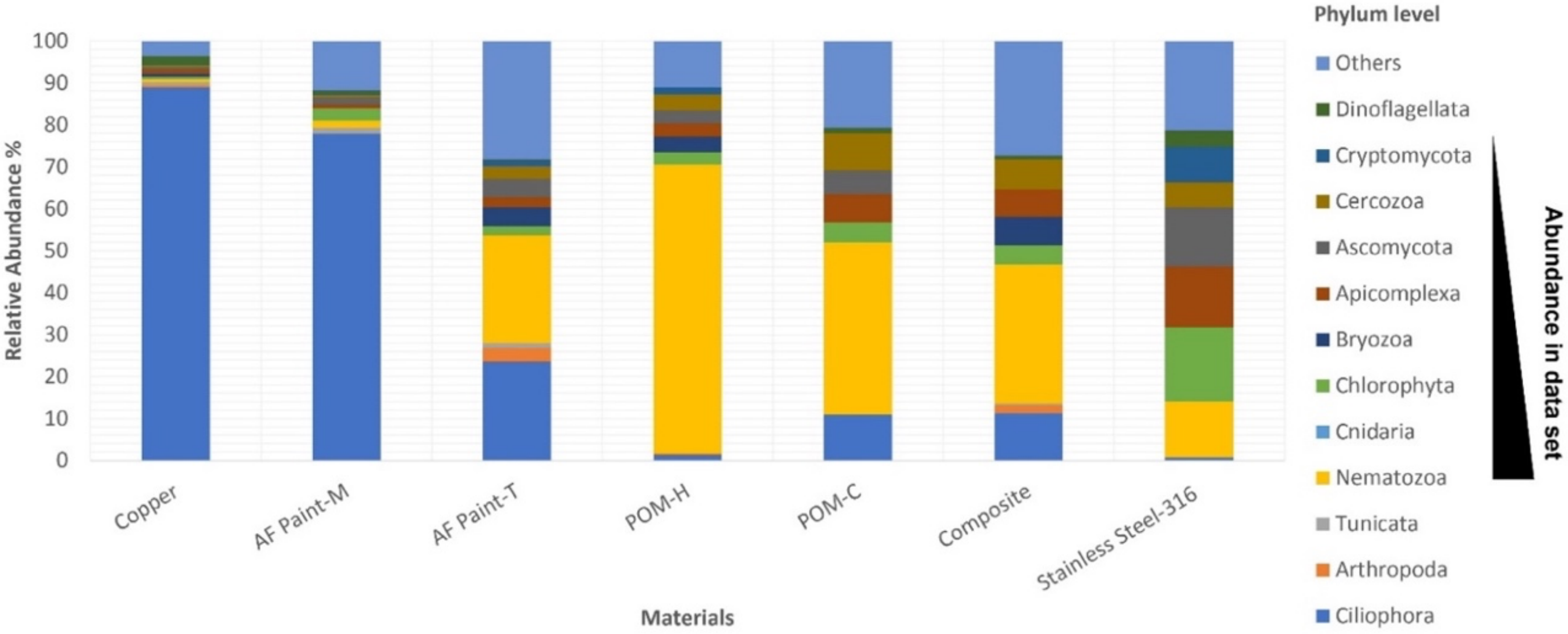

Figure 18: Relative abundance of phylum based on 18S rRNA sequencing.

Table 5: Percentage taxonomic abundance for each sample at level 2 (phylum) for the 10 most frequent results amongst all samples for 18S rRNA.

Phylum	Copper	F. Composite	POM-C	POM-H	AF P-M	AF P-T	316L S. Steel
Ciliophora	88.92	8.12	10.88	1.31	77.91	23.56	0.63
Arthropoda	0.41	47.11	0	0.27	0	3.25	0
Nematozoa	0.83	27.02	41.07	68.96	1.62	3.25	13.15
Chlorophyta	0.48	3.84	4.75	2.99	2.95	25.75	7.79
Apicomplexa	0.90	1.81	6.74	3.17	0.98	2.14	4.52
Tunicata	0.75	0	0	0	1.42	2.40	0.21
Ascomycota	0.56	2.28	5.67	3.15	1.59	1.17	14.04
Cercozoa	0.43	1.64	8.97	3.75	0.49	4.39	6.01
Cryptomycota	0.21	0.75	0	1.73	0.33	2.87	8.43
Dinoflagellata	2.08	0	1.23	0	0.87	1.44	3.87
Others	4.45	7.43	20.69	14.67	11.84	29.78	41.35

Although supervised image classification exhibits impressive performance in sample analysis, it remains a relatively constrained tool when compared to metabarcoding in terms of its ability to extract comprehensive information. This is primarily due to the significant processing power required, particularly in situations where samples are heavily covered. This can be seen in materials such as the fiberglass composite and POM-H where the slime-class (in red colour) cannot be detected correctly, and the percentage covered is underestimated. However, this analysis technique is cheaper, faster and does not destroy the sample compared to metabarcoding, and provides us with more information than the analysis of the temporary colonization of barnacles.

The metabarcoding approach, unlike the other techniques, provides a greater detail on the groups of organisms that colonize each material, and enables custom material selection based on the application environment [37]. For example, materials such as POM-C and POM-H polymers showed very similar performance in the three techniques. Composite and 316L stainless steel were found to be the worst performing materials in the high biofouling environment for one year. The relative abundance of all classes observed for these two samples was found to be considerably high through the use of the 18S rRNA marker. Consequently, the ecological community established on these panels is much more resilient and less susceptible to environmental changes compared to copper or antifouling paints, which exhibit a lower relative abundance and therefore, lower biodiversity.

This is the first time that marine grade materials used in sensing devices have been evaluated to establish the link between biofilm community and material composition. Using multiple methods for biofilm progression and characterisation our results indicate that biofilm diversity is linked with quantitative biofilm accumulation. Healthy biofilm (those with greatest diversity of organisms) formation was noticed on most of the materials tested with the exception of copper and antifouling paints. For this materials, additional antifouling strategies are needed to protect the immersed surfaces, whereas, for those made from copper or coated in antifouling paints the antifouling performance could be sufficient for most applications.

2.5 Conclusion

In conclusion, this study aimed to evaluate the performance of various materials and coatings employed in sensor construction using a combination of image analysis techniques, supervised classification, machine learning, and metabarcoding analysis of the 18S rRNA marker. By employing these multidimensional approaches, a comprehensive assessment of the sensor materials' effectiveness in mitigating biofouling was achieved.

The utilization of image analysis techniques allowed for the visual identification and characterization of fouling organisms on the sensor surfaces, enabling a qualitative assessment of fouling severity. Moreover, supervised classification and machine learning algorithms not only offered quantitative measurements but also established the groundwork for employing deep learning techniques and methodologies. These advancements will enable researchers and manufacturers to swiftly and effectively evaluate various materials for equipment construction in a significantly more accurate manner than manual counting.However, more classical techniques like metabarcoding analysis using 18S rRNA marker, enhanced the study's accuracy and resolution by providing insights into the taxonomic composition of the fouling communities. This molecular approach offered a more comprehensive understanding of the biofouling species present and their potential impacts on sensor performance. The use of biofilm-DNA-based metabarcoding for biodiversity assessment may prove to be a more cost-effective approach for environmental biomonitoring as it allows detection of large organisms in relatively small samples [152–154], but, it has its limitations. For example, PCR biases, stemming from preferential amplification during DNA sequencing, can introduce inaccuracies in estimating species abundance. Reference database completeness and accuracy are crucial for precise taxonomic assignments. The method may inadvertently co-amplify non-target DNA, leading to contamination in environmental samples. Quantitative uncertainties arise from variations in PCR efficiency and DNA extraction. Metabarcoding targets conserved DNA regions, potentially overlooking intraspecific variation and hindering differentiation between closely related species. Adequate sample size, replication, and computational resources are essential for robust statistical analyses, and the method may not capture temporal and spatial dynamics or accurately reflect ecological interactions.

By combining these analytical methods, a holistic evaluation of the sensor materials' biofouling resistance was achieved demonstrating that certain materials have favorable properties for biofouling management. For example, copper, in combination with antifouling paints, is an ideal choice for sensor housings or optical head protectors, especially in areas with high biological activity. Although materials such as POM-H and POM-C have intermediate performance, they offer advantages such as high mechanical strength, low cost and ease of handling, making them ideal for reducing manufacturing costs.

However, materials such as fiberglass-composite and stainless steel need to be supplemented with antifouling paints or other antifouling strategies [138–140].

Chapter 3 :

Establishment of an Antifouling Performance Index derived from the assessment of biofouling on typical marine sensor materials

3.1 Introduction

In recent years, materials technology has undergone and is undergoing a remarkable change for the marine industry in terms of corrosion and fouling by biofouling. Marine biofouling is the unwanted accumulation of living organisms on submerged surfaces. It is a complex process that depends on a variety of environmental factors. These environmental factors include, among others, water temperature, salinity, pH, nutrient abundance, water flow velocity, depth and light exposure which all depend on the ecosystem in which they are submerged [155–158]. Other parameters intrinsic to the materials, such as hydrophobicity and porosity among others, also play a role.

The International Maritime Organization (IMO) has identified marine biofouling as a major economic and ecological issue. Depending on the area of interest, biofouling has a different relevance. In sectors such as marine commerce, biofouling represents a major problem due to the drag problems it causes on the hulls of ships, leading to a decrease in hydrodynamic efficiency and an increase in fuel consumption and CO_2 emissions from diesel engines and the consequent evolution of greenhouse gases [159–161]. In the energy sector, the use of offshore constructions such as tidal turbines, biofouling control plays a key role in terms of efficiency. For example, hard calcareous organisms such as barnacles can produce not only more drag, but also cavitation processes which can structurally compromise turbine blades [162]. In addition, these systems are usually anchored to the seabed, making them difficult and costly to access and maintain. Similarly, in the context of ocean monitoring, biofouling has long been considered a limiting factor and is recognised as one of the main obstacles to autonomous environmental monitoring in aquatic environments [59,64].

Therefore, sensor manufacturers are paying more and more attention to effective antifouling strategies [8]. As a result, measures to manage biofouling in submerged structures and devices require periodic maintenance and application of coatings. [163–165]. These coatings may involve textures and/or functionalities (hydrophilic or chemically responsive) that reduce biofouling, like copper-based coatings, or hydrogel coatings that swell or change their hydrophilic properties in response to environmental conditions and can create a surface that is inhospitable to fouling organisms and easily sheds attached biofouling [166–168]. One of the ways in which industries deploying both in-water sensors and those building large offshore infrastructures are studying biofouling is by using growth models that allow them to see how different materials and coatings perform against biofouling over specific periods of time.

3.1.1 Why a biofouling growth model is needed

Only a few studies have attempted to provide models aimed at describing and predicting the growth of biofouling on different materials. For example, in marine structures, after their construction, they are inevitably subject to colonization by micro-organisms that can induce aesthetic but also mechanical degradation [169]. These micro-organisms can be bacteria, algae, fungi, lichens and others. It has been proven that, except for ubiquitous bacteria, algae are the first colonizers. The establishment of micro-organisms depends on various parameters of origin. Indeed, in temperate or tropical climates, the composition of a biofilm and the dominant species are respectively different [170]. According to several authors, in an ecosystem, the microclimate to which samples are subjected is regulated by different parameters that control the nature and growth of microorganisms.[171,172]. The microclimate is influenced by sun exposure, water flow velocity, nutrients in the water, depth, temperature. Substrate characteristics, such as porosity, surface roughness, chemical composition and surface pH, are obviously important [173–175]. Several studies have focused on the influence of these parameters on biofouling, both at laboratory and full-scale. However, to our knowledge, very few studies have attempted to model this phenomenon. Studies conducted by B. Chen-Charpentier and co-workers developed a numerical simulation of biofilm growth in porous materials [176]. The biofouling of algae growing on porous materials was calculated by mathematical modelling using a system of hyperbolic-elliptic partial differential equations. Thanks to this mathematical modelling, it was found that the physical phenomenon of algal cell growth and multiplication generally follows a trend similar to a sigmoidal curve [177]. In fact, microalgae culture growth is characterized by three phases; an initial lag phase in which the algae begin to adapt to the growing conditions called "latency time", a phase of rapid exponential growth and finally a stationary phase, in which the surface area covered remains constant over time (Figure 19).

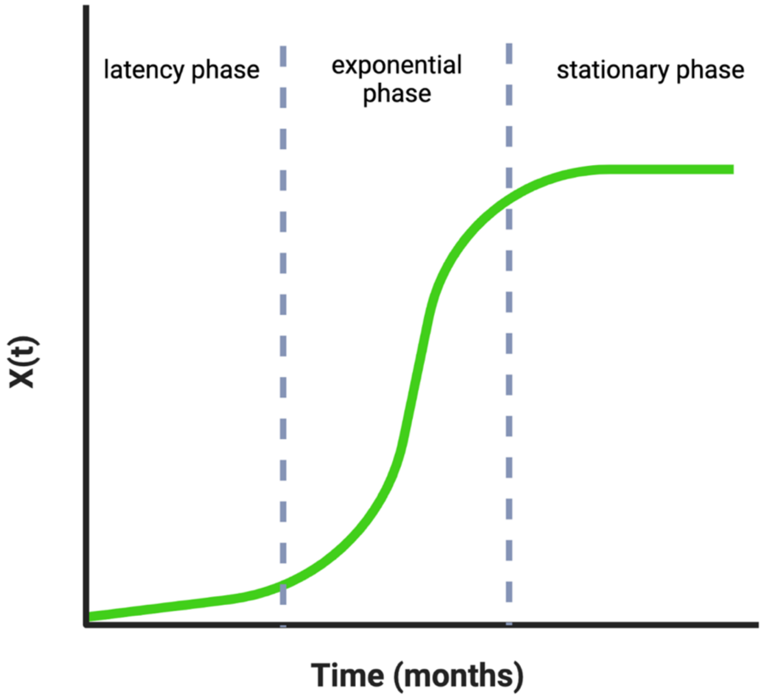

Figure 19: Typical growth-phases of an algae culture

3.1.2 Avrami´s model

Additional studies by Ruot and Barberousse showed that it was possible to study the process of biofouling under accelerated conditions under highly regulated conditions in the laboratory using Avrami's law applied to specific points for a single organism [178]. Avrami's law was developed in the form of an exponential equation by Avrami, Johnson and Melh [179–182]. This law was originally used to describe the kinetic phase transformation of solids [183,184], although it is used in different fields: crystallisation of polymers, heat treatment or solids decomposition [185,186]. For example, it is a model commonly used to study the formation of ice crops in the different layers of the atmosphere. This mathematical model mainly has two phases, nucleation, which corresponds to the appearance of a nucleus that gives rise to a new phase and on which the second phase takes place, which is the expansion or growth phase in which this nucleus begins to grow larger over time (Figure 18). In the same way, the process of biofouling in different materials can be described by means of these two phases.

In the colonisation phase, organisms begin by attaching to the substrate. Specifically, the primary colonisers, in this case microscopic algae such as diatoms and/or benthic cyanobacteria, adhere to the surface, identified as green spots that correspond to the nucleation points of Avrami's model. From then on, this nucleation point will expand over time, which corresponds to the growth phase.

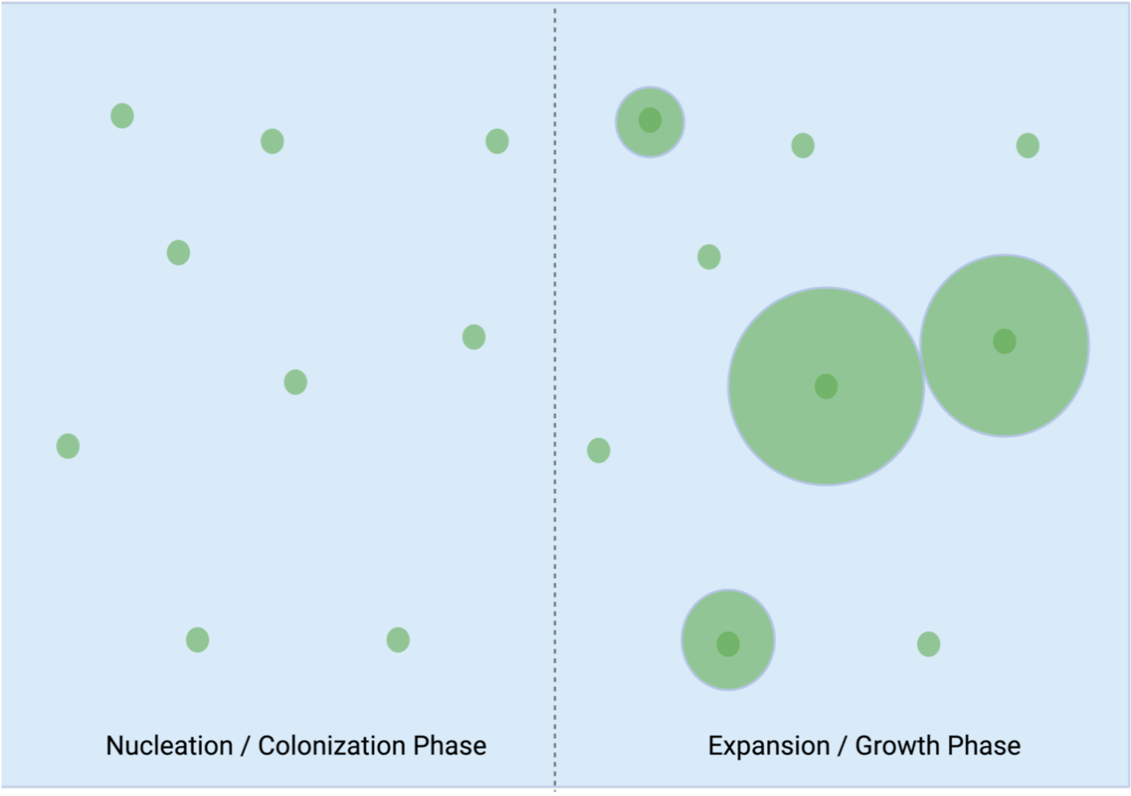

Figure 20: Simplified representation of Avrami's model. Transformation of one phase from another by the growth of randomly formed nuclei. Each dot represents a colonizing organism like a microscopic alga (image on the right) that is expanding/growing (image on the left).

3.1.3 Biofouling growth study using supervised image classification

In our biofouling studies shown in this chapter, the possibility of using this method for the calculation of biofouling growth was considered. However, one of the negative points of this Avrami's model is that it can only be applied to a certain group of organisms (microscopic algae) for a short period of time (1-2 weeks), which is not feasible for prolonged deployments of several months at sea to assess the growth of macroscopic species such as barnacles or tunicates. On the other hand, in Avrami's model the chromatic change is used for the calculation of the covered surfaces. In our experiments, however, the changes in colour and luminosity are not constant because they are field studies and the submerged samples are exposed to chemical oxidation and above all to numerous organisms of different colour, shape and size. This is why we discarded the possibility of using Avrami's model and proceeded to create a sigmoidal model to explain the growth in a similar way, but using techniques based on image classification by artificial vision techniques using machine learning algorithms in a fast way that could be applied to a wide range of materials and biofouling studies very similar to the one applied in the previous chapter but in much more depth.

Currently, biofouling quantification is often a painstaking, manual and complex task. [187]. However, the increasingly stringent requirements of biofouling management are stimulating efforts to develop reliable methods to quantify, analyse and assess biofouling damage in an efficient and rapid manner that allows different industries and sectors to evaluate which materials are better in terms of biofouling performance.

To this end, this study develops a rapid method to quantify, classify and evaluate the performance of different materials in marine sensors construction and marine-rated materials.

3.2 Aims and objectives

The aim of this chapter is to study the growth of biofouling on different materials used in the marine industry and in the construction of autonomous marine sensors.

- Investigate by using of simple image segmentation techniques assisted by machine learning algorithms the area covered and to generate classification groups.
- Generate models of biofouling growth in materials deployed at sea for extended periods of time.
- Rank materials according to their biofouling performance using the surface area covered by different groups of organisms.

3.3 Materials and Methods

3.3.1 Sampling area

The analysis of biofouling colonization on the submerged materials was carried out in Dublin Bay at Poolbeg Marina 53° 20'39 "N, 6° 13' 03 "W (Figure 19).

Figure 21: End of the mouth of the River Liffey which forms a brackish environment estuary surrounded by cargo ships and subject to a constant tidal variation. A represents the sampling site at Poolbeg Marina (A), Dublin Bay, Ireland. The arrow represents the movement of waterflow.

3.3.2 Selection of materials and deployment setup.

Seven materials used for engineering purposes like structures in tidal energy turbines or deployed equipment like sensors were selected for the study (Figure 20 C). The materials used were copper, 316L stainless steel, titanium, high chemical resistance polyoxymethylene (POM-C), high density polyoxymethylene (POM-H) and polyethylene terephthalate glycol (PETG) (Radionics ltd Ireland) commonly used in sensor housing, and fiberglass composite used in the construction of other structures like tidal turbine blades. The composite material tested were designed by INPRE Composites S.L., Spain, from fiberglass and vinyl ester resin with a 200 µm thick coating made from Policor® GEL ISO NPG PA Ral 9003 gelcoat from Polynt with the Luperox® K12 G catalyst from Arkema (Paris; France). The samples included in the study were made and supplied by CANOE technological platform, France. For this purpose, a triangular structure was designed with PMMA panels on which 10x10 cm panels of the different materials were screwed in triplicate in such a way that they had a multiple orientation to reduce variations due to exposure, sunlight, or water flow, among others. This structure was protected by a cylindrical mesh cage (Figure 20 A and B) that supported it and at the same time allowed the panels to be kept submerged at a depth of 1 meter, this being in the ideal photic zone for the study of biofouling and communities of photosynthetic benthic organisms. The reason for this configuration is that it allows for triplicates and allows for some rotation of the structure in order to obtain the least variation between them due to orientation and water flow.

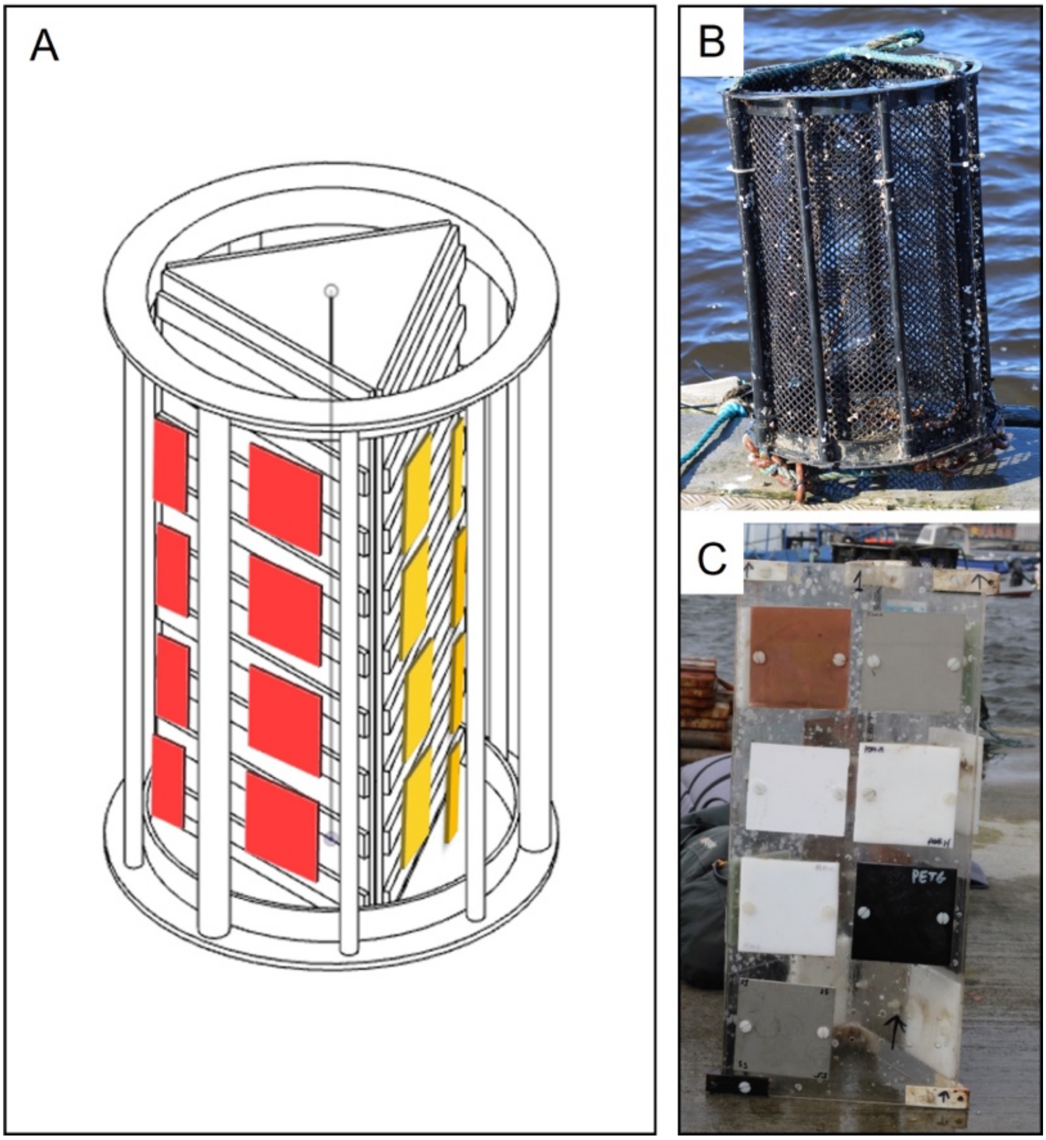

Figure 22: Deployment setup and materials deployed. Render of the sampling cage with the holder structure that has the panels in red and yellow colours (A). Real sampling cage (B). Triangular PMMA holding structure with the different material panels (C).

Table 6 : Materials deployed and characteristics.

Materials	Application
316L-Stainless Steel	Housing in freshwater sensors, good anticorrosion resistance
Copper	Antifouling guards, mesh for housing and shutters to protect optical head, good mechanical strength and antifouling resistance
High chemical resistance polyoxymethylene POM-C	Used in economic sensors, used in sensors housing, inexpensive and easy to use for models and concepts using CNC machining
High density polyoxymethylene POM-H	Used in economic sensors, used in sensors housing, inexpensive and easy to use for models and concepts using CNC machining
Titanium	Used in ships hulls to protect against biofouling. Requires water flow to be effective. Ablative paint
PETG (Polyethylene terephthalate glycol)	Used in economic water sensors, used in sensors housing, inexpensive and easy to use for models and concepts made with 3D printers
Fiberglass	Used in the manufacture of tidal turbine blades and recreational boat hulls

3.3.3 Imaging of panels and biofouling macroscopic identification

The samples were evaluated according to standard ASTM D6990-05 “Standard Practice for Evaluating Biofouling Resistance and Physical Performance of Marine Coating Systems [188]. Photographs of the panels were taken in situ on the pontoon in order to minimise any removal or interference with the biofouling. Sampling was conducted monthly from March 2021 to September 2021. The panels were submerged and removed once per month to gather measurements using a camera. High resolution photographs 3084x3078 pixel of each panel were taken each month using a Canon EOS 2000D fitted with a Canon EF 50mm f/1.8 STM Lens after rinsing each panel with seawater using low-pressure syringes in order to remove debris and sediments transported by the river. The camera was mounted on a conventional tripod at a consistent distance from the samples. The surface not covered by biofouling, which was used as a reference/control in each triplicate separately, underwent post-processing correction for illumination, saturation, and exposure of the images. Rapid identification of the organisms was carried out using Ireland's Seashore, a field guide [189], and involved the use of morphological features as well as field dissections to identify their basic structures. [28]

3.3.4 Image analysis: Supervised classification

A Fiji distribution in ImageJ called Trainable Weka Segmentation (TWS) (University of Waikato, Hamilton, New Zealand) was used to evaluate the photographs from the panels exposed after 6 months immersed in triplicate [97].

Weka segmentation plugin uses features such as pixel intensity, edge filters and texture descriptors for modelling. A total of 4 classes were established (table 5). Once established the classes, a random forest classifier was used which performs semantic segmentation. The random forest classifier is a machine learning tool which contains decision trees. In this case, 1000 decision trees were used using 2 random features with an out-of-bag (OOB) estimate of less than 8% and using the default pre-set training features Gaussian blur, Hessian, Membrane projections, Sobel filter, Difference of gaussians and Neighbours. The out-of-bag (OOB) estimate is a method of estimating the test error of a Random Forest, which is an ensemble of decision trees. The idea is that for each tree in the forest, only a subset of the data is used to train it, and the remaining data is referred to as the "out-of-bag" (OOB) data. The OOB estimate is computed by averaging the prediction errors made by each tree on its own OOB data. This can give an estimate of the test error of the forest without the need for an additional holdout set or cross-validation. A high out-of-bag (OOB) error rate means that the predictions made by the Random Forest model on the out-of-bag data (data that was not used to train a specific tree) are not accurate, and therefore the model is not performing well on unseen data. This can indicate overfitting, where the model has learned the noise in the training data rather than the underlying pattern, and therefore it does not generalize well to new data. A high OOB error rate might also be an indication of poor quality or imbalance of the data, or that the model is not complex enough to capture the underlying pattern in the data.

The random forest classifier is a machine learning tool that utilizes decision trees. In this case, 1000 decision trees were built with 2 random features, resulting in an out-of-bag (OOB) error estimate of less than 8%. The default training features used include Gaussian blur, Hessian, Membrane projections, Sobel filter, Difference of gaussians, and Neighbours. The OOB estimate is a method for evaluating the test error of the random forest, which is a collection of decision trees, by averaging the prediction errors of each tree on its own OOB data. A high OOB error rate suggests poor accuracy of the model's predictions on unseen data, potentially due to overfitting, poor quality or imbalanced data, or insufficient model complexity.

Once we were satisfied with the segmentation, we obtained a final image with the result of the classification process which contained the four colours of the four classes (table 5). This image was then reopened with ImageJ and the percentage of surface area covered by clustering colour analysis was calculated using an open-source plugin developed by the Biomedical Imaging Group from Swiss Federal Institute of Technology (Lausanne EPFL, Switzerland) [190].

In colour analysis using clustering, two approaches can be used: independent colour channels and a combined colour space. The independent colour channels option involves treating each channel (e.g., red, green, blue) as separate features for the clustering algorithm to identify distinct clusters based on variations in each channel. The combined colour space approach combines the channels into a single feature vector, allowing the algorithm to identify clusters based on the relationships between the channels. The choice between these two options depends on the specifics of the problem and data type. Independent colour channels are used when channel variations are important, while the combined colour space approach is better when the relationships between channels are more relevant.

Table 7: Classes of organisms used in supervised classification.

Colour of each class	Description of the class
Purple	Background: Clean, unfouled surface
Red	Slime: Debris particles, microscopic bacteria, algae and extracellular polymeric substances (EPS)
Green	Hard biofouling: Barnacles and tube worms
Yellow	Soft biofouling: Tunicates

3.3.4.1 Classification using pixel detection algorithms. How it works.

The different organisms such as algae, barnacles, tunicates, sediment and microscopic organisms were identified and located in the images visually by assigning them a classification (hard biofouling, soft biofouling, slime). The background (clean surface) was used to train the programme in the subtraction and identification of the remaining classes. Representative patches of the identified organisms and the clean surface were selected to create a library defining the visual characteristics of each type of fouling. The software was trained until a satisfactory result was achieved. Classification using pixel detection algorithms, sparse coding and morphological filters is a recent method successfully applied in numerous studies [191]. This chosen method was used assisted by the TWS software. In computer vision, a feature is often defined as the part of an image of particular interest, and image features are frequently used as a starting point for many algorithms [97]. Therefore, the overall algorithm is usually only as good as its feature detector. This software was chosen because it includes a wide range of image features most of which are extracted by common filters or plugins in ImageJ-Fiji. This software by default calculates more than 70 features using generic data and spherical filters ranging from 1 to 16 pixels. Once the software is provided with an image to be classified, as well as the different classes to be detected previously identified visually, TWS transforms the segmentation problem into a pixel classification problem in which each pixel is classified as belonging to a specific segment or class. The set of input pixels that has been labelled is used as the training set for a given classifier. Once the classifier is trained, it is used to classify the rest of the input pixels or new image data to be recognised and classified. Once a segmentation map or vector was obtained for each image containing the different classes grouped by colour, the analysis was combined with the plugin developed by the biomedical imaging group of the Swiss Federal Institute of Technology Lausanne, which allows the segmentation of a colour image by grouping pixels [190] allowing to obtain the percentage of area covered by each colour that would correspond to each class assigned at the beginning of the process.

3.3.5 Building a biofouling growth regresion for each material

For the construction of a biofouling growth regression, the segmentation maps obtained with TWS were used in combination with the plugin of the Swiss Federal Institute of Technology Lausanne, which allowed us to obtain the total percentage of surface area covered assigned to each colour of the segmentation map/vector. For each triplicate, the areas covered for the three classes slime, hard and soft biofouling were summed, and the mean value of the triplicates was calculated.

The average values of the percentage of total biofouling covered for each of the materials were then plotted for each month.

A 4-parameter sigmoidal regression fit (equation 3) was performed for each of the graphical representations using Sigmaplot version 11 (build 11.0.0.77). The default number of interactions was 200 to achieve the best fit. The tolerance was $1x10^{-10}$ and Chi-Square was used to compute parameter standard errors in weighted regression. Normality of the data was ensured by the Shapiro-Wilk test with a sample size ≤5000 and a P-Value to reject of 0.05.

The exponential growth phase was studied and a linear regression was performed in order to compare the growth/colonisation rates of biofouling on the different materials. For this purpose, 10 data values of the exponential phase were extrapolated from the sigmoidal model constructed and the equation of the line was calculated. The slope of each line was then used to compare the growth/colonisation rate between each material [94,102,192,193].

$$Y = Y_0 + \left(\frac{a}{1+e^{-\left(\frac{x-x0}{b}\right)}}\right) \qquad \text{(Eq 3)}$$

There are four such function parameters: Y_0, x_0, a and $1/b$. The initial biofouling coverage is represented by Y_0. This should be negligible for a clean surface at immersion. The delay due to the latency phase and the initial part of the exponential phase is captured by x_0. The biofouling coverage at the end of the stationary phase is measured by a while the rate of relaxation that is the slowdown in the growth of biofouling coverage at the end of the exponential phase is given by $1/b$. The three parameters a, x_0 and $1/b$ have been used to compare the growth and colonization rates between the various materials tested.

3.3.6 Fouling rating calculation

The fouling rating (FR) was calculated at the end of the study after 6 months as a measure of the performance of the different materials against the percentage of surface area covered by biofouling and thus benchmarking these materials. At the end of the study, the percentages of surface area covered by biofouling were calculated for each of the above-mentioned classes for each triplicate using the image analysis and the mean value was calculated. Each percentage covered in each group was multiplied by a severity factor modified from [194] (Table 8 and

Table 9). The Antifouling Performance Index (API) was calculated using equation 4.

Table 8 Different classes identified according to severity factor (modified from [194]).

Description of the Class	Severity Factor
Slime	0.2
Hard biofouling	15
Soft biofouling	0.5

Table 9: Antifouling performance evaluation of marine coatings.

Fouling rating		Antifouling Performance Index (API)	
Fouling rating	**Covered area (%)**	**Performance**	**API (%)**
0	0	Excellent	100–90
1	0-2	Good	89–70
2	3-5	Weak	69–40
3	6-25	Poor	39–30
4	26-50	Bad	29-0
5	51-100		

(Eq 4)

API = 100−(0:2 x Area covered by slime + 0:5 x Area covered by soft biofouling + 15 x Area covered by hard fouling) (modified from [194]).

3.4 Results and discussion

3.4.1 Biofouling identification

Different organisms such as barnacles, tunicates, typical of the more advanced stages of biofouling, were found (Figure 23). Sediment and unidentified microscopic organisms that were not identified, were observed and classified as slime.

Three different barnacle species were identified, *Semibalanus balanoides*, *Chthalamus spp* and the most predominant specie in this estuarine ecosystem *Austrominius modestus* which were classified as hard biofouling for the image classification analysis. Next to it, tubeworms like *Spirobranchus triqueter*, from the Serpulidae family were identified and included in the hard biofouling group as previous ones because of their hard calcareous shell. Another of the organisms found and included in this group was *Membranipora membranacea* belonging to the Membraniporidae family. As for the soft foulers organisms, *Ascidia sp.* from the Ascidacea family was identified.

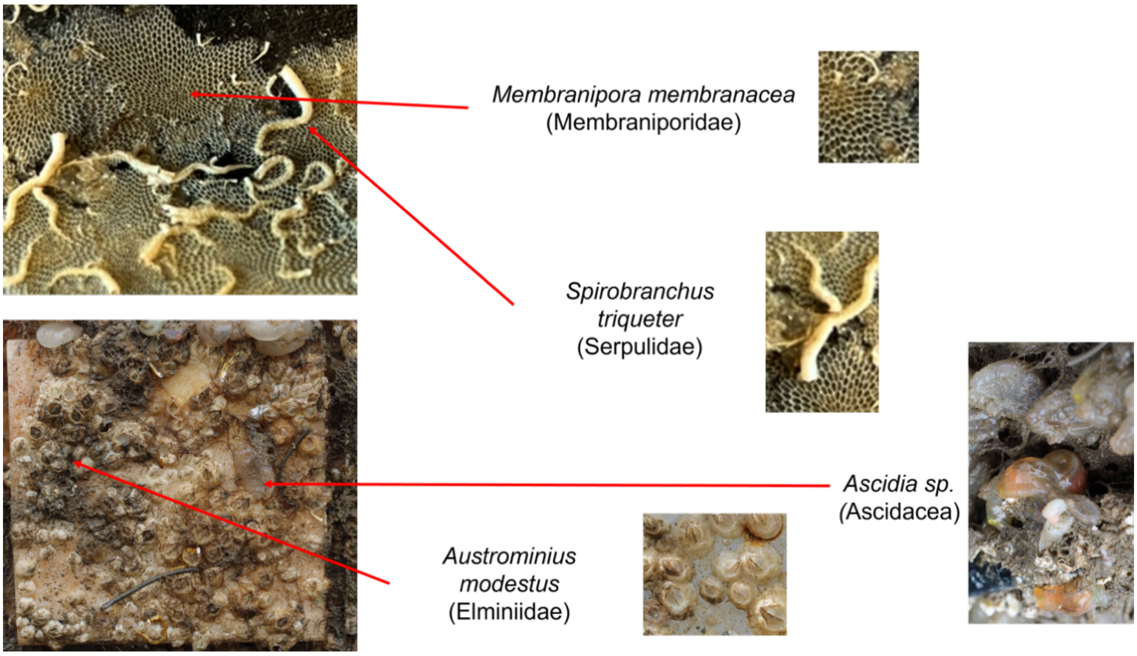

Figure 23: Main macroscopic biofouling organisms identified on PETG panel and fiberglass composite panel after 6 months of exposure.

3.4.2 Imaging and supervised classification results

In view of the results of the supervised classification (Figure 24 and Figure 25), it is clear that the materials showed a very diverse behaviour. In figure 24 it can be seen that in the first 2 months the biofouling, colonisation is very low, hardly any changes can be seen with respect to month 0, however, after 4 months of being submerged coverage of different organisms is evident. In materials such as copper hardly any changes were observed, however, in the rest of the material's hard biofouling (green colour), notably more pronounced in titanium and coverage by slime (red colour) in all the samples was noted. After about 6 months the hard biofouling coverage increased considerably except for copper. Soft biofouling (yellow colour) was notably high on PETG, POM-H and Stainless Steel and low on the POM-C, titanium, and fiberglass samples. However, there was no trace in the copper samples.

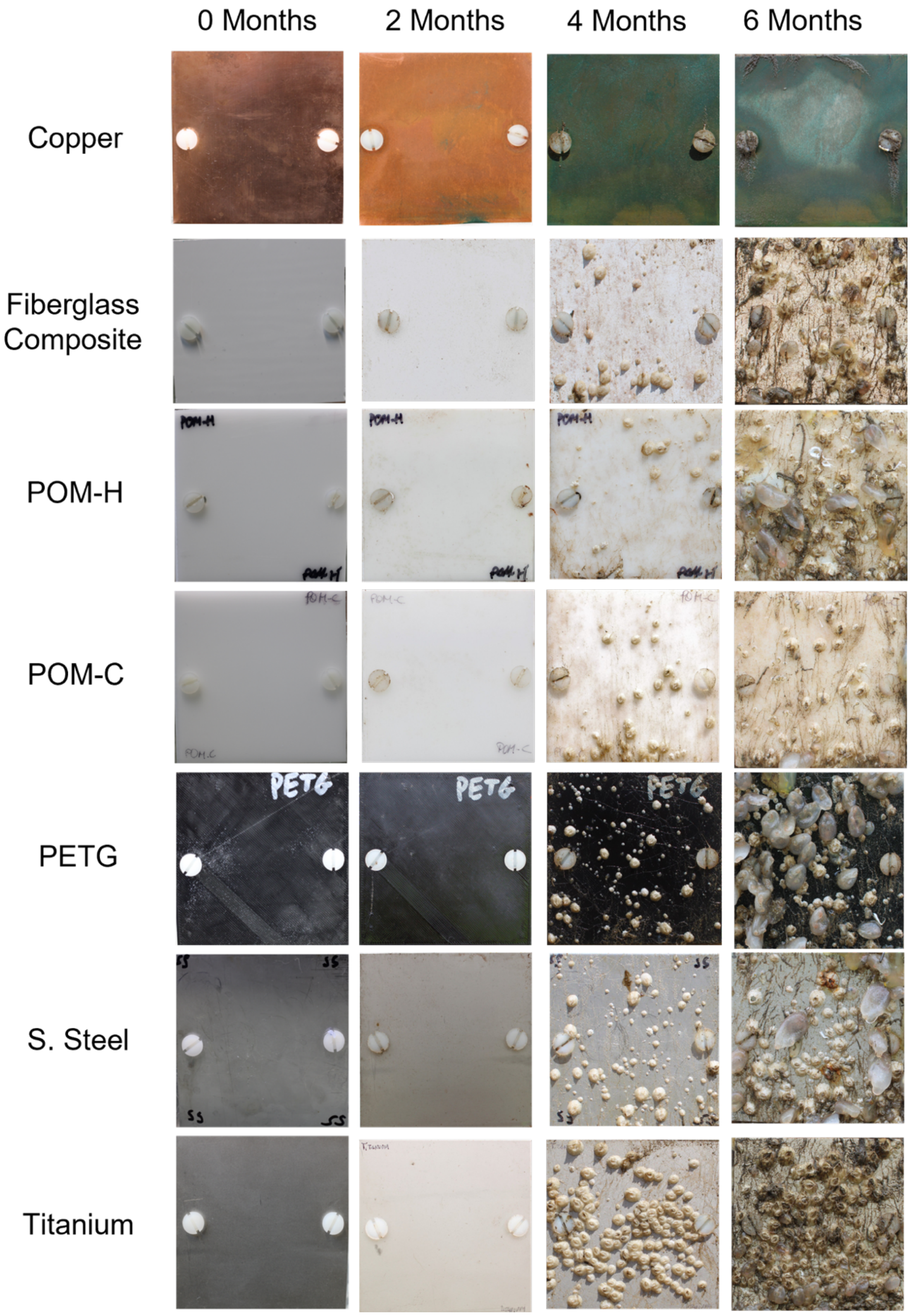

Figure 24: Photographs showing the progression of the biofouling in a period of 6 months on the different panels of the different materials proposed in this study

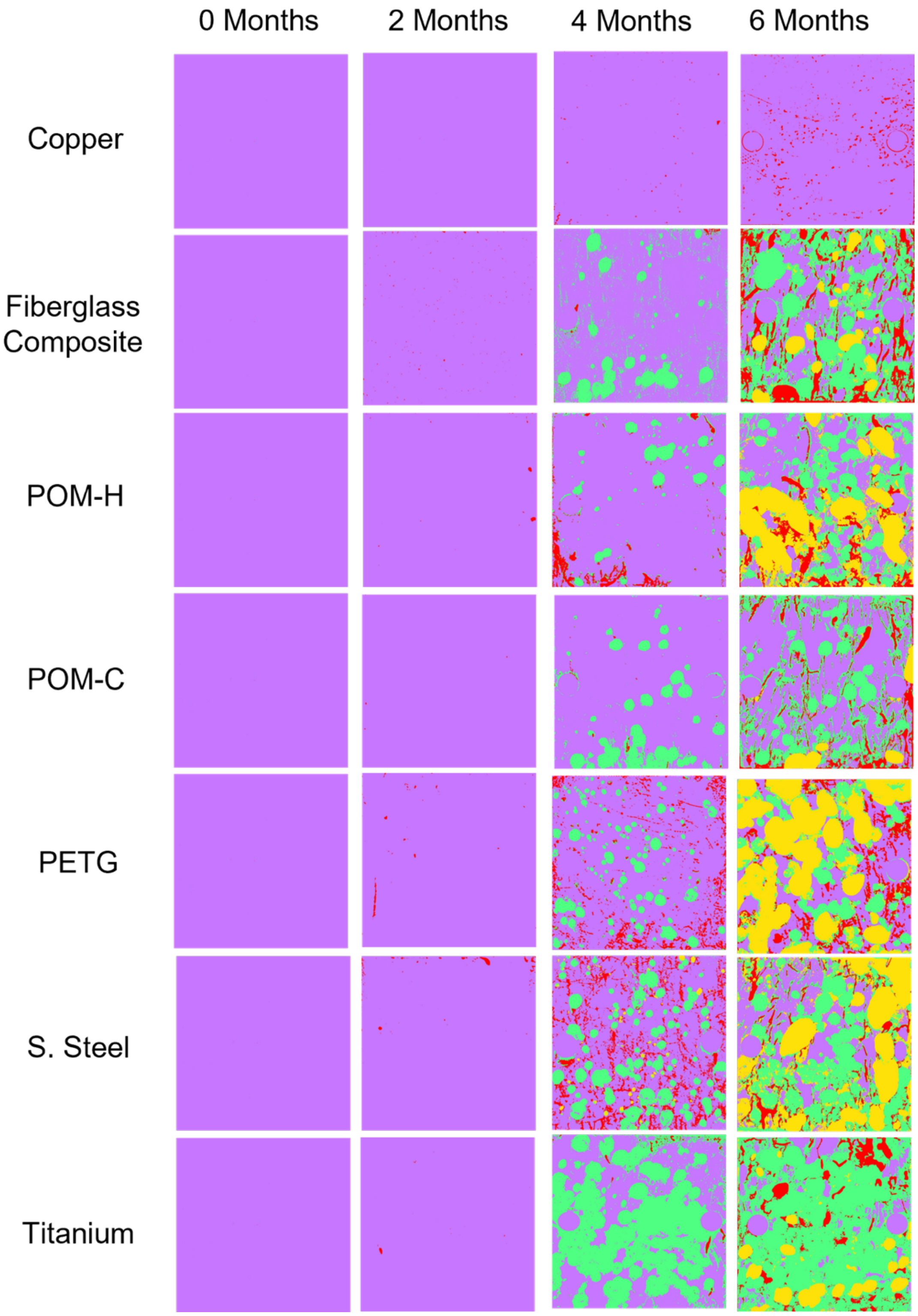

Figure 25: Image segmentation showing the progression of the biofouling in a period of 6 months on the different panels of the different materials proposed in this study. Each colour represented corresponds to a different biofouling group. Purple: clean surface, red: slime, green: hard biofouling, yellow: soft biofouling.

3.4.3 Overview of the progression of the biofouling process on each sample. Sigmoidal growth.

The growth patterns for each of the materials were found to be very diverse, (Table 10). The growth patterns calculated for each of the materials showed a sigmoidal pattern (Figure 26). In all materials the three typical stages of biofouling growth can be clearly identified, a first latency phase in which microscopic colonising organisms such as algae and bacteria adhere and acclimatize to the surfaces, then the exponential growth phase takes place, with the exception of copper. As can be seen in all the materials, the exponential phase begins 90-100 days after the start of the field trial, which coincides with the third month (June). The temperature and the higher number of daylight hours characteristic of the summer season favoured the faster biofouling development rate during this period. The results shown for copper are very different to the rest of the materials due to its toxicity to organisms. High concentrations of copper in water can be harmful to a variety of aquatic organisms, including algae or bacteria [195].

This material can also be toxic to bacteria, but the effect depends on the specific type of bacteria and the concentration of copper in the environment. In general, copper can be effective at killing a wide range of bacteria, including those that are resistant to other antimicrobial agents, such as antibiotics or toxic compounds embedded in antifouling coatings. However, high concentrations of copper can also be harmful to other aquatic organisms, including as we mention before algae, but also some invertebrates like barnacles which makes it an ideal antifouling agent. A sigmoidal growth regression was not observed and only a simple polynomial regression was used to represent the growth of some microscopic organisms included in the slime, which are difficult to observe with a conventional camera used in this investigation.

In the segmentation map form figure 25 and in figure 26 in which is showed the sigmoidal regression for all materials, it can be seen that materials such as titanium showed some settlement for hard fouling such barnacles compared with the other materials. Titanium is not known to be heavily fouled in marine ecosystems. In fact, titanium is a relatively unreactive metal that does not corrode easily in seawater, making it a popular choice for marine applications. Its shows low growth-rate with 0.92. For this reason, it is commonly used in the construction of ships, boats, and offshore platforms. However, while titanium is not toxic to aquatic organisms, it is possible for marine organisms like barnacles to attach to the surface of titanium structures or objects which may explain this behaviour after 4 months of exposure. On the other hand, in the same way as titanium, stainless steel also started to show a significant coverage after 4 months of exposure, however its exponential growth phase was greater than the titanium, 1.26 compared with 0.92. Despite these results stainless steel is not particularly prone to biofouling. In fact, stainless steel is a durable and corrosion-resistant material that is often used in marine environments because of its ability to resist the corrosive effects of seawater same as titanium material. However, it is possible for marine organisms like barnacles to attach to the surface of stainless steel, just as they do with other types of materials like titanium.

Fiberglass growth-rate was found to be 1.06. Fiberglass is a strong and lightweight material that is often used in the construction of boats, as well as in a variety of other applications however its application as an antifouling material is not effective. It is for this reason that fiberglass surfaces must be treated as same as stainless-steel and titanium with antifouling coatings with toxic compound for organisms (i.e., copper, zinc) to prevent the settlement and growth of marine organisms. These coatings contain biocides that are released into the surrounding water and help to prevent the attachment of marine organisms to the surface. Some of these biocides include copper compounds (such as cuprous oxide), zinc compounds, and booster biocides like Irgarol and Diuron. Antifouling coatings are typically applied to the hulls of boats, other watercraft and are even used in the tidal industry to help reduce drag and improve performance and efficiency of the hydrodynamics of a body in water. They can be found used in structures that are submerged in water, such as offshore oil platforms, bridge pilings or tidal turbines. There are a variety of antifouling coatings available, and the most effective ones typically contain a combination of different biocides that are effective against a wide range of marine organisms. However the release of these biocides into the environment can have broader ecological impacts. While effective in deterring fouling organisms, the environmental release of biocides raises concerns about ecotoxicity, bioaccumulation, and non-target effects. Biocides can be harmful to non-fouling marine organisms, leading to disruptions in ecosystems. Additionally, the development of resistance in fouling organisms, as well as regulatory restrictions due to environmental concerns, has prompted ongoing research into alternative, more environmentally friendly antifouling strategies.

PETG (glycol-modified PET) is a type of plastic that is often used for 3D printing and for the manufacture of a variety of products, including packaging, automotive parts, and medical devices. It is a strong, cheap and durable material that is easy to work with and has good chemical resistance. It is sometimes used in sensor developments due to the ease of 3D printing. In this case PETG was used because is had good weather resistance able to withstand UV and moisture. It is also strong and durable for withstanding impact, resistant to harsh chemicals and abrasion. It is also easier to print relative to materials with similar robust properties such as abs and nylon which are prone to warping during the printing process. However, it is not common to use PETG as an antifouling material, as it is not naturally resistant to the attachment and growth of marine organisms such as barnacles, algae, and mussels. PETG samples showed the highest growth-rate of all the materials studied with 2.71. On the other hand, this material is generally considered to be hydrophilic. The wettability of a surface affects the attachment of organisms to it because they can more easily retain water and allow for the formation of a thin film of water between the surface and the organism [135–140]. Rough hydrophilic surfaces can provide more surface area for attachment and can create microenvironments that are more favourable for settlement. Some studies reported the apparent preference of some fouling organisms like *B. amphitrite* for hydrophilic surfaces [141–143]. On the other hand, smooth hydrophobic surfaces, may be less attractive for settlement because they provide less surface area for attachment. However, some authors reported that *B. improvisus* demonstrated an opposite tendency for settling on hydrophobic (low-surface-energy) surfaces [145] and even others highlighted the absence of a correlation between surface wettability and the temporary adhesion strength of *B. amphitrite* cyprids [146].

Materials such as POM-C and POM-H which are hydrophobic, showed a growth-rate for the exponential phase of 0.81 and 0.56 respectively which explains its lower value compared to PETG and are very similar to titanium or stainless-steel numbers. However, in titanium and stainless-steel samples roughness plays an important role. The roughness of a surface can affect the adhesion of biofouling organisms because influences the surface wettability as the air pocket affords a larger contact angle θ, which relates to wettability [196]. Rougher surfaces tend to have a greater surface area, which can provide more attachment points for biofouling organisms because increases the contact points. However, smoother surfaces like titanium and stainless-steel may be more difficult for biofouling organisms to adhere to, due to the lack of surface roughness and the presence of a more uniform and continuous surface. However, although calculating the roughness and wettability of panels can be a valuable aspect of assessing their performance, this parameter is only one of many factors that influence anti-incrustation properties. Bearing in mind that measuring roughness can be resource intensive, requiring specialised equipment and expertise, but above all bearing in mind that the main interest was in understanding biological fouling rather than the physical characteristics of the surface, the statements made in this chapter are only based on previous studies and hypotheses.

The roughness of titanium can vary depending on the specific grade and treatment of the material. In general, titanium has a relatively smooth surface finish, with an Ra value in the range of 0.1 to 0.5 µm and stainless steel and 0.5 to 3 µm which make them a very good anti-adhesion material. However, manufacturers combine the use of these materials with antifouling coatings of paints to provide them an extra protection layer.

.

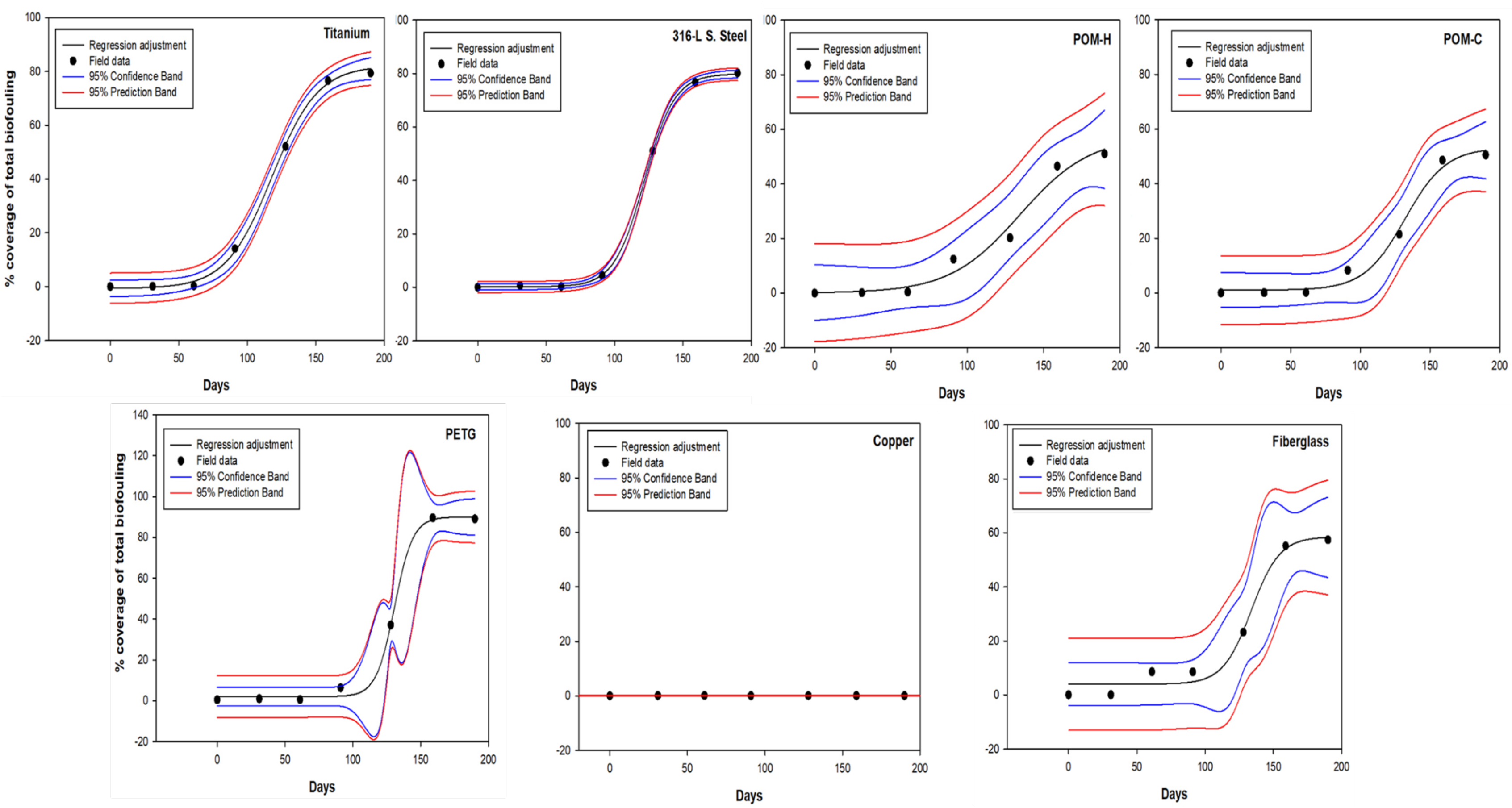

Figure 26: Representation of biofouling growth for each panel of each material over a 6-month period. Each black dot represents the average of the percentage of the biofouling covered from field data done in triplicate (n=3).

Table 10: Sigmoidal growth regression over the 6 months duration of the study for each material. Linear regression to calculate the growth rate in the exponential phase for each material.

Material	Sigmoidal growth regression for 6 months	Linear regression for the exponential growth phase	Growth-rate for the exponential phase
Fiberglass	Y = 4.01+54.55(1+e^(−((X−133.81)/(−10.41)))	Y = -110.51+1.0595*X	1.06
Titanium	Y = -0.68+82.84(1+e^(−((X−118)/(−16.78)))	Y = -68.51+0.92*X	0.92
Stainless-steel	Y = 0.15+79.71(1+e^(−((X−121.86)/(11.71)))	Y = -114.85+1.26*X	1.26
POM-C	Y = 1.03+52.16(1+e^(−((X−132.07)/(14.74)))	Y = -81.09+0.81*X	0.81
POM-H	Y = 0.03+53.35(1+e^(−((X−134.51)/(23.09))	Y = -46.45+0.56*X	0.56
PETG	Y = 2.08+87.97(1+e^(−((X−130.76)/(6.79))	Y = -308.34+2.71*X	2.71
Copper	_	Y = 0.10	0

3.4.4 Fouling Rating

Taking the observations after the 6-month deployment, a fouling rating was calculated so that the different materials could be evaluated according to the different biofouling groups previously identified (slime, soft biofouling and hard biofouling). The results obtained reveal and confirmed the data obtained in the previous section, which showed the development of biofouling throughout the study. In table 11 and figure 27 where the results are shown, it can be seen that results are in line with what is shown in the previous section. Copper shows the best results with an excellent antifouling rate which is explained by a high FR (99.8) as it was hardly covered with any type of biofouling except slime. This slime, as mentioned above, is usually composed of algae, bacteria, debris and extracellular polymeric substances (EPS). These can be found on this type of material because although copper generates a toxic environment for most organisms [197]. However, for the rest of the materials we found very similar results at the end of the 6-month deployment. All the materials performed between the weak and poor antifouling grade. POM-H showed slightly higher values with a weak antifouling rate (FR = 52.9) as same as the 316L-stainless steel that also showed a weak grade (FR= 52.6). These samples show very similar values which means that both a smooth rough surface and a hydrophobic surface provide a high FR although it should be noted that the deviation between triplicates for the hard biofouling group was considerably high. However, titanium, POM-C and the fibreglass showed a poor antifouling grade (FR = 37.9) due to barnacles’ coverage which was one of the highest in the entire study. The material with the lowest antifouling grade was PETG (FR = 22.4). This is explained by the large percentage of area covered by both hard biofoulings, i.e., mainly barnacles, but also the high percentage of area covered by soft biofouling, mainly tunicates. This also coincides with its growth rate which was the highest in the whole study ranking it at the bottom of the antifouling materials of this study.

Table 11: Percentages of surface area covered by biofouling for each group and calculated Fouling-rate. Each percentage represent an average of a triplicate plus its standard deviation.

Materials	Slime	Soft Biofouling	Hard biofouling	Fouling Rating	AF-Grade
316L-Stainless Steel	4.77 ± 1.98 %	52.85 ± 22.10 %	18.42 ± 15.88 %	52.6	Weak
Copper	1.48 ± 0.83 %	0 %	0 %	99.8	Excellent
Polyoxymethylene POM-C	9.05 ± 0.80 %	5.88 ± 2.27 %	33.67 ± 29.07 %	37.9	Poor
Polyoxymethylene POM-H	7.38 ± 1.89 %	15.69 ± 14.01 %	23.42 ± 3.85 %	52.9	Weak
Titanium	8.62 ± 5.62 %	12.32 ± 3.65 %	42.31 ± 6.90 %	37.9	Poor
PETG	9.51 ± 0.88 %	27.05 ± 5.64 %	53.06 ± 10.89 %	22.4	Bad
Fiberglass Composite	19.18 ± 3.63 %	6.17 ± 3.25 %	37.90 ± 7.39 %	37.9	Poor

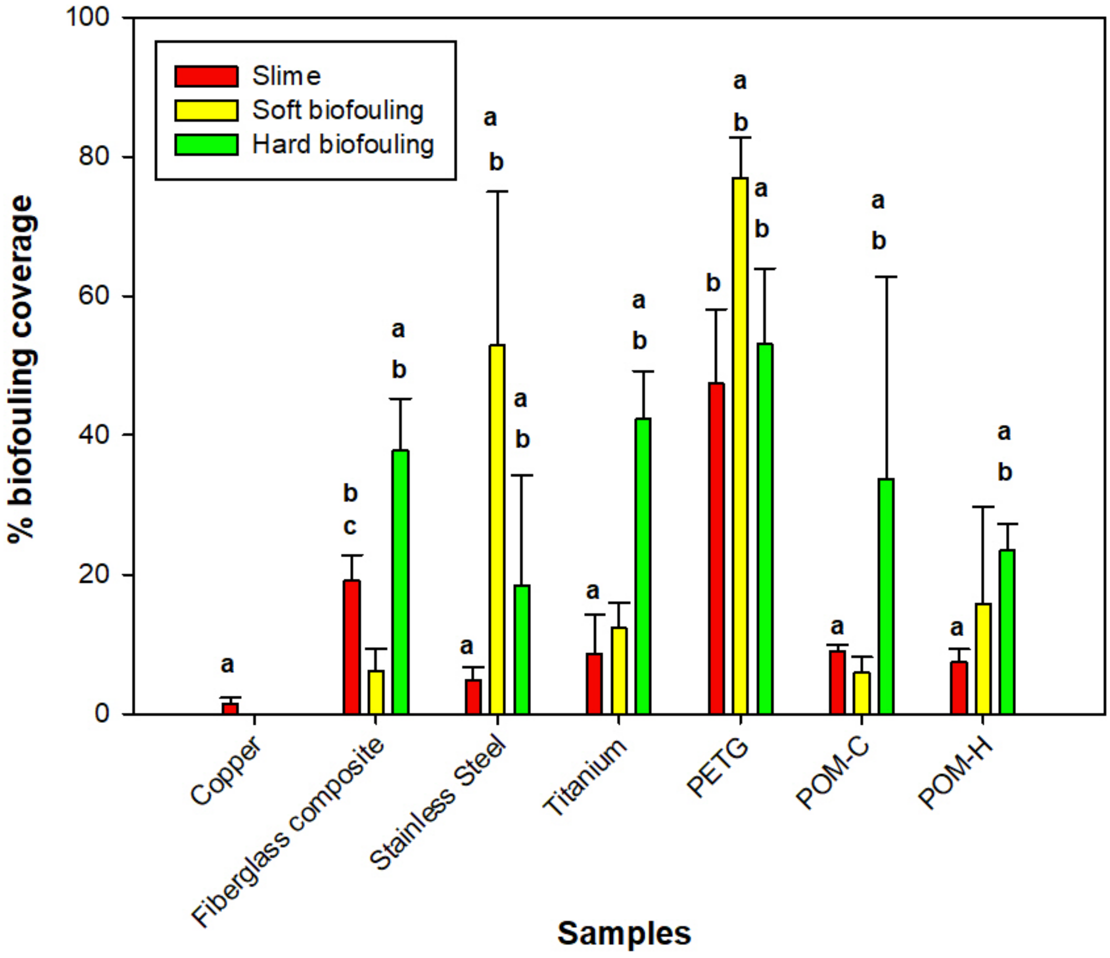

Figure 27: Percentage of biofouling coverage on deployed marine industry manufacturing materials in the marine environment after a period of 6 months deployed in Dublin Bay. Each bar plot is the average of a triplicate with its standard deviation.

3.4.5 Statistical analysis

Statistical tests were performed using SigmaPlot software Version 11 Build 11.0.0.77. In all studies the analyses were done in triplicate. Subsequently, means and standard deviations were calculated. A comparison of many groups was made using the One Way Anova (One Way Analysis of Variance) method to establish whether or not there were significant differences between the samples in each different class of this study (slime: Table 13; soft biofouling: Table 15; hard biofouling: Table 17).

In all analyses the power of performed test alpha was 0.050. Subsequently, multiple comparisons were also made between all samples when treatments were significantly different (≤ 0.001). The test chosen for this was the Holm-Sidak test. The Holm-Sidak test can be used for both pairwise comparisons and comparisons versus a control group. It is more powerful than the Turkey and Bonferroni test and is recommended as the first line procedure for most multiple comparison testing.

One Way Analysis of Variance for slime, soft biofouling and hard biofouling % coverage was performed separately. The differences in the mean values among the treatment groups were greater than would be expected by chance; there is a statistically significant difference for every single group studied.

Table 12: One Way Analysis of Variance for slime % coverage. The differences in the mean values among the treatment groups are greater than would be expected by chance; there is a statistically significant difference (P = <0.001). SEM= Standard Error of the mean; DF= Degrees of freedom; SS= The sum of squares due to the source; MS= The mean sum of squares due to the source; F= variation between sample means / variation within the samples; P= Probability that the null hypothesis is true.

Power of performed test with alpha = 0.050

Group Name	**N**	**Missing**	**Mean**	**Std Dev**	**(SEM)**
Copper	3	0	1.483	0.83	0.479
Fiberglass Composite	3	0	19.183	3.627	2.094
Stainless Steel	3	0	4.77	1.982	1.144
Titanium	3	0	8.617	5.622	3.246
PETG	3	0	47.467	10.623	6.133
POM-C	3	0	9.047	0.798	0.461
POM-H	3	0	7.377	1.887	1.09
Source of Variation	**DF**	**SS**	**MS**	**F**	**P**
Between Groups	6	539,541	89,923	11,582	<0,001
Residual	14	108,701	7,764		
Total	20	648,242			

Table 13: All Pairwise Multiple Comparison Procedures for slime % coverage (Holm-Sidak method). Overall significance level = 0.05.

Comparison	Diff of Means	t	Unadjusted P	Critical Level	Significant?
Fiberglass vs. Copper	17.7	7.78	<0.001	0.002	Yes
Fiberglass vs. 316L S.Steel	14.413	6.335	<0.001	0.003	Yes
Fiberglass vs. POM-H	11.807	5.189	<0.001	0.003	Yes
Fiberglass vs. Titanium	10.567	4.644	<0.001	0.003	Yes
Fiberglass vs. POM-C	10.137	4.455	<0.001	0.003	Yes
Fiberglass vs. PETG	9.67	4.25	<0.001	0.003	Yes
PETG vs. Copper	8.03	3.529	0.003	0.003	Yes
POM-C vs. Copper	7.563	3.324	0.005	0.004	No
Titanium vs. Copper	7.133	3.135	0.007	0.004	No
POM-H vs. Copper	5.893	2.59	0.021	0.004	No
PETG vs. 316L S.Steel	4.743	2.085	0.056	0.005	No
POM-C vs. 316L S.Steel	4.277	1.88	0.081	0.005	No
Titanium vs. 316L S.Steel	3.847	1.691	0.113	0.006	No
316L S.Steel vs. Copper	3.287	1.445	0.171	0.006	No
POM-H vs. 316L S.Steel	2.607	1.146	0.271	0.007	No
PETG vs. POM-H	2.137	0.939	0.364	0.009	No
POM-C vs. POM-H	1.67	0.734	0.475	0.01	No

Titanium vs. POM-H	1.24	0.545	0.594	0.013	No
PETG vs. Titanium	0.897	0.394	0.699	0.017	No
PETG vs. POM-C	0.467	0.205	0.84	0.025	No
POM-C vs. Titanium	0.43	0.189	0.853	0.05	No

Table 14: One Way Analysis of Variance for soft biofouling % coverage. The differences in the mean values among the treatment groups are greater than would be expected by chance; there is a statistically significant difference (P = <0.001). SEM= Standard Error of the mean; DF= Degrees of freedom; SS= The sum of squares due to the source; MS= The mean sum of squares due to the source; F= variation between sample means / variation within the samples; P= Probability that the null hypothesis is true.

Power of performed test with alpha = 0.050

Group Name	N	Missing	Mean	Std Dev	SEM
Copper	3	0	0	0	0
Fiberglass Composite	3	0	6.17	3.25	1.877
Stainless Steel	3	0	52.85	22.098	12.758
Titanium	3	0	12.323	3.653	2.109
PETG	3	0	76.977	5.8	3.349
POM-C	3	0	5.883	2.274	1.313
POM-H	3	0	15.687	14.014	8.091
Source of Variation	**DF**	**SS**	**MS**	**F**	**P**
Between Groups	6	5819.268	969.878	9.106	<0.001
Residual	14	1491.099	106.507		
Total	20	7310.367			

Table 15: All Pairwise Multiple Comparison Procedures for soft biofouling % coverage group (Holm-Sidak method). Overall significance level = 0.05

Comparison	Diff of Means	t	Unadjusted P	Critical Level	Significant?
Stainless Steel vs. Copper	52.85	6.272	<0.001	0.002	Yes
Stainless Steel vs. POM-C	46.967	5.574	<0.001	0.003	Yes
Stainless Steel vs. Fiberglass	46.68	5.54	<0.001	0.003	Yes
Stainless Steel vs. Titanium	40.527	4.809	<0.001	0.003	Yes
Stainless Steel vs. POM-H	37.163	4.41	<0.001	0.003	Yes
PETG vs. Copper	27.06	3.211	0.006	0.003	No
Stainless Steel vs. PETG	25.79	3.061	0.008	0.003	No
PETG vs. POM-C	21.177	2.513	0.025	0.004	No
PETG vs. Fiberglass	20.89	2.479	0.027	0.004	No
POM-H vs. Copper	15.687	1.862	0.084	0.004	No
PETG vs. Titanium	14.737	1.749	0.102	0.005	No
Titanium vs. Copper	12.323	1.462	0.166	0.005	No
PETG vs. POM-H	11.373	1.35	0.199	0.006	No
POM-H vs. POM-C	9.803	1.163	0.264	0.006	No
POM-H vs. Fiberglass	9.517	1.129	0.278	0.007	No
Titanium vs. POM-C	6.44	0.764	0.457	0.009	No
Fiberglass vs. Copper	6.17	0.732	0.476	0.01	No

Table 16: One Way Analysis of Variance for hard biofouling % coverage. The differences in the mean values among the treatment groups are greater than would be expected by chance; there is a statistically significant difference (P = 0.007). SEM= Standard Error of the mean; DF= Degrees of freedom; SS= The sum of squares due to the source; MS= The mean sum of squares due to the source; F= variation between sample means / variation within the samples; P= Probability that the null hypothesis is true.

Power of performed test with alpha = 0.050

Group Name	N	Missing	Mean	Std Dev	SEM
Copper	3	0	0	0	0
Fiber-Glass Composite	3	0	37.897	7.385	4.264
Stainless Steel	3	0	18.417	15.881	9.169
Titanium	3	0	42.31	6.897	3.982
PETG	3	0	53.063	10.888	6.286
POM-C	3	0	33.667	29.071	16.784
POM-H	3	0	23.417	3.854	2.225
Source of Variation	**DF**	**SS**	**MS**	**F**	**P**
Between Groups	6	5.509.659	918.276	4.823	0.007
Residual	14	2.665.623	190.402		
Total	20	8.175.282			

Table 17: All Pairwise Multiple Comparison Procedures for hard biofouling % coverage group (Holm-Sidak method). Overall significance level = 0.05

Comparison	Diff of Means	t	Unadjusted P	Critical Level	Significant?
PETG vs. Copper	53	5	<0.001	0.002	Yes
Titanium vs. Copper	42	4	0.002	0.003	Yes
Fiber-Glass Composite vs. Copper	38	3	0.005	0.003	No
PETG vs. Stainless Steel	35	3	0.008	0.003	No
POM-C vs. Copper	34	3	0.01	0.003	No
PETG vs. POM-H	30	3	0.02	0.003	No
Titanium vs. Stainless Steel	24	2	0.052	0.003	No
POM-H vs. Copper	23	2	0.057	0.004	No
Fiber-Glass Composite vs. Stainless Steel	19	2	0.106	0.004	No
PETG vs. POM-C	19	2	0.107	0.004	No
Titanium vs. POM-H	19	2	0.116	0.005	No
Stainless Steel vs. Copper	18	2	0.124	0.005	No
POM-C vs. Stainless Steel	15	1	0.197	0.006	No
PETG vs. Fiber-Glass Composite	15	1	0.2	0.006	No
Fiber-Glass Composite vs. POM-H	14	1	0.22	0.007	No
PETG vs. Titanium	11	0.954	0.356	0.009	No
POM-C vs. POM-H	10	0.91	0.378	0.01	No

3.5 Conclusion

This chapter demonstrates that, using a low-cost conventional camera and standard classification routines available in many software packages, it is possible to perform biofouling classification and benchmarking different materials used in industry in a more automated way and with less variability as subjectivity of observations would be eliminated. The technology required to implement this approach is well developed. Combining these simple observational elements with computational neural networks for image classification is a major step forward in efforts to quickly and easily classify biofouling without the intervention of human specialists. For example, the images could be captured by a diver or a remote operated vehicle (ROV), which are used for the inspection of ship hulls and submerged structures in general. The supervised classification approach is a tool that allows the incorporation of new classes into the analysis scheme as they are identified, potentially increasing the number of classes and therefore the taxonomic specificity of the analysis. This in turn allows us to assess the impact, degree of biofouling settling and physical performance of different materials over extended periods of time, which can be useful for industry in making material selection decisions in their deployments. For example, on ships there are areas of limited access such as propellers where biofouling could have a major hydrodynamic and structural impact due to cavitation, not to mention the impact on 20 m blades on a tidal turbine. In these hydrodynamically crucial areas, it is very important to control biofouling to prevent maintenance cost overruns. It is therefore crucial to develop methods that reliably and accurately assess fouling in key areas.

In view of the results obtained in this work, we can conclude that copper is one of the best materials to combat biofouling and that it can be used by the industry as a strategy against this problem that can be incorporated into instruments such as sheaths or meshes. Materials such as stainless steel or titanium are the two most common materials that have been used in the construction of sensors (stainless steel mainly for freshwater ecosystems and titanium for saltwater ecosystems). However, the manufacturing and machining costs of these are usually high, which makes the price of the instruments significantly more expensive, so alternatives such as the POM-C or the POM-H can be a good solution to this problem for the development of cheaper sensors due to that they are easily to work with, and the antifouling advantages are not very different from those of titanium or 316L-stainless steel. The fiberglass composite commonly used in the manufacture of turbine blades and ship hulls showed poor performance and also its difficult machining by forming extrusion molds and the superimposition in multiple layers of the fiberglass itself makes it difficult to machine. and unlikely material for other than light duty marine applications. Finally, PETG, although its use is recommended for making small-scale prototypes since it can be used in 3D printing, its use at a commercial level is not recommended if effective protection against biofouling is desired, so its use can it be recommended only if coatings and/or paints that reduce the colonization of biofouling are used on this material.

Chapter 4 :

Rapid Quantification of Biofouling using machine learning approach on different coatings and bioinspired textures using selected fouling organisms under laboratory conditions

4.1 Introduction

Marine biofouling is a serious problem for maritime industries and other marine activities worldwide [128,165,198], caused by the accumulation of microorganisms, plants, and marine animals on submerged surfaces. Antifouling coatings are usually applied to these surfaces to prevent or control biofouling. However, traditional coatings containing harmful substances such as tributyltin (TIN) or cuprous oxide (CuO_2) with organic biocides can have harmful effects on non-target organisms and the environment [199,200]. Therefore, efforts have been made to develop environment-friendly materials such as low surface energy elastomers [201–203], bioinspired engineered topographies [204,205], amphiphilic nanostructured coatings [206–209] , enzymes [210,211], and antifoulants made of natural products [212,213]

Antifouling coatings are an essential technology used in various industries to protect surfaces from the unwanted attachment of marine organisms, such as algae, barnacles, and molluscs. These organisms can cause severe damage to ships, offshore structures, and other marine equipment, resulting in increased maintenance costs, reduced efficiency, and shortened lifespan. Antifouling coatings work by preventing the settlement and growth of these organisms on the coated surface, reducing the need for frequent cleaning, and ensuring the smooth operation of marine equipment. The development of effective antifouling coatings has been a major focus of research and development in the marine industry, with new technologies continually being developed to address the challenges posed by marine fouling.

Coatings for marine fouling are very diverse and there are several types of antifouling coatings available, including biocidal coatings, which contain chemicals that kill or inhibit the growth of fouling organisms, and physical/mechanical coatings, which create a difficult surface for organisms to adhere to. Biocidal coatings are generally effective in preventing biofouling, but can have negative impacts on the environment, including the potential to harm unwanted organisms and contribute to the development of antibiotic resistance in bacteria.

Physical/mechanical coatings or engineered antifouling topographies are generally considered more environmentally friendly but may be less effective in preventing biofouling in some cases like polyurethane-based coatings.

However, in recent years, there has been a growing interest in developing more environmentally friendly antifouling coatings that are less toxic and more biodegradable. These coatings can be based on natural materials such as plant extracts or nanoparticles and can be less harmful to unwanted organisms. Some examples are silicon dioxide (SiO_2) coatings.

Non-biocidal coatings to prevent biofouling may be based on physical or mechanical properties of the coating material. For example, a coating with a smooth, slippery surface may be less attractive to fouling organisms than a rough, porous surface. Similarly, a coating with a high surface energy may be less prone to fouling.

4.1.1 Polyurethane-based coatings

Polyurethane-based coatings are a type of coating used in the prevention of biofouling. They can be used as physical/mechanical coatings, as their surface is smooth and resistant to the adhesion of fouling organisms. Polyurethane is a tough and durable material, and polyurethane coatings can be applied to a variety of surfaces, including metals, plastics and wood. In addition, they can also be modified with additives to improve their resistance to biofouling and corrosion.

However, it is important to note that some polyurethane coatings may contain toxic chemicals that can have a negative impact on the environment. Therefore, it is important to select and use polyurethane coatings that are environmentally friendly and do not harm unwanted organisms.

4.1.2 Silicon dioxide nanoparticles-based coatings

Silicon dioxide (SiO_2) based coatings are a type of antifouling coating that has gained popularity due to their non-toxic and environmentally friendly properties. These coatings use nanoparticles of silica, which have a high surface area and a negative charge, to create a surface that is inhospitable to marine organisms. The negative charge of the silica particles repels the negatively charged bacteria and algae, preventing them from attaching to the surface.

SiO_2-based coatings have several advantages over traditional antifouling coatings. They do not contain toxic biocides that can harm marine life and are resistant to fouling for a longer period, reducing the need for frequent maintenance. Moreover, they have excellent mechanical and chemical properties, including resistance to abrasion, chemicals, and UV radiation, making them suitable for a wide range of applications.

The effectiveness of SiO_2-based coatings has been demonstrated in various studies, where they have shown superior antifouling performance compared to other coatings. These coatings have been used in the marine industry for applications such as hull coatings, offshore structures, and underwater sensors.

Despite their advantages, SiO_2-based coatings also face some challenges. One of the main challenges is their high production cost, which limits their widespread adoption. Another challenge is their durability in harsh marine environments, where they can degrade over time, reducing their effectiveness. Researchers continue to work on improving the durability and cost-effectiveness of these coatings to overcome these challenges and make them more widely accessible for the marine industry.

4.1.3 Bioinspired surfaces

Bioinspired textures are a promising eco-friendly solution to reduce biofouling in various marine applications. These textures imitate the physical features of marine organisms that have evolved to resist fouling, such as sharks, dolphins, and whales [214]

Sharks, for example, have dermal denticles that are arranged in a specific pattern on their skin, which reduces drag and resists the attachment of marine organisms. Researchers have mimicked this texture in the design of antifouling coatings and demonstrated their effectiveness in reducing biofouling [12].

Another example is the texture of the lotus leaf, which has a surface that repels water droplets, preventing the attachment of dirt and bacteria. Researchers have developed coatings that mimic this texture, which have shown promising results in reducing biofouling in marine environments.

Bioinspired textures offer several advantages over traditional antifouling coatings. Firstly, they are non-toxic and environmentally friendly, as they do not rely on toxic chemicals to prevent fouling. This aspect ensures the protection of marine ecosystems and reduces potential harm to aquatic life. Secondly, the application of bioinspired textures involves a low-energy, environmentally friendly process. This not only reduces energy consumption but also minimizes the carbon footprint associated with the manufacturing and application of the coatings. As a result, bioinspired textures are both cost-effective and sustainable, aligning with the growing global emphasis on environmentally conscious solutions. [4,12,43,215–217].

Despite their advantages, bioinspired textures also face challenges in terms of durability and scalability. Designing surfaces that can effectively regulate cellular behaviour in natural environments is a difficult task due to the diverse array of cell types that exist in environments like marine waters. These environments contain many different variations in cell size, shape, and adhesion strategies, making it challenging to develop a surface that can accommodate all of them [218]. However, bioinspired approaches offer a promising avenue for the development of new antifouling technologies. By studying naturally occurring non-fouling species and identifying common features, scientists can gain valuable insights into how to replicate or modify these features to create natural antifouling mechanisms for commercial use [219]. Over billions of years, nature has evolved effective solutions to the fouling problem, and by drawing inspiration from these solutions, we can develop more effective antifouling strategies.

Researchers have investigated the antifouling properties of the natural surfaces like the Brill fish scale, *Scophthalmus rhombus* (Figure 28). Using the latest microfabrication techniques, an artificial surface inspired by the natural surface of S. rhombus was created and tested under controlled static and dynamic conditions in the laboratory and in the field (see chapter 6). The results of the study demonstrate that the surface topography can have both positive and negative effects on cell behaviour, as evidenced by experiments conducted on *Nitzschia ovalis*. This research provides a roadmap for the future design of non-toxic antifouling materials, based on the insights gained from studying the natural antifouling properties of the Brill fish scale.

The cross section was replaced with a rectangular design for increased mechanical stiffness, replacing the sharp edge of the ridge with a flat surface measuring 10 μm in width. The length was increased to 85 μm to reduce machining requirements.

Figure 28: Electron microscopic view of the Brill fish scale structure

4.1.4 Laboratory-scale biofouling analysis

Model organisms, such as diatoms, can be instrumental in studying biofouling and adhesion on various surfaces in the laboratory. Diatoms are unicellular photosynthetic organisms that can attach to different substrates, and they are commonly used as model organisms due to their small size and ease of cultivation under laboratory conditions.

In the laboratory, researchers can study the adhesion of diatoms to different surfaces, including coatings and textures, by observing the percentage coverage of diatoms on these surfaces. By quantifying the percentage coverage of diatoms, researchers can determine the efficacy of different antifouling coatings and textures in preventing diatom attachment and biofouling.

In this study the possibility of using two different diatom species was considered (*Nitzschia ovalis* and *Amphora coffeaeformis).* However, *Nitzschia ovalis* was selected over *Amphora coffeaformis* because it was more easily observed under the microscope and grew faster than *Amphora coffeaeformis* under laboratory conditions.

Nitzschia ovalis is a specie of diatom, a type of microalga that is commonly found in marine and freshwater environments (Figure 29 B). It is a common biofouling organism that can attach to surfaces and form colonies in aquatic environments.

Nitzschia ovalis is often used as a model organism in laboratory studies of biofouling and other aquatic processes. It is relatively easy to culture and maintain in the laboratory, and it has a number of characteristics that make it suitable for experimental studies. For example, it has a simple cellular structure that is easy to observe and manipulate, and it is capable of rapid growth and reproduction.

In biofouling studies, *Nitzschia ovalis* can be used to investigate the factors that influence the attachment and growth of fouling organisms on different surfaces. It can also be used to test the effectiveness of different methods for preventing or reducing biofouling, such as antifouling coatings and biocides.

Nitzschia ovalis is a useful model organism for laboratory studies of biofouling and other aquatic processes, and it has contributed to our understanding of these phenomena and the development of effective strategies for preventing and controlling biofouling and because of this we have chosen this organism for our studies.

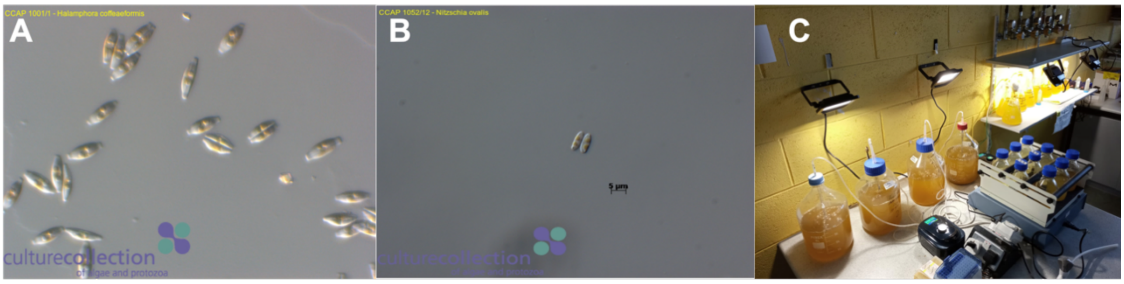

Figure 29: Microscopy images taken from the Culture Collection of Algae and Protozoa; *Amphora coffeaeformis*, (A) (left) and *Nitzschia ovalis*, (B) (right). (C) The image on the far right is of the cultures growing under laboratory conditions in a 'batch' growth system. (A) and (B) Image sourced from the Culture Collection of Algae and Protozoa, SAMS, Scotland, U.K

4.2 Aims and objectives

The main objective of this chapter is to explore how topographical features inspired by the scale of the common brill fish, *Scophthalmus rhombus* and different coatings, behave under laboratory conditions using benthic organisms as a model.

This work aims to achieve the following objectives:

Evaluate the surface topography of the Brill fish, *Scophthalmus rhombus*, for its potential in preventing fouling in laboratory using a model organism that replicates early stages of biofouling.

Evaluate the surface of different coatings for its potential in preventing fouling in laboratory using a model organism that replicates early stages of biofouling.

Generate a database of images in order to train an AI to learn to recognize microfouling patterns that will be used in chapter 6.

4.3 Materials and methods

4.3.1 Microtextures fabrication

The microtextures were fabricated and designed by Dr. Chloe Richards, DCU and were derived from measurements of real *S. rhombus* scales (Figure 30 and Table18) [42,220]

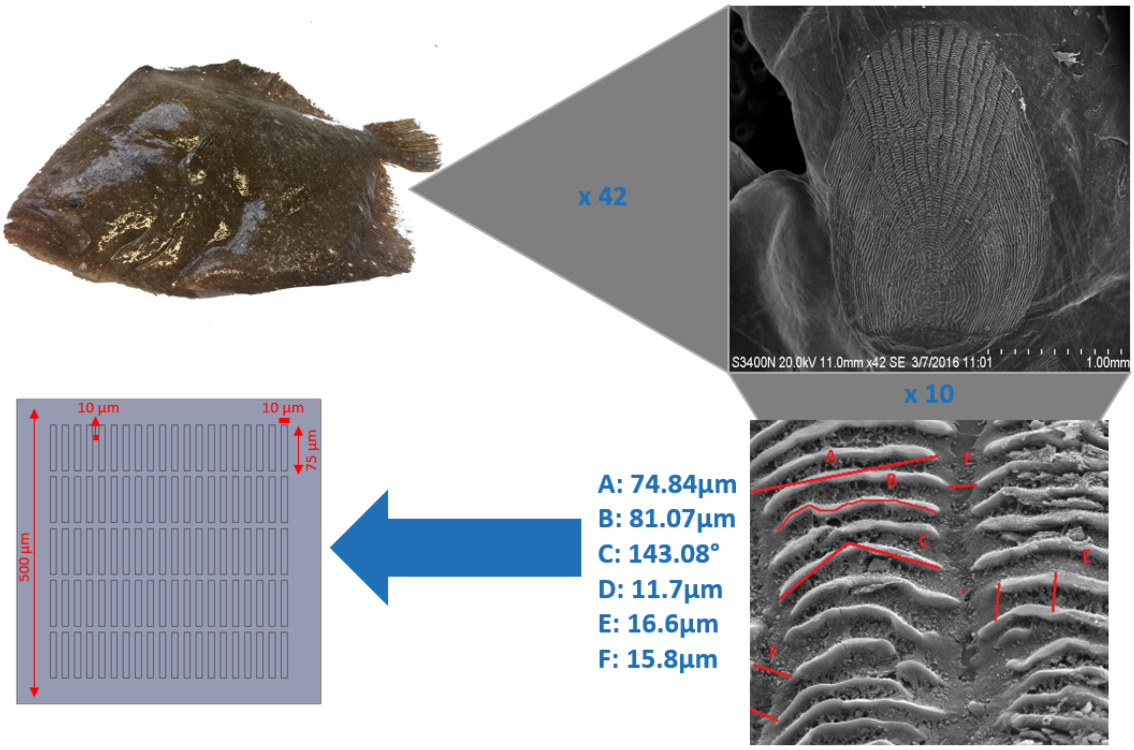

Figure 30: Simplified process of transforming Brill fish scales into a bio-inspired artificial design

Using SolidWorks, several designs were created and fabricated using the Nanoscribe Photonic Professional GT 3-D printing system, as shown in Figure 2.16. This 3D printing system utilizes a 150 mW femtosecond solid-state laser operating at a wavelength of 780 nm, and a x25 Dip-in laser lithography (Dill) objective with a NA of 0.8 was employed to focus the laser. The negative-tone photoresist IP-S was used in the process, and the DeScribe software provided by Nanoscribe was utilized to convert the writing files from SolidWorks 2017 STL files to files compatible with Nanowrite software.

Table 18: Summary of the bioinspired textures analysed, their characteristics and their 3D design.

Name	Description	3D Model
A1	Raised Bar Array with sharpened edges and 10 µm spacing	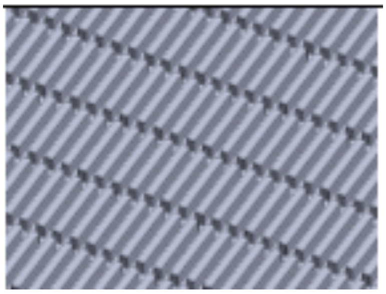
A2	Raised Bar Array with filleted/rounded edges and 10 µm spacing	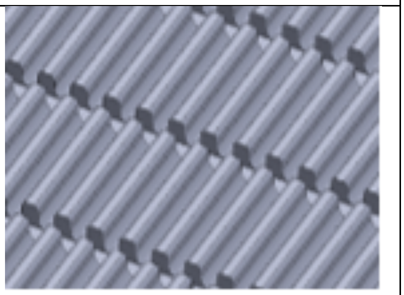
A3	Recessed Cavity Array with sharpened edges and 10 µm spacing	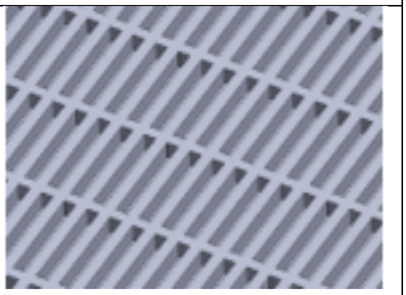

The direct laser writing process employed by this printer involves deflecting a laser beam into a photosensitive material using alternating X and Y laser scanning directions to form polymer structures. To remove any uncured photoresist, the structures were placed in a solution of PGMEA (Propylene glycol monomethyl ether acetate, >99.5%) for 30 minutes, followed by washing with Novec 7000 engineering fluid (methyl perfluoro propyl ether, Sigma, Ireland).

For this study, 3 textures mounted on Indium tin oxide-coated glass (ITO) were selected and compared against two control groups, one with smooth-flat texture, and the second control with no photoresist material only the ITO-coated glass surface (Table 18).

4.3.2 Coatings fabrication

The coatings were synthesized by Funditec company (Madrid, Spain) as part of the European Project Nemmo collaboration (available here: http://nemmo.eu/).

4.3.2.1 Silica nanoparticles synthesis

Sol-gel technology is a commonly used method for synthesizing silica nanoparticles due to its advantages:

1) It does not require expensive equipment,

2) It provides highly stable colloidal dispersions,

3) It uses mild reaction conditions.

To synthesize silica nanoparticles sol-gel alkoxide route was used. This route allows precise control over the microstructure of the material by regulating the relative rates of hydrolysis and condensation reactions of the precursors. Under basic conditions, small and highly branched agglomerates form a colloidal sol that can be used to prepare particles.

Silicon alkoxide precursor used was tetraethyl ortho silicate (TEOS) $Si(OR)_4$ and the functional organic silane used was 3-(trimethoxysilyl)-propyloctadecyldimethyl ammonium chloride (QAS). The QAS provides biocide properties for a long time without leaching of the agent, as its organic group is covalently linked to the inorganic network via a non-hydrolysable C-Si bond.

4.3.2.2 Polyurethanes-based coatings synthesis

Polyurethane-based coatings have emerged as a favoured choice in antifouling applications, drawing on a synthesis strategy that originated from the versatile properties inherent in polyurethane chemistry. The durability and chemical resistance of polyurethane coatings stem from their unique molecular structure, which can be tailored to achieve specific performance characteristics. Developed from the combination of polyols and isocyanates, this synthesis strategy allows for formulations with strong adhesion to diverse substrates, flexibility to accommodate dynamic marine conditions, and the creation of smooth surfaces with low energy that deter fouling organisms. The origin of this synthesis strategy lies in the extensive research and development efforts within the field of polymer chemistry, leading to the optimization of polyurethane formulations for effective and long-lasting antifouling applications.

In this chapter the synthesis of Polyurethanes-based coatings two components were used, a component A synthesized by Funditec company and a commercial B component (Figure 31).

Component A was synthesised in a two-step process starting with a first step consisting of the reaction of a highly functionalised polyol. This has excess isocyanate to produce an NCO-terminated polyurethane prepolymer. In the second step, free NCO groups were then blocked with an acrylate monomer so that the combination of the different chemical structures within the polymer produces different properties in the final coating. This component A was then mixed with a commercially available component B called LUMIFLON LF910L, a fluoroethylene vinyl ether solvent borne polyol used in applications requiring outstanding exterior durability and excellent chemical resistance, solvents and additives to form the final coating which was applied to the surface prior to the curing process.

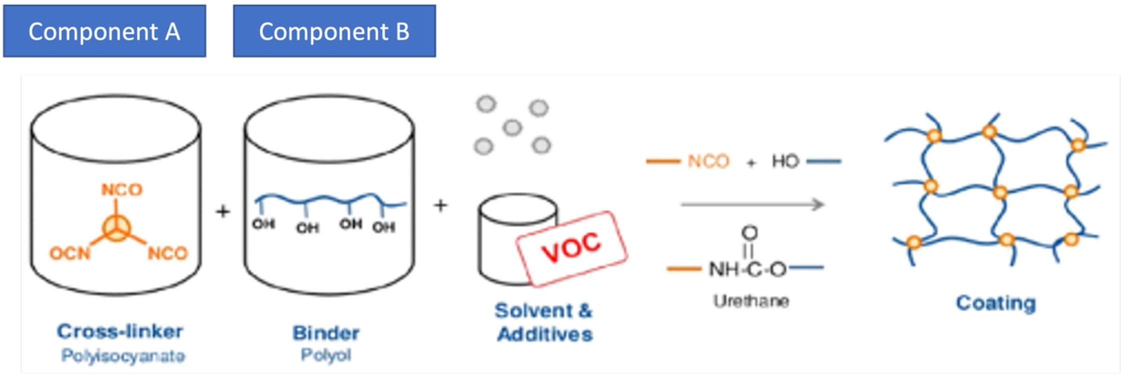

Figure 31: Simplified process for the creation of a two-component polyurethane coating

Table 19: Overview of the samples analyzed in the lab and the commercial antifouling paint. (n=3)

Coating identification	Description
PUD	Water-based polyurethane 1K
C15	Solvent-based polyurethane 2K
C15 + SiO_2	Solvent-based polyurethane 2K + 1% silica nanoparticles

Fiberglass composite	Fiberglass and vinyl ester resin with a 200 μm thick coating made from Policor® GEL ISO NPG PA Ral 9003 gelcoat from Polynt with the Luperox® K12 G catalyst from Arkema
Commercial Antifouling Paint	Solvent-based PUR 2K (HEMPEL HARD RACING TecCel 7688W)

4.3.3 Laboratory test

4.3.3.1 Culture conditions

Marine diatom species, *Amphora coffeaeformis* and *Nitzschia ovalis* were selected for biofouling laboratory studies which were purchased from the Scottish Marine Institute (SAMS Limited, Scotland, UK). To cultivate these organisms, water with 0.45 μm filtered sea salt was supplemented with nutrients for Guillard's F/2 + Si medium, prepared according to the instructions in Table 2.1 and adjusted to pH 8.0 with 1 M NaOH or 1 M HCl before autoclaving at 15 psi for 15 minutes. The cultures were grown in 5L Pyrex bottles using a 'batch-type' growth system, maintaining a temperature range of 15°C to 23°C and a 12:12 light:dark cycle with continuous light of 65 μmoles/m2/s. The cultures were homogenized using filtered-air pumps and soft bubblers (See the setup diagram in figure 32)

Table 20: The components of f/2 + sodium metasilicate medium (f/2 + Si) (Guillard's medium) used to grow laboratory diatoms, *A. coffeaeformis* and *N. ovalis*.

	Solution	Component	mL per L
1	Sodium nitrate	$NaNO_3$	1
2	Sodium phosphate monobasic dihydrate	$NaH_2PO_4.2H_2O$	1
3	Trace elements	NA_2EDTA $FeCl_3.6H_2O$ $CuSO_4.5H_2O$ $ZnSO_4.7H_2O$ $CoCl_2.6H_2O$ $MnCl_2.4H_2O$ $Na_2MoO_4.2H_2O$	0.1
4	Vitamin mix	Cyanocobalamin Biotin	1
5	Sodium metasilicate	$Na_2SiO_3.9H2O$	1

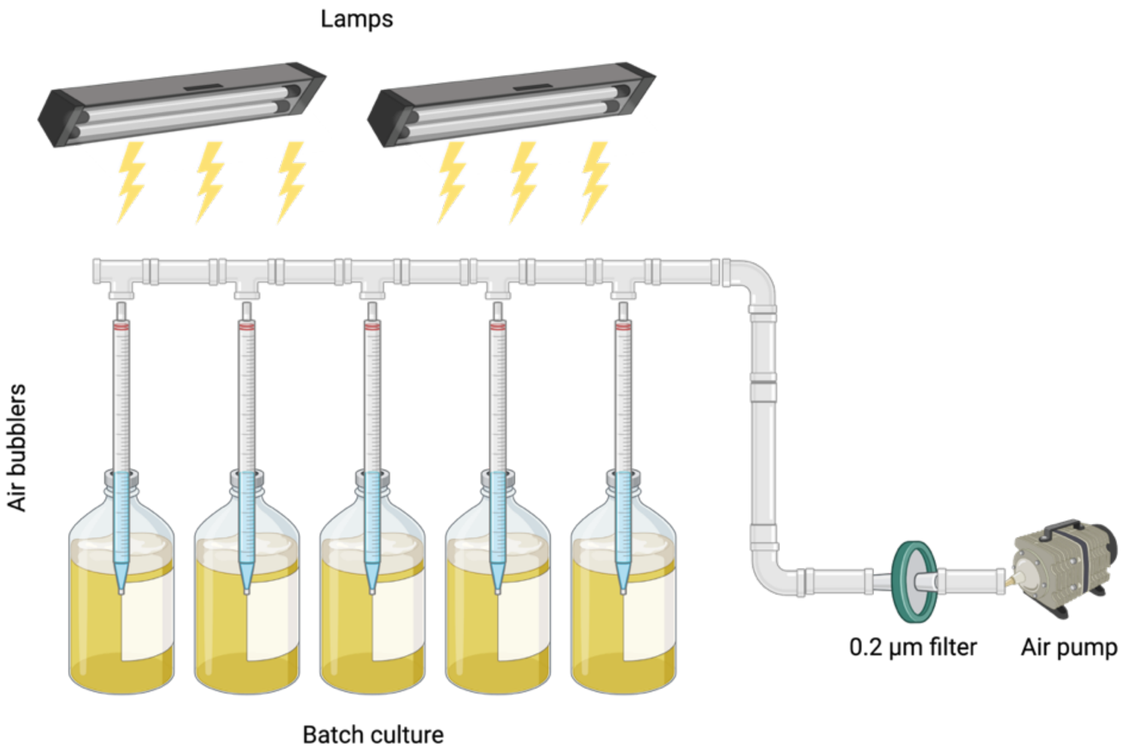

Figure 32: Schematic representation of the setup constructed to grow algae cultures in batches for exposure experiments. The diagram shows the system used in the laboratory in which the algae were kept in a semi-continuous liquid culture in batches to which filtered air was supplied to homogenise the sample and prevent the algae from settling on the walls of the bottles due to their benthic nature.

4.3.3.2 Culture growth monitoring

The culture growth was monitored every week using optical density at 750nm and *Chlorophyll-a* as an estimation of biomass before starting every experiment in combination with the number of cells per millilitre using light microscope and an improved Neubauer bright line hemocytometer (Figure 33 E).

Optical density was measured every week at a wavelength of 750nm using the UVmini-1240 spectrophotometer, keeping the cells always in their exponential growth phase in the range of 0.3 – 0.5 AAU.

Chlorophyll-a concentration was used as an estimation of biomass and it was determined in 25 mL aliquots that were filtered in low pressure (700 mb) through GF/F glass fibre filters (Whatman GF/F, pore size 0.7 µm) kept in the dark at -20 ºC for 12 hours. Subsequently, 8 mL of 90 % (v/v) acetone was added to each 25 mL filtered aliquot, followed by sonication in an ultrasound bath for 5 min, extraction in the dark at 4 ºC for at least three hours, centrifugation (5000 r.p.m., 10 minutes) and recovery of the supernatant. Absorbance was read at 665 nm and 750 nm in a Shimadzu UV-1800 UV-Vis double beam spectrophotometer allowing the calculation of *Chl-a* concentration according to [221]

The number of cells per millilitre was estimated using a light microscope and an improved Neubauer bright line hemocytometer with a depth of 0.100mm and a surface area of 0.0025 mm^2. The culture was filtered 3 times directly through an 0.45 µm pore size, 47 mm diameter Whatman nylon filters (VWR, Ireland) and then 10 uL of culture was injected with a micropipette into the improved Neubauer chamber. The cells were then counted in the four corners of the chamber in duplicate (Figure 33 F). The mean and standard deviation were then calculated.

The cultures were diluted using Guillard's F/2 + Si medium (Scottish Marine Institute, SAMS Limited, Scotland, UK) or concentrated by centrifugation in order to always obtain a cell density of approximately 3x10^6 cells per millilitre (n=3).

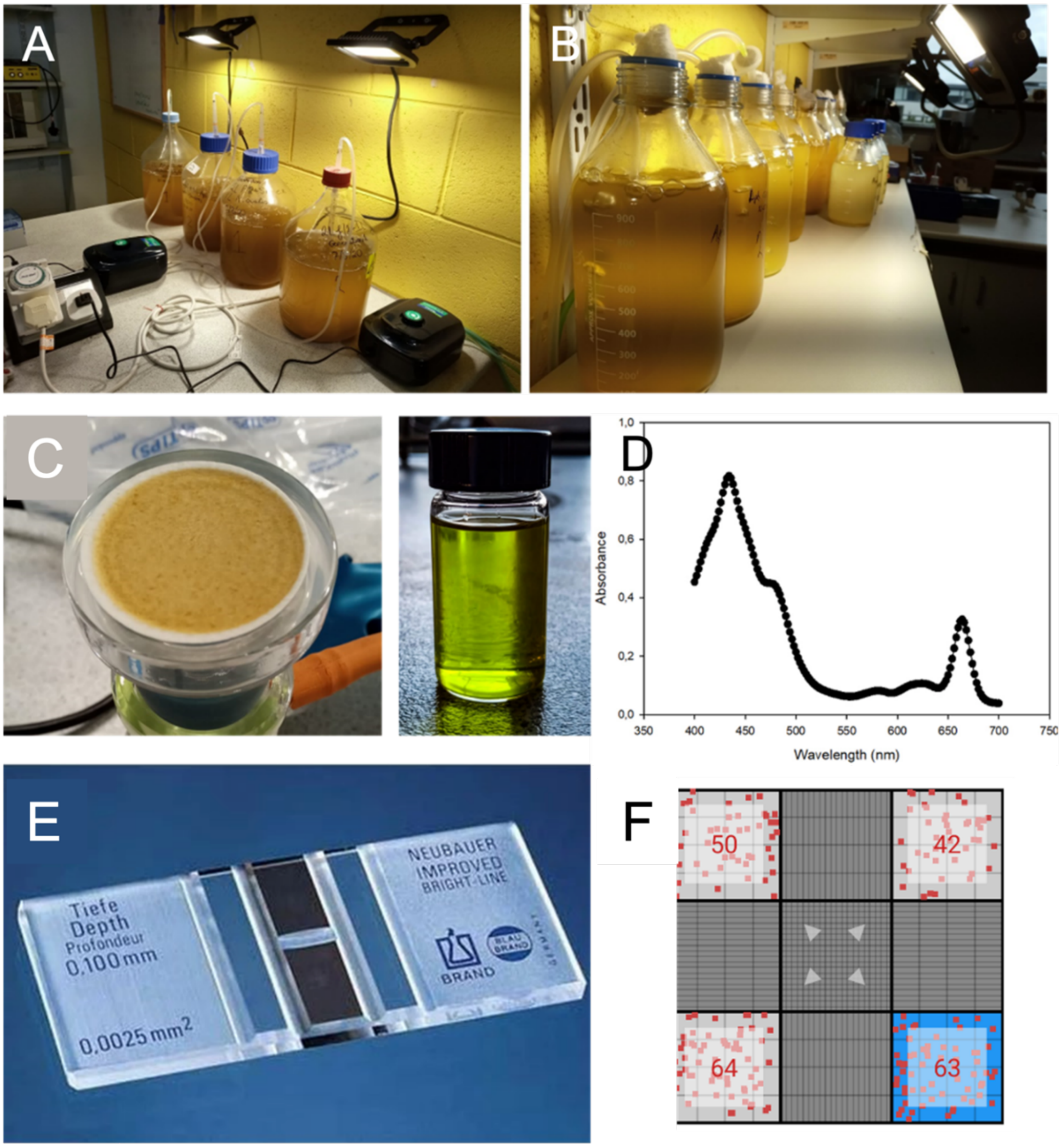

Figure 33: General overview of the laboratory equipment used in this chapter. A: represents a large volume 20 L *Nitzschia ovalis* culture system for maintenance of laboratory stock. B: represents a small volume 7 L culture system for maintenance of the stock shown in A. C: represents the membrane filtration for concentration, extraction and quantification of chlorophyll-a from the laboratory cultures in order to know their biomass and therefore their optimal growth. D: represents a spectrophotometric absorption curve for chlorophyll-a. E: represents a Neubauer chamber (hemocytometer) for the quantification of cells per millilitre in cultures A and B. F: is a representation of the quadrants in which the cells were counted in the Neubauer chamber.

4.3.3.3 Static testing of *Nitzschia ovalis* settlement

Rapid biofouling assessment was performed using a 10 mL culture suspension of fouling organisms, *Nitzschia ovalis*. The use of *Amphora coffeaeformis* was discarded because it could not be observed clearly under the microscope due to low numbers of individuals.

The textures and coatings were firstly purged with nitrogen (N_2) gas to remove air pockets. Designed micro-textures were immersed in the cell suspension for 4 h in individual petri dishes. Colonization of textures and coatings was observed by removing them from the cell suspension and dipping twice sequentially in solutions of 50:50, artificial seawater: deionized water and deionized water. Samples were stained by immersion in 10 µg mL-1 of acridine orange (AO) dye for 3 min at room temperature. Samples were rinsed three times sequentially in deionized water to remove excess stain and allowed to dry. Colonization of organisms on the candidate micro-textures and the coatings was observed using the Keyence VHX2000E 3D digital light microscope with high resolution zoom lens VH-Z500R (500 x to 5000 x). Images were acquired at a magnification of 500 x for each sample in triplicate for the textures (n = 3) and ten for the coatings (n=10) (see the schematic methodology in the figure 34)

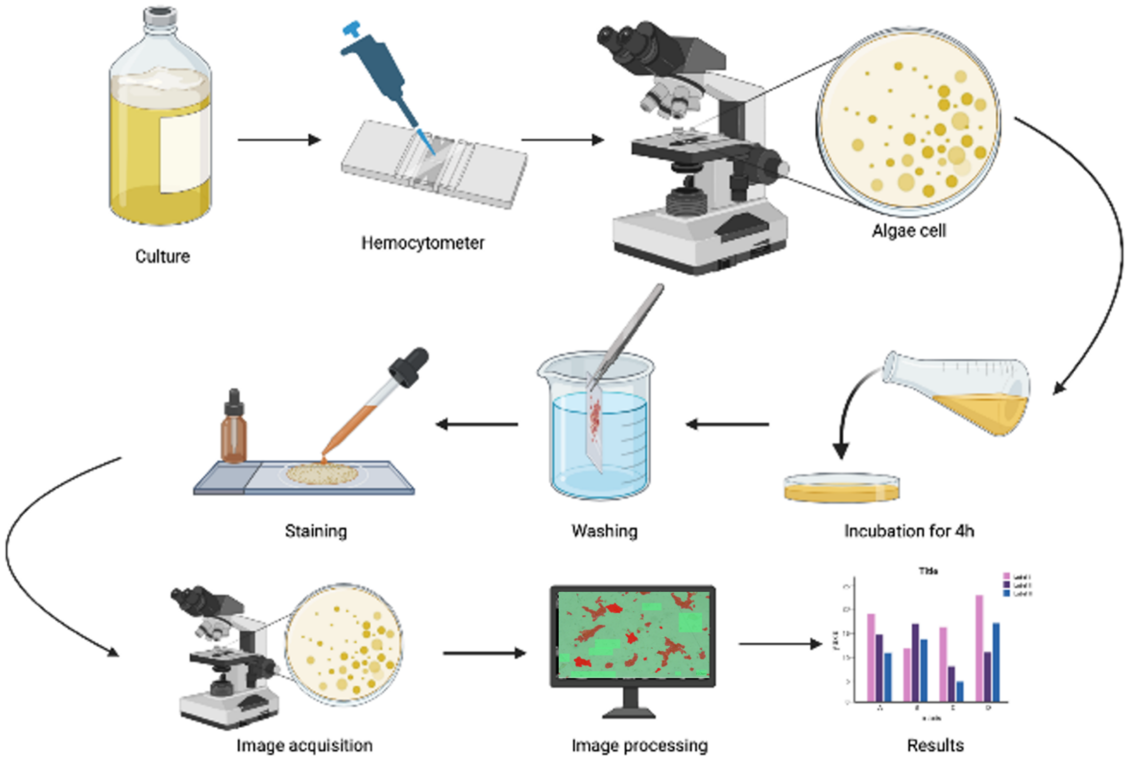

Figure 34: General representation of the procedure carried out in this chapter for the quantification of the adhesion of *Nitzschia ovalis* on the different samples tested. The process starts with counting with the haemocytometer in order to estimate the cell concentration, followed by incubation of the samples with the desired cell suspension. After a certain period of time (4h) the excess of unattached cells is removed and stained with a stain to be photographed under the microscope for computer analysis and calculate the percentage of surface covered.

4.3.4 Image Analysis

All image Pre-Processing were performed using Fiji (ImageJ) for the textures and Ilastik for the coatings. Exposure and saturation levels were adjusted to obtain the highest contrast between image and the image-features.

4.3.4.1 Adhesion test and percentage covered calculation for textures

For analysis of textures all image analyses were performed in a ASUS ROG Strix computer with a Intel I7 8750H 6+6 cores CPU and 16 Gb of RAM with the software Weka segmentation (V3.3.2) to evaluate the exposed surface (see chapter 3)

The images used in the analysis were scaled using the scale bar given in the images taken on the Keyence VHX2000E 3-D digital microscope. Images were cropped a to approximately 300 x 300 μm to remove noise or imperfections such as unwanted particles, material/texture defects.

Image segmentation was performed using the TWS plugin which uses machine learning algorithms to classify an image into different classes. The user trained the software by drawing strokes defined as a training set of pixels (STP) over the region of interest (ROI) for each class. An STP of two classes is necessary to start the segmentation. Two classes were used. Class 1 corresponds to the particles to be detected, in this case benthic diatom specie, *N. ovalis*, appearing red. Class 2 corresponds to the background of the image, appearing green (Figure 35). These classes are comprised of sets of pixels that share similar visual characteristics such as colour, shape, or size.

The segmentation process was carried out using the Fast Random Forest algorithm which employs machine learning using decision trees to classify data based on user-defined patterns for each class. This algorithm was chosen because of its computational efficiency (see chapter 3). In addition, this algorithm avoids over-fitting the data by injecting randomness in the training trees and combining the output of multiple random trees into the final classifier; in our case 1000 trees were performed using always in each analysis an out of bag error lower than 8 % to arrive at the final classifier from which a probability image was obtained. The Random Forest algorithm proves to have robust performance when compared using eight evaluation metrics [222]. Once satisfied with the segmentation, a final image was obtained with the result of the classification process which contained the two colours relating to the two classes (Red = *N. ovalis*; Green = clean background). This image was then reopened with ImageJ and the percentage of surface area covered by clustering colour analysis was calculated using an open-source plugin developed by the Biomedical Imaging Group from Swiss Federal Institute of Technology (Lausanne EPFL, Switzerland) [190].

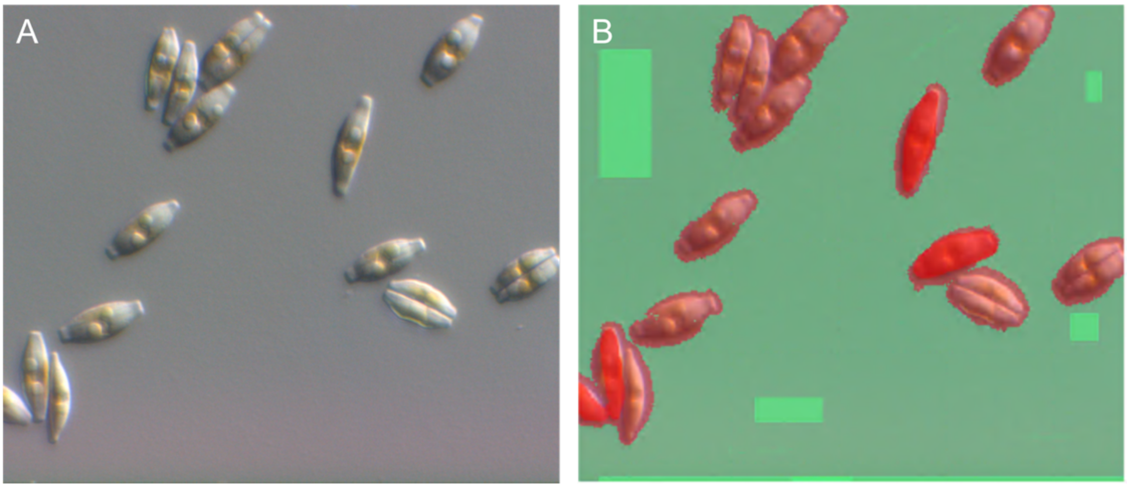

Figure 35: A glimpse of how artificial intelligence is able to recognise the organisms in the original microscopy image (A) and transform it into a segmented colour image (B). This system works through a user-friendly interface in which patterns are drawn to detect the different artefacts required. In this case the background was selected in green and green rectangles were drawn while for the cells the colour red was selected and an oval shape was drawn around the cell.

4.3.4.2 Adhesion test and percentage covered calculation for coatings

For the analysis of coatings Ilastik software (v.1.4) was used to create a data base of images to train an AI to be able to recognize patterns like slime cells that was used in chapter 6

Ilastik is an open-source software for image analysis very similar to Weka Segmentation. It provides a user-friendly interface for interactive image segmentation, tracking, and multi-dimensional data visualization. It is designed to be flexible and extensible and can be used for a wide range of applications, including microscopy, satellite imagery, and medical imaging. It is written in Python and built on top of several open-source libraries, including the Insight Toolkit (ITK) and the Visualization Toolkit (VTK).

So, for this particular experiment the analysis was done by creating a classification model based on pixel segmentation. The pixel characteristics used in this model were smoothed pixel intensity, edge filters and texture features. For the developed model, all sigma values were chosen to obtain the best result. The pixel classification model was then trained using the samples from microscopic images previously acquired a part of the experiment on the machine learning tool called random forest classifier (same as we did with the textures with TWS) which performs semantic segmentation. In this software, 100 decision trees were made by default. These decision trees contain a set of binary decisions and terminal nodes that are connected as branches. The tree grows with each interaction until all branches end at an end node.

The software was trained using 53 microscopy images containing both classifiers (algae and background). Each of these images used for training contained information on the different patterns, shapes, sizes, etc. of *Nitzschia ovalis*, particles of debris attached and the surface.

Once a satisfactory segmentation model was obtained, all the images of each coating and control were batch-processed to obtain probability image.

Percentage coverage of a total of ten randomized microscopic fields of each coating were performed in triplicate (n=30) and then the mean and standard deviation were calculated. Once all the probability maps were obtained, they were run with ImageJ's Fiji software and the area covered for each class was calculated using the K-Means algorithm in the ImageJ plugin to cluster colour pixel driven by the user input, same as we did with analysis with the textures [190].

4.3.4.3 Aggregation / cluster area formation analysis.

A diatom cluster refers to a grouping or accumulation of two or more diatoms in a relatively localized area (Figure 36). For the calculation of the areas of the algal clusters, ImageJ software was used. The scale of the image was used and a correlation was made between this and the pixels, obtaining a scale expressed in pixels per micrometre (pixels/μm). The clusters of organisms were outlined with the brush tool in ImageJ and their area (μm^2) calculated using the scale-bar. The area and centroid were incorporated in the measurements, and the "Analyse Particles" feature was utilized to calculate nearest neighbor distances with the "nnd" plugin located in the "Plugins" tab of ImageJ. A total of 10 measurements were made per sample and they were averaged and standard deviation was measured.

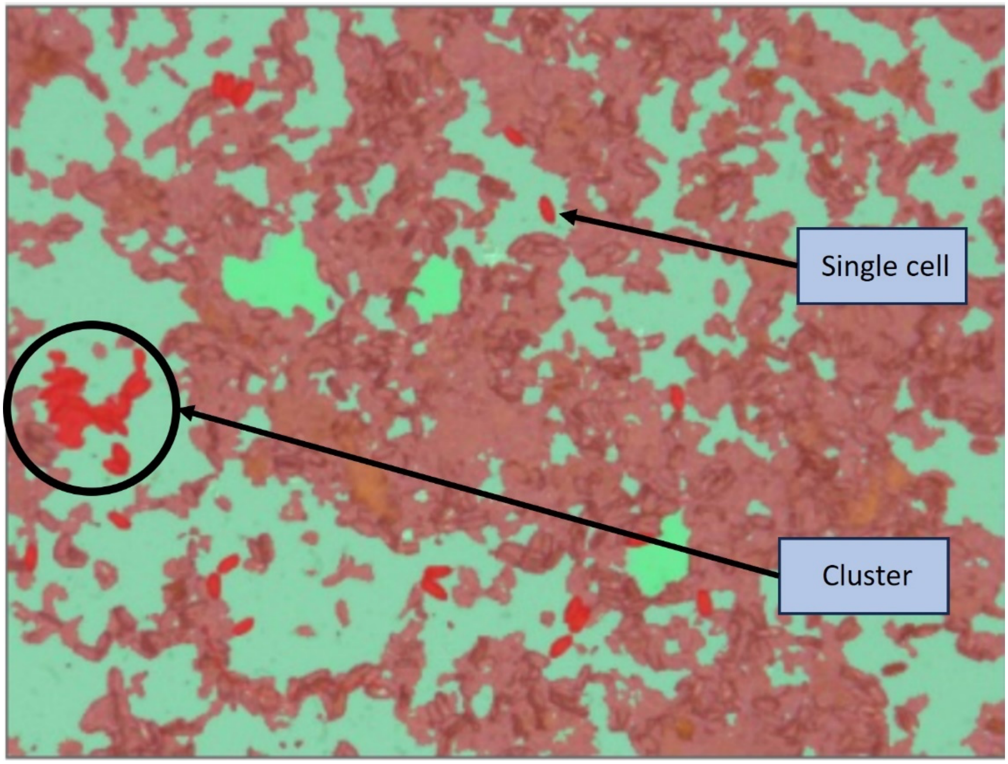

Figure 36: Result of the segmentation process (red are cells, green is background), showing the clustering of cells in comparison to an isolated cell.

4.3.5 Statistical analysis.

In the statistical analysis a one-way analysis of variance was used taking into account the number of photographs in triplicate (n=30). The power of performed test with alpha = 0.050. A multiple pairwise comparison was also performed (Holm-Sidak method) with an overall significance level = 0.05.

4.4 Results and discussion

4.4.1 Adhesion test, percentage coverage and cluster area analysis on textures

Laboratory assessment of *N. ovalis* settlement on textured surfaces was performed using the 4 h rapid adhesion assay described previously. Micro-textures inspired by the Brill fish, *Scophthalmus rhombus*, revealed lower algae adhesion to the surface's micro-topographical features, while the smooth-flat control texture and ITO-coated glass showed higher percentage coverage after the image analysis (Figure 38 and Figure 40). Significance testing was determined via 2-way ANOVA followed by Holm-Sidak method. Textured surfaces, A1 (Mean = 16.37 ± 7.63 %), A2 (Mean = 27.74 ± 5.93 %) and A3 (Mean = 22.20 ± 1.11 %) indicated a reduction in the adhesin of *N. ovalis* cells to the controls used ITO-coated glass (Mean = 54.98 ± 6.66 %) and flat texture (Mean = 30.19 ± 5.44 %). The differences in the mean values among the treatment groups were greater than would be expected by chance; there was a statistically significant difference between the ITO-coated glass control used and the textures ($P \leq 0.001$). On the other hand we couldn´t find any statistically difference between different types of textures and smooth-flat control texture (Table 21 and Table 22). This was probably due to the sample pool used which should be increased to be statistically stronger. However, we can say that visually A1 gave better results than the other textures. These results for A1 texture which has sharp edges at 90 degrees angle can be explained by the theory of attachment points (Figure 37) [223]. *Nitzschia ovalis* used in the laboratory which has dimensions of approximately 7 x 14 μm (n=10) may find it difficult to attach to the designed textures due to the 10 μm space between the cavities, however it will find it much easier to attach to a texture with rounded edges as the contact surface will be more accessible and will therefore be able to develop multiple attachment points.This is why sample A2, which has rounded edges, has a higher colonisation rate than the other textures because the rounded edge provides a larger contact surface and the diatoms can orient themselves to position to maximise contact with it, promoting colonisation. However, for texture A3, which corresponds to the recessed cavity array, it could be acting as a wells in which diatoms accumulate and can therefore form aggregates more easily and which can explain the behaviour of the larger cluster formation.

Average cluster area (μm^2) on each of the textured surfaces and smooth surfaces showed very similar results (Figure 39). Textured surfaces, A1 (Mean = 94.28 ± 42.83 μm^2), A2 (Mean = 97.27 ± 44.93 μm^2) and A3 (Mean = 321.57 ± 171.87 μm^2) indicated a reduction in the cluster and colonization process of *N. ovalis* cells compared to the controls used Glass (Mean = 1823.65 ± 441.65 %) and flat texture (Mean = 618.23 ± 251.24 %). The differences in the mean values among the treatment groups were greater than would be expected by chance; there was a statistically significant difference between the control and the textures ($P \leq 0.001$). However, no statistically difference could be found between the different types of textures (Table 23 and Table 24)

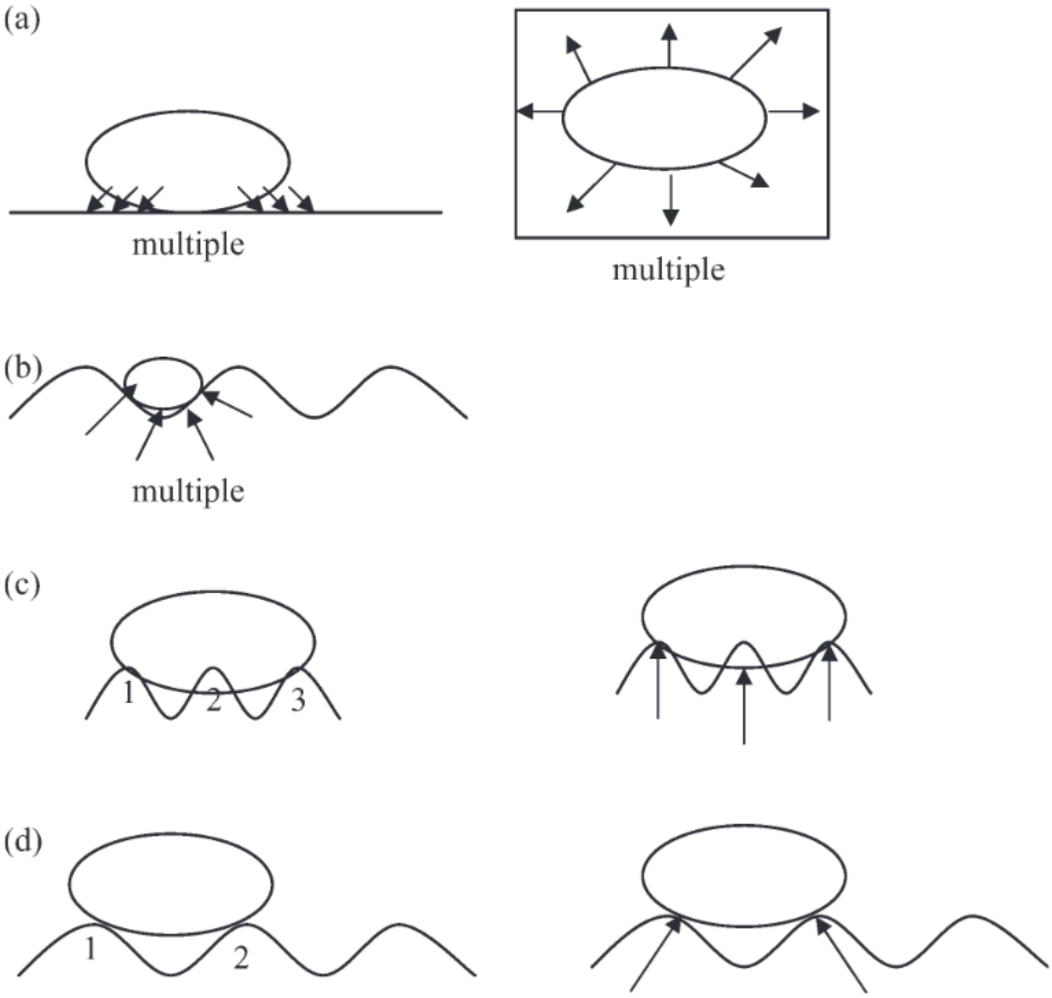

Figure 37: Schematic illustration of theoretical attachment points theory for (a) all diatoms on a smooth surface with multiple attachment points; (b) F. carpentariae on 2 μm ripples with multiple attachment points; (c) N. jeffreyi settling on 2 μm ripples with 3 attachment points; (d) Amphora sp. Settling on 4 μm ripples with 2 attachment points [223].

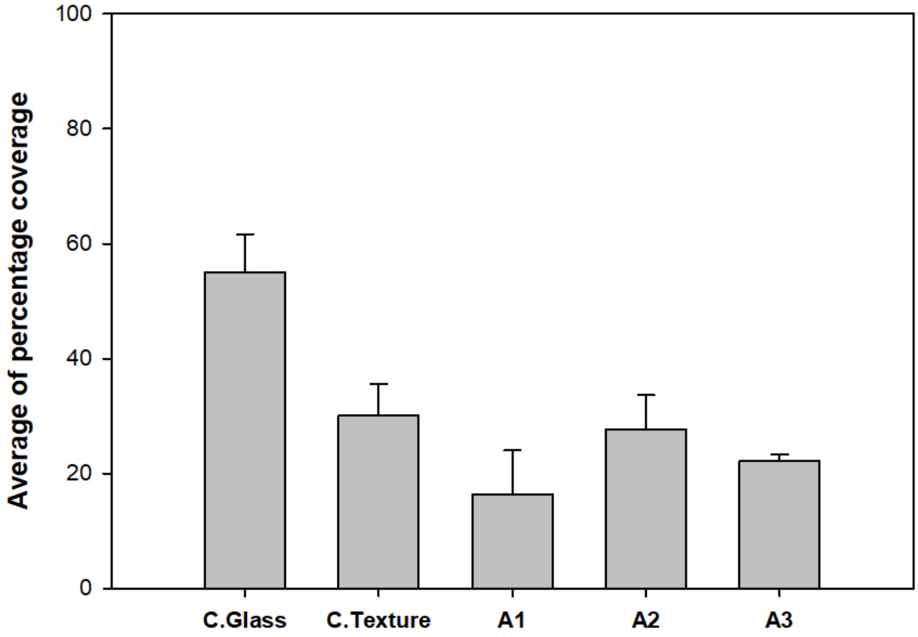

Figure 38: Average of percentage coverage per texture (n=3) directly calculated by colour analysis of the segmented images obtained using Fiji software (ImageJ) and the plugin [190].

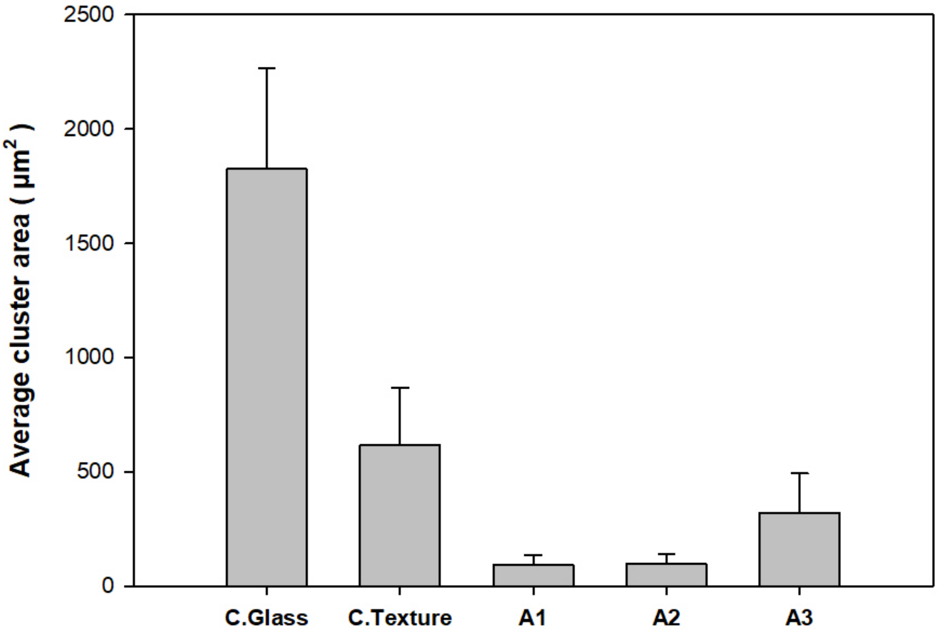

Figure 39: Average of cluster area per texture (n=10) calculated using pixels per micrometre (pixels/μm) and the brush tool around each red patch.

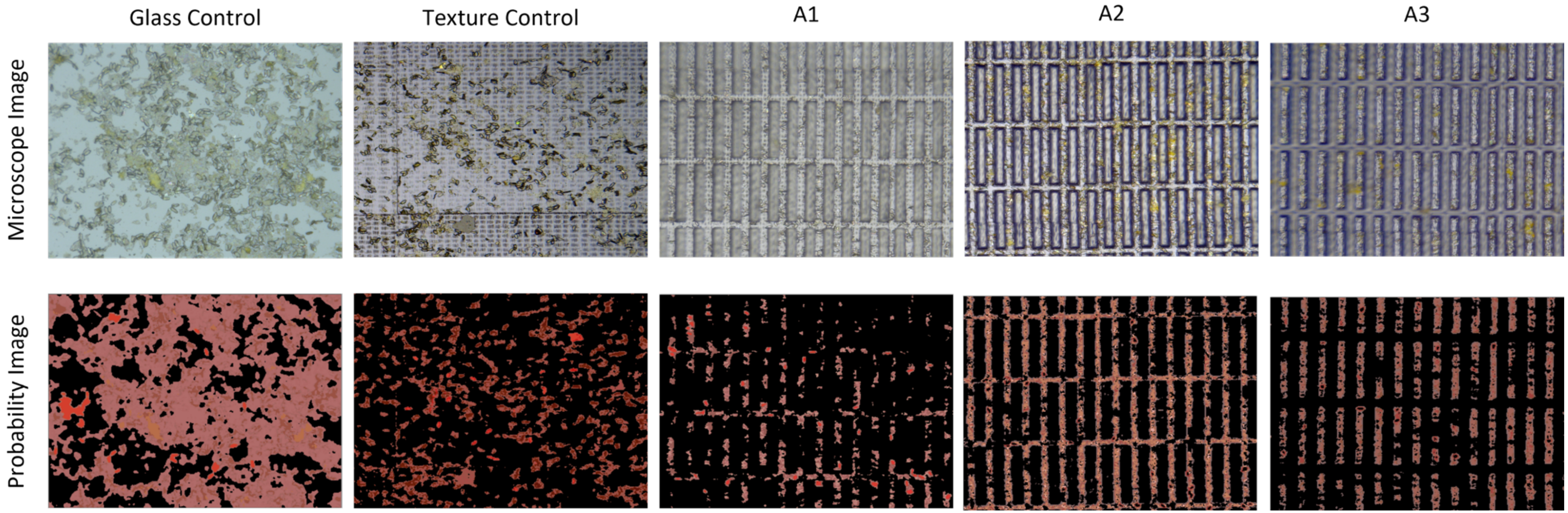

Figure 40: Representation of the microscopy image and its probability image after the segmentation process for the different texture samples. The images in the first row were obtained directly with the microscope Keyence VHX2000E 3D digital light microscope at a magnification of 500X using VH-Z500R lens (500 x to 5000 x magnification). The images in the second row show the segmented images (probability images) where the red colour shows the surface covered by the organisms and the black colour the uncovered area.

Table 21: One Way Analysis of Variance for the average percentage coverage on textures. The differences in the mean values among the treatment groups are greater than would be expected by chance; there is a statistically significant difference (P = <0.001). SEM= Standard Error of the mean; DF= Degrees of freedom; SS= The sum of squares due to the source; MS= The mean sum of squares due to the source; F= variation between sample means / variation within the samples; P= Probability that the null hypothesis is true.

Power of performed test with alpha = 0.050: 1.000

Group Name (%)	**N**	**Missing**	**Mean**	**Std Dev**	**SEM**
Control Glass	3	0	54.982	6.663	3.847
Control Texture	3	0	30.194	5.441	3.141
A1	3	0	16.371	7.63	4.405
A2	3	0	27.739	5.934	3.426
A3	3	0	22.203	1.112	0.642
Source of Variation	**DF**	**SS**	**MS**	**F**	**P**
Between Groups	4	2626.049	656.512	19.462	<0.001
Residual	10	337.332	33,733		
Total	14	2963.38			

Table 22: All Pairwise Multiple Comparison Procedures for average percentage coverage (Holm-Sidak method). Overall significance level = 0.05

Comparison	Diff of Means	t	Unadjusted P	Critical Level	Significant?
Control Glass vs. A1	38.611	8.142	<0.001	0.005	Yes
Control Glass vs. A3	32.779	6.912	<0.001	0.006	Yes
Control Glass vs. A2	27.243	5.745	<0.001	0.006	Yes
Control Glass vs. Control Texture	24.788	5.227	<0.001	0.007	Yes
Control Texture vs. A1	13.823	2.915	0.015	0.009	No
A2 vs. A1	11.368	2.397	0.037	0.01	No
Control Texture vs. A3	7.991	1.685	0.123	0.013	No
A3 vs. A1	5.832	1.23	0.247	0.017	No
A2 vs. A3	5.536	1.167	0.27	0.025	No
Control Texture vs. A2	2.455	0.518	0.616	0.05	No

Table 23 One Way Analysis of Variance for the average clustering formation area for the textures tested. The differences in the mean values among the treatment groups are greater than would be expected by chance; there is a statistically significant difference (P = <0.001). SEM= Standard Error of the mean; DF= Degrees of freedom; SS= The sum of squares due to the source; MS= The mean sum of squares due to the source; F= variation between sample means / variation within the samples; P= Probability that the null hypothesis is true.

Power of performed test with alpha = 0.050

Group Name (cluster)	**N**	**Missing**	**Mean**	**Std Dev**	**SEM**
Control Glass	10	0	1823.65	441.654	139.663
Control Texture	10	0	618.227	251.235	79.447
A1	10	0	94.281	42.829	13.544
A2	10	0	97.267	44.929	14.208
A3	10	0	321.568	171.871	54.35
Source of Variation	**DF**	**SS**	**MS**	**F**	**P**
Between Groups	4	20832703.71	5208176	89.313	<0.001
Residual	45	2624128.739	58314		
Total	49	23456832.45			

Table 24: All Pairwise Multiple Comparison Procedures for the clustering formation area for the textures tested (Holm-Sidak method). Overall significance level = 0.05

Comparison	Diff of Means	t	Unadjusted P	Critical Level	Significant?
Control Glass vs. A1	1729.37	16.014	<0.001	0.005	Yes
Control Glass vs. A2	1726.39	15.986	<0.001	0.006	Yes
Control Glass vs. A3	1502.09	13.909	<0.001	0.006	Yes
Control Glass vs. Control Texture	1205.43	11.162	<0.001	0.007	Yes
Control Texture vs. A1	523.946	4.852	<0.001	0.009	Yes
Control Texture vs. A2	520.96	4.824	<0.001	0.01	Yes
Control Texture vs. A3	296.659	2.747	0.009	0.013	Yes
A3 vs. A1	227.287	2.105	0.041	0.017	No
A3 vs. A2	224.301	2.077	0.044	0.025	No
A2 vs. A1	2.986	0.0276	0.978	0.05	No

4.4.2 Adhesion test. percentage coverage and cluster area analysis on antifouling coatings

Laboratory assessment of *N. ovalis* settlement on coated surfaces was performed using the 4 h rapid adhesion assay described previously with the textures. Different probability images and subsequently segmentation images were created, which allowed us to analyze the surface area covered by *Nitzschia ovalis* compared to the clean surface area (Figure 43). In figure 43 and the bar chart showed in figure 41 it can be seen a reduced adhesion performance of *Nitzschia ovalis* on PUD (Mean = 19.71 ± 3.34 %), C15 (Mean = 15.02 ± 2.50 %) and C15 + SiO_2 (Mean = 12.13 ± 3.13 %) against the two controls used as a reference, commercial paint (23.41 ± 3.47 %) and the fiberglass composite (Mean = 24.60 ± 3.83 %) on which the coatings are applied using 10 random microscope observations fields per triplicate (n=30). However, C15 + SiO_2 showed the best results. Statistically significant differences were found between the control groups and the coatings ($P \leq 0.001$) (Table 25 and Table 26). This is because these compounds have various components that make them more effective. For example PUD is a “waterborne polyurethane coating” which showed the highest average coverage percentage using *N. ovalis* compared to the rest of the coatings. Despite this, its smooth surface reduces the amount of surface area available for organisms to attach, which is directly related to the attachment points theory [223] making it more difficult for them to establish a foothold and grow. However, coating 15, which is very similar to PUD with the particularity that it is a solvent-based two-component polyurethane, showed a better result compared to the average coverage percentage. The reason to explain this could very diverse. For example in terms of biofouling specifically, one study found that waterborne polyurethane coatings were more susceptible to biofouling than solvent-based coatings [224] Two component solvent-based polyurethane is preferred over a one-component coating for antifouling paints for several reasons but mainly in relation with their formulation and curing process. Two-component polyurethane coatings consist of a resin (normally a polyacrylic resin) and a hardener (normally polyisocyanate hardener), which react with each other to form a strong, crosslinked polymer network. This curing mechanism results in a coating that is more durable and resistant to wear and tear than a waterborne polyurethane coating, which cures through a different mechanism (typically moisture cure) [225]. The crosslinked network of a two-component polyurethane provides better adhesion to the surface, and overall protection against biofouling and harsh conditions in the sea and the lab conditions used in this chapter like high salinity (30 g/L) compared to water-based coatings such as PUD coating tested. This is because they are have a less dense molecular structure and lower crosslinking density and less ability to form a hard, impermeable barrier on the surface they are applied to, which can allow marine organisms to adhere and colonize the surface more easily Therefore, these coatings often have to be supplemented with biocides or nanoparticles.

Another reason why there may be differences between PUD and C15 could be the impact of the potential toxicity of the solvent of the coating which was not pre-treated or pre-conditioned to remove any toxic agents due to its to the limited number of samples and replicates available at the time of testing. Prior exposure to artificial seawater might have shown clearer results,

In the case of C15 + SiO_2 its low percentage coverage results, may be due to a number of factors. For example the SiO_2 components provides a low surface energy of SiO_2 surfaces makes it difficult for microorganisms to adhere to the material. This reduces the chance of fouling and biofilm formation. Silica nanoparticles have been shown in studies to have the ability to increase the presence of lysozyme on the surface of bacteria which is highly effective for antibacterial activity and can inhibit the growth of bacteria, specifically *E. coli*, for an extended period of up to 3 days [226]. In addition, SiO_2 coatings often create a smooth surface, which makes it difficult for microorganisms and particles to attach and easy to clean. This makes it convenient to maintain the antifouling properties by removing any accumulated particles or organisms, so probably more cells were removed in the rinsing process after staining with acridine orange when we performed the adhesion test in the lab. Nonetheless, SiO_2 is applied in nanoparticulate form (1% concentration), and its small size may potentially allow it to be absorbed by organisms, leading to cellular damage or other harmful consequences. Some studies reported that SiO_2 particles result in IL-6 increase in humans, DNA damage and apoptosis [227–229]. The toxicity of SiO_2 nanoparticles remains an active area of investigation, with potential risks influenced by factors such as size, shape, and surface characteristics.

As for the results of average cluster area formation (μm^2) on each coatings, similar cluster area formation was found between coatings; PUD (Mean = 194.61 ± 126.60 μm^2), C15 (Mean = 154.73 ± 73.16 μm^2) and C15 + SiO_2 (Mean = 199.78 ± 123.40 μm^2) (Figure 42) with no notable statistically significant differences between them (P = 0.021) with the exception of the two controls used; commercial paint respect to the fibre glass composite (Mean = 92.73 ± 55.07 μm^2) (Mean = 199.78 ± 123.40 μm^2) (Table 27 and Table 28). These differences shown as standard deviations would probably be reduced if we used a slightly larger data pool to make our statistical test more robust. However, the data pool used was just at the limit of the capacities and resources available at the time..

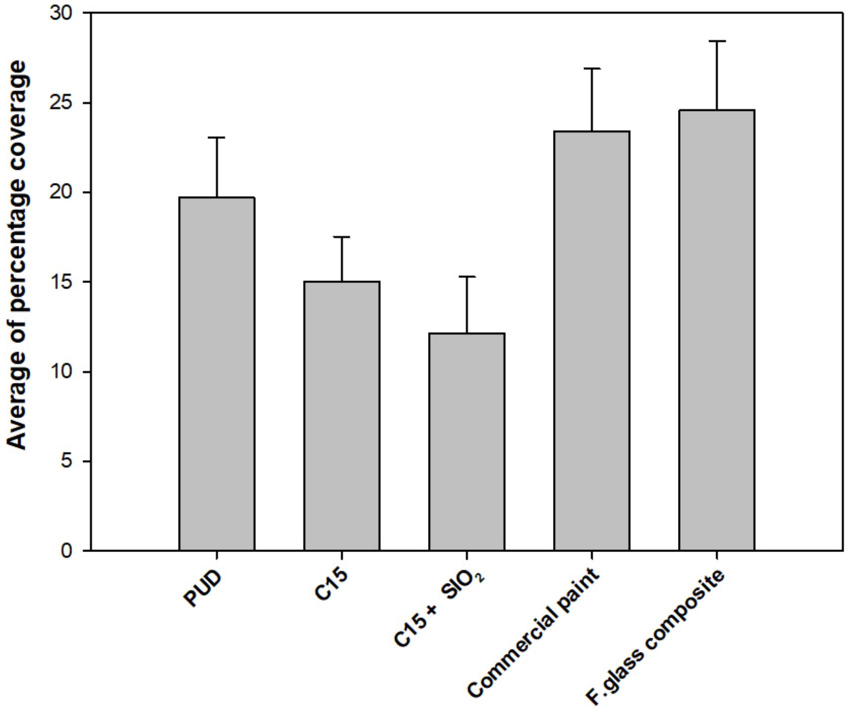

Figure 41: Average of percentage coverage per coating (N=30) directly calculated by colour analysis of the segmented images obtained using Fiji software (ImageJ) and the plugin [190].

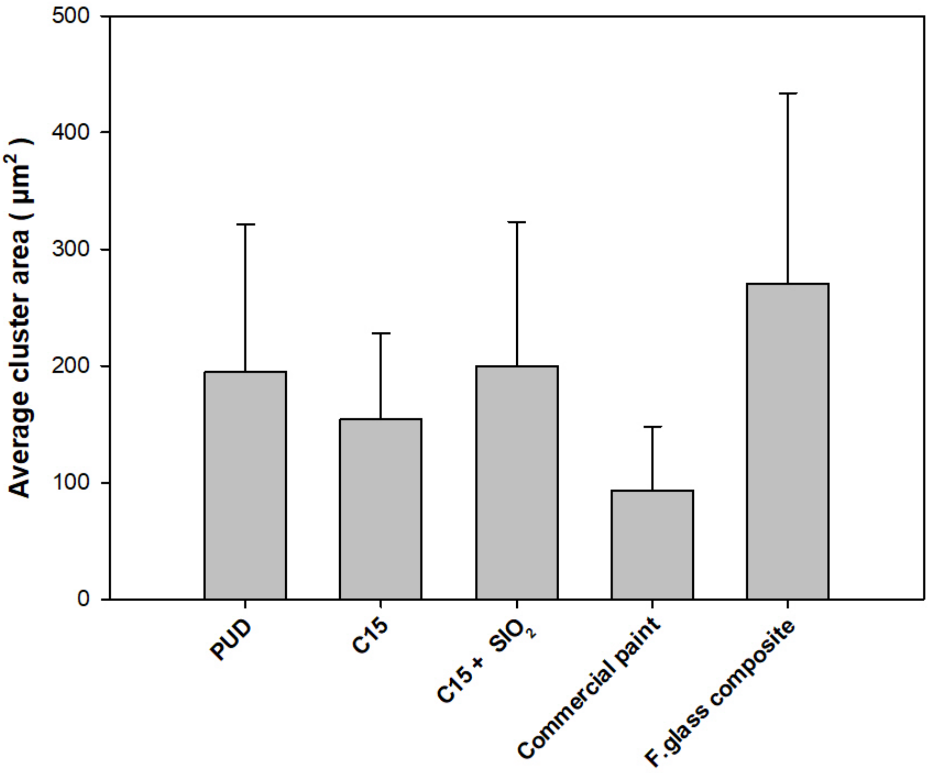

Figure 42: Average cluster area per coating (N=10) calculated using pixels per micrometer (pixels/µm) and the brush tool around each red patch.

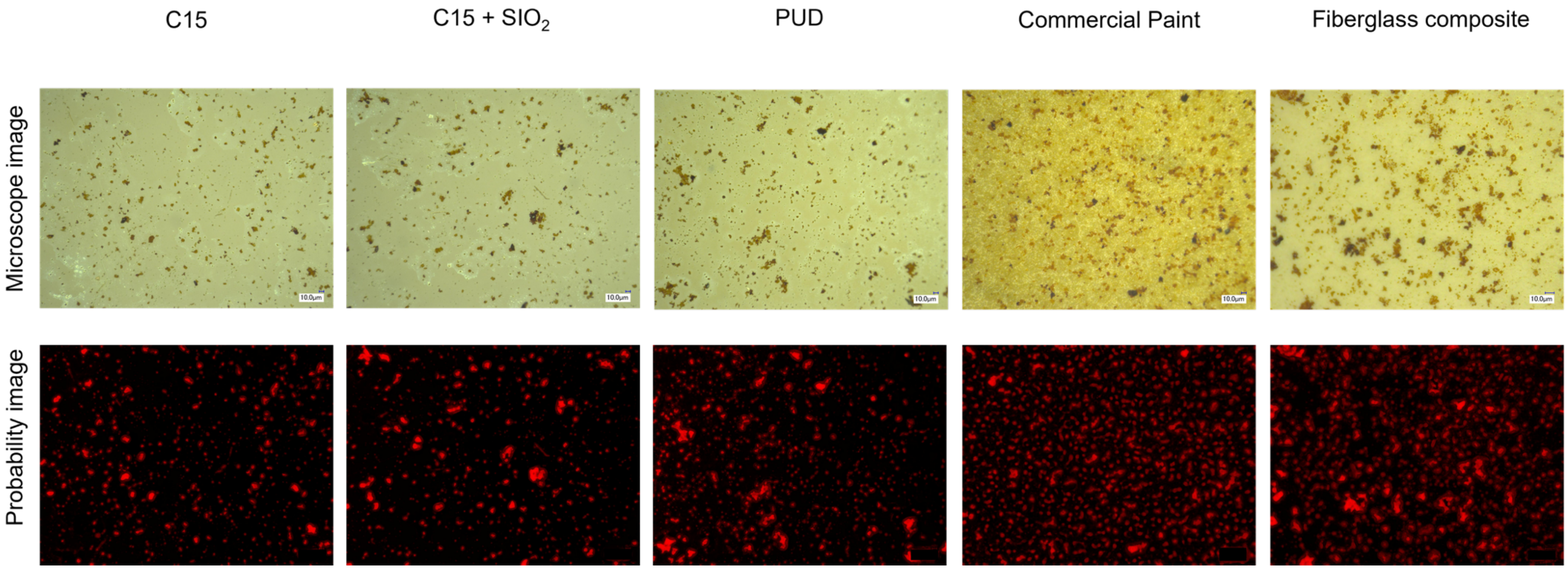

Figure 43: Representation of the microscopy image and its probability image after the segmentation process for the different coatings tested The images in the first row were obtained directly with the microscope Keyence VHX2000E 3D digital light microscope at a magnification of 500X using VH-Z500R lens (500 x to 5000 x magnification). The images in the second row show the segmented images (probability images) where the red colour shows the surface covered by the organisms and the black colour the uncovered area.

Table 25: One Way Analysis of Variance for the average percentage coverage on coatings. The differences in the mean values among the treatment groups are greater than would be expected by chance; there is a statistically significant difference (P = <0.001). SEM= Standard Error of the mean; DF= Degrees of freedom; SS= The sum of squares due to the source; MS= The mean sum of squares due to the source; F= variation between sample means / variation within the samples; P= Probability that the null hypothesis is true.

Power of performed test with alpha = 0.050

Group Name (%)	**N**	**Missing**	**Mean (%)**	**Std Dev**	**SEM**
PUD	30	0	19.709	3.339	0.61
C15	30	0	15.021	2.5	0.457
C15+ SiO_2	30	0	12.136	3.131	0.572
Commercial Paint	30	0	23.408	3.467	0.633
F. glass composite	30	0	24.597	3.832	0.7
Source of Variation	**DF**	**SS**	**MS**	**F**	**P**
Between Groups	4	3426.26	856.565	79.434	<0.001
Residual	145	1563.58	10.783		
Total	149	4989.84			

Table 26: All Pairwise Multiple Comparison Procedures for the average percentage coverage (Holm-Sidak method). Overall significance level = 0.05

Comparison	Diff of Means	t	Unadjusted P	Critical Level	Significant?
F. glass composite vs. C15 + SiO_2	12.461	14.697	<0.001	0.005	Yes
Commercial Paint vs. C15 + SiO_2	11.272	13.295	<0.001	0.006	Yes
F. glass composite vs. C15	9.576	11.294	<0.001	0.006	Yes
Commercial Paint vs. C15	8.387	9.892	<0.001	0.007	Yes
PUD vs. C15 + SiO_2	7.573	8.932	<0.001	0.009	Yes
F. glass composite vs. PUD	4.888	5.765	<0.001	0.01	Yes
PUD vs. C15	4.688	5.529	<0.001	0.013	Yes
Commercial Paint vs. PUD	3.699	4.363	<0.001	0.017	Yes
C15 vs. C15 + SiO_2	2.885	3.403	<0.001	0.025	Yes
F. glass composite vs. Commercial Paint	1.189	1.402	0.163	0.05	No

Table 27: One Way Analysis of Variance for the clustering formation for the coatings tested. The differences in the mean values among the treatment groups are greater than would be expected by chance; there is a statistically significant difference (P = <0.001). SEM= Standard Error of the mean; DF= Degrees of freedom; SS= The sum of squares due to the source; MS= The mean sum of squares due to the source; F= variation between sample means / variation within the samples; P= Probability that the null hypothesis is true.

Power of performed test with alpha = 0.050

Group Name (Cluster)	**N**	**Missing**	**Mean (μm^2)**	**Std Dev**	**SEM**
PUD	10	0	194.61	126.603	40.035
C15	10	0	154.727	73.162	23.136
C15+ SiO_2	10	0	199.78	123.404	39.024
Commercial Paint	10	0	92.972	55.067	17.414
F. glass composite	10	0	270.527	163.422	51.679
Source of Variation	**DF**	**SS**	**MS**	**F**	**P**
Between Groups	4	169806.029	42451.51	3.199	0.021
Residual	45	597138.027	13269.73		
Total	49	766944.055			

Table 28: All Pairwise Multiple Comparison Procedures for the clustering formation area for the coatings tested (Holm-Sidak method). Overall significance level = 0.05

Comparison	Diff of Means	t	Unadjusted P	Critical Level	Significant?
F. glass composite vs. Commercial paint	177.555	3.447	0.001	0.005	Yes
F. glass composite vs. C15	115.8	2.248	0.03	0.006	No
C15 + SIO_2 vs. Commercial paint	106.808	2.073	0.044	0.006	No
PUD vs. Commercial paint	101.638	1.973	0.055	0.007	No
F. glass composite vs. PUD	75.917	1.474	0.148	0.009	No
F. glass composite vs. C15 + SIO_2	70.747	1.373	0.176	0.01	No
C15 vs. Commercial paint	61.755	1.199	0.237	0.013	No
C15 + SIO_2 vs. C15	45.053	0.875	0.386	0.017	No
PUD vs. C15	39.883	0.774	0.443	0.025	No
C15 + SIO_2 vs. PUD	5.17	0.1	0.921	0.05	No

4.5 Conclusion

The aim of this work was to study and explore how different Scophthalmus rhombus bio-inspired topographic textures and coatings perform against biofouling under laboratory conditions using the benthic algal model organism N. ovalis, in order to have a holistic test both at laboratory level and its application in a real situation such as a tidal turbine (Chapter 5).

Initial results from adhesion studies involving *N. ovalis*, under static laboratory conditions showed that the textures A1, A2 and A3 show promise as an alternative non-toxic antifouling solution that could be tested in real marine conditions with a small-scale turbine.

This findings despite the results of percentage coverage led to the hypothesis that Brill's micro-topographical features could inspire the design of a novel antifouling surface for laboratory scale because not only reduce the percentage of organisms covered in the surface, they disrupt the formation of agregates and clusters formation and allowing us to suggest the hypothesis or premise for chapter 6 in which one of these textures will be tested under dynamic conditions using a marine turbine.

We can also conclude that the use of image segmentation techniques in the laboratory in combination with the use of benthic organisms such as the diatom *Nitzschia ovalis* can help us to understand the performance of different materials and coatings against the early stages of biofouling which is mainly composed of microscopic organisms such as bacteria, algae, as well as the adsorption of extracellular polymeric substances (EPS).

These types of easy-to-implement techniques allow small-scale analyses to be carried out in controlled laboratory environments for the selection of materials and coatings for the marine environment..

In terms of coating selection, coating 15 and PUD showed good performance compared to the controls, however, coating 15 with SIO_2 nanoparticles showed the best performance in percentage surface area covered of the coatings tested. However, although these values were slightly lower than the reference antifouling paint and certainly much better than the composite on which they are applied, it is still far from the commercial antifouling paint in terms of cluster formation. This formation of clusters favouring the formation of a biofilm and in the long term and therefore potentially faster colonisation by higher organisms typical of more advanced stages of the biofouling process could potentially cause structural problems on tidal turbine rotors and blades.

Chapter 5

A novel approach to assessment of biofouling in a tidal turbine

5.1 Introduction

Marine tidal energy is a form of renewable energy that harnesses the power of tides to generate electricity [230]. Tidal energy is generated by the movement of water caused by the gravitational pull of the moon and sun on the earth. The tides cause a rise and fall in sea level, which can be captured and converted into electricity using a variety of technologies.

One common method for generating tidal energy is the use of tidal turbines. These are similar to wind turbines, but they are placed in the water and are driven by the movement of tides (Figure 44). Tidal turbines can be installed in a variety of locations, including in shallow water near the coast, in estuaries, and in deeper water offshore.

Other technologies for generating tidal energy include tidal fences and tidal barrages [230,231]. Tidal fences consist of a series of turbines that are suspended from a floating platform and are driven by the movement of water passing through them. Tidal barrages are large structures that are built across an estuary or tidal channel and use gates or turbines to capture the energy of the tides as they flow in and out.

Marine tidal energy has several potential benefits as a source of renewable energy. It is a reliable source of power because the tides are predictable, and it does not produce greenhouse gases or other pollutants [231]. However, there are also some challenges associated with tidal energy, including the cost of building and maintaining the necessary infrastructure and the potential impact on marine ecosystems [232–234].

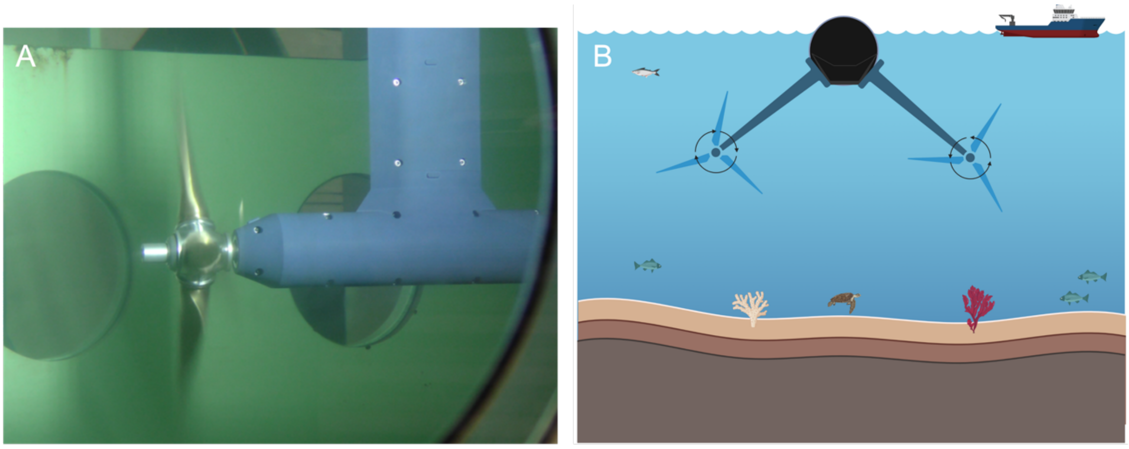

Figure 44: A: Small-scale marine turbine test rig. B: Schematic-design of a structure for tidal power production in the sea. (Figure A source: Nemmo Project 2020 available here http://nemmo.eu/)

5.1.1 Maintenance in marine energy

Maintaining marine tidal energy systems in the sea can be a challenging task due to the harsh and corrosive nature of the marine environment [235,236]. These systems are exposed to saltwater, waves, storms, and other environmental factors that can wear down and damage the equipment over time. In addition, biofouling and other forms of marine growth can interfere with the operation of tidal energy systems and require regular cleaning and maintenance.

To maintain marine tidal energy systems, it is important to have a robust and well-planned maintenance program in place. This might include regular inspections, cleaning and maintenance of the equipment, and the use of protective coatings and other measures to prevent corrosion and biofouling. It is also important to have a plan in place for repairing any damage or failures that may occur.

The key to maintaining marine tidal energy systems is to be proactive and to implement regular and effective maintenance and repair procedures [236]. By taking a proactive approach, it is possible to extend the lifespan of these systems and ensure their continued operation.

5.1.2 How biofouling affects marine energy

Biofouling can be a significant problem for marine tidal turbines and other underwater structures. As organisms such as algae, barnacles, and mussels attach to the surfaces of these structures, they can interfere with their operation and reduce their efficiency. Biofouling can also increase the weight and drag of the structures, making them more difficult to move and requiring more energy to operate.

For example, cavitation phenomenon, occurs when the pressure of a fluid at a specific point decrease so much that water vapour is generated, and when the pressure increases again, that vapour collapses generating shock waves and gas bubbles [71]. This process can cause erosion of metal surfaces and can have a significant impact on the durability of underwater structures such as ships propellers or turbine impellers (Figure 45) [237].

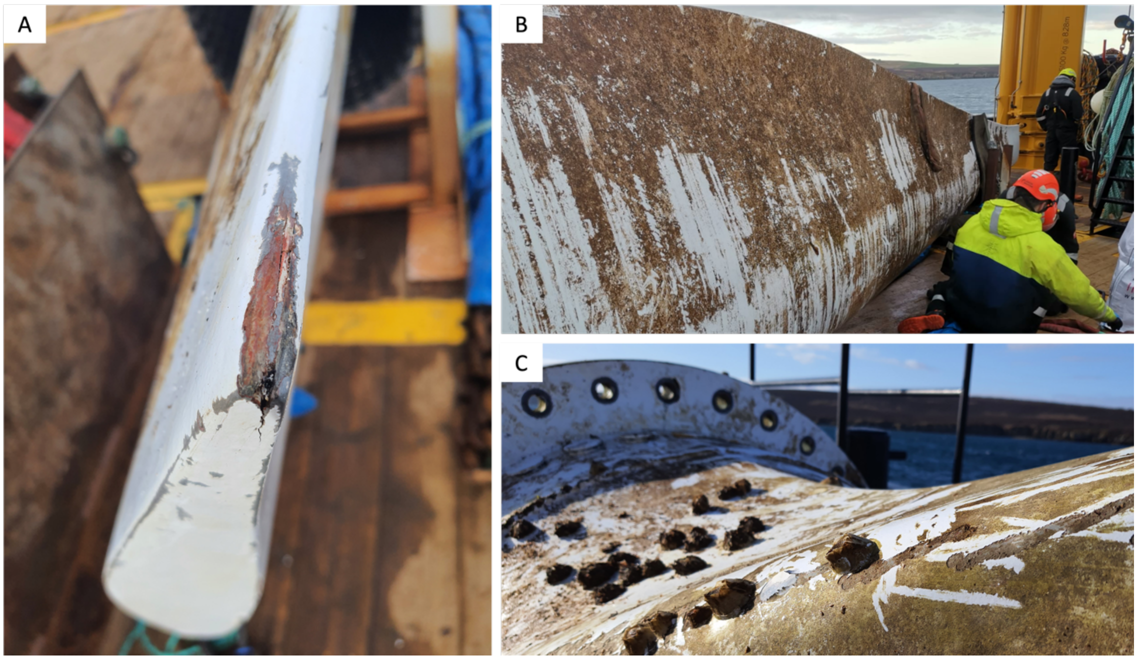

Figure 45: Effect of biofouling on tidal turbines. Image A shows the damage of the composite on the blade tip, probably due to cavitation processes. B shows the surface of the turbine blade completely covered by algae and slime and C shows the colonisation of barnacles on the part closest to the axis of rotation where the speed and shear stress is lower than at the tip (A) [238]

In terms of how it affects biofouling, studies suggest that cavitation can have a positive effect on the prevention of biofouling due to mechanical erosion caused by shock waves and gas bubbles [239]. Some studies in the area of human health in particular dentistry, the use of cavitation techniques is very useful for biofilm removal [240]. In addition, cavitation can also create an unfavourable environment for fouling organisms due to pressure fluctuations and high-water velocities. Therefore, further research is needed to assess precisely how cavitation affects biofouling. Furthermore, it is important to note that prevention of biofouling requires a holistic approach that includes mechanical as well as chemical and biological measures.

There are several ways to prevent or reduce biofouling on marine tidal turbines and other underwater structures. One common method is the use of antifouling coatings, which are applied to the surface of the structure and release chemicals that inhibit the growth of fouling organisms [8,18,65,131,211]. Other methods include the use of physical barriers such as screens and the application of biocides or other chemicals. Regular cleaning and maintenance can also help to reduce biofouling.

In recent years, there has been increasing interest in developing more environmentally friendly methods of preventing biofouling, such as the use of biodegradable coatings [18,65,131,194,201,211]. It is important to consider the potential impact of these methods on the marine environment and to carefully assess the risks and benefits of different approaches.

Antifouling coatings are a common method for preventing or reducing biofouling on man-made structures such as ships, oil platforms, pipes but in tidal turbines too. These coatings are applied to the surface of the structure and release chemicals that inhibit the growth and attachment of fouling organisms such as algae, barnacles, and mussels.

5.2 Aims and objectives

The objectives of this chapter were to test the non-disruptive biofouling quantification technique employed in previous chapters based on pixel segmentation and machine learning on the best performing coatings in chapter 4 and the bioinspired textured coatings designed by Dr Chloe Richards, DCU based on *Scophthalmus rhombus*.

5.3 Materials and methods

5.3.1 Sampling location and test-rig description

Flow induced stresses are known to impact biofilm formation over marine surfaces slowing down growth and reducing its sensitivity to surface properties [241]. The effect is particularly noticeable on the exposed surfaces of marine tidal turbines which experience large increases in mean stresses as the radial position over the blade varies from root to tip. There is evidence from sea trial by the Magallanes that larger hard fouling organisms are found only near the hub mostly in the relative shelter of the lee. Further from the centre of rotation, biofouling growth develops as a slime layer. In collaboration with DCU School of Mechanical and Manufacturing Engineering a new and unique marine test platform was developed to expose sample materials to a non-uniform stress distribution to mimic this effect. The system was designed to reproduce hydrodynamic stresses which are characteristic of conditions experienced over the turbine used for tidal energy (Figure 47).

This custom floating test platform was designed and built at Dublin City University (DCU), Ireland and was deployed in the Malahide marina in Dublin Bay (Figure 46) This location was chosen as it is a sea water estuarine environment with a high peak tidal flow and flushing. The marina has the additional benefit of providing access to a very sheltered sea water berth offering improved safety and reducing additional hydrodynamic stresses that the motion of the platform could otherwise induce.

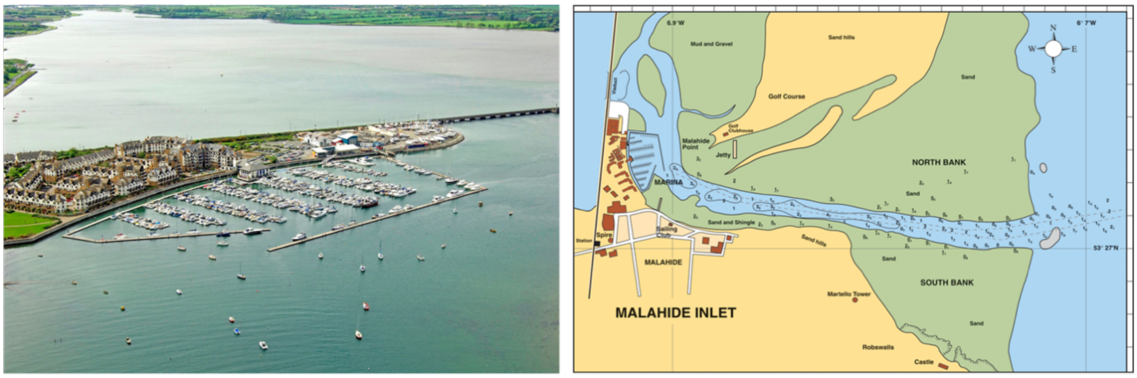

Figure 46: Deployment site at the Malahide Marina. Left: aerial photograph of the Malahide estuary. Right: detailed plans of the Malahide inlet and surrounding sandbanks.

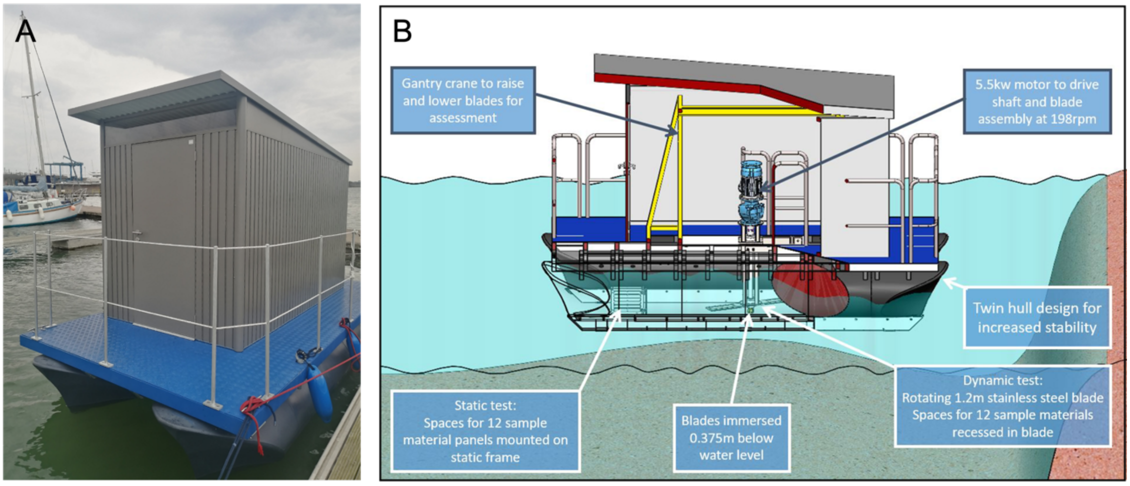

Figure 47: Marine test platform in the sea, [A] Image of the system moored at the Malahide Marina, [B]. (Images courtesy of the School of Mechanical & Manufacturing Engineering in DCU)

The system comprises a two-blade impeller assembly with a diameter of 1.2 meters (Figure 49). Each blade is capable of accommodating a maximum of six flat panels, with three panels positioned on each blade surface. These rectangular panels measure 330 mm in length and 40 mm in width. To ensure a flush and aligned installation with the blade surface, the panels are recessed accordingly. The blade rotation is powered by a 5.5 kV motor, enabling precise speed control. The rotating assembly was contained within the structure of the rig above the waterline and a fully encapsulating steel mesh below the waterline, providing a layer of protection. The blade and rotating assembly can be raised and lowered using a permanently mounted gantry crane and chain hoist, this allows for regular detailed assessments of the biofouling on the dynamic samples mounted on the blade. The evolution of the biofouling coverage was used to develop material specific behavioural model intended to characterize biofouling growth. Images of the marine test platform are shown in figure 48 while the rotating turbine assembly is shown in figure 49

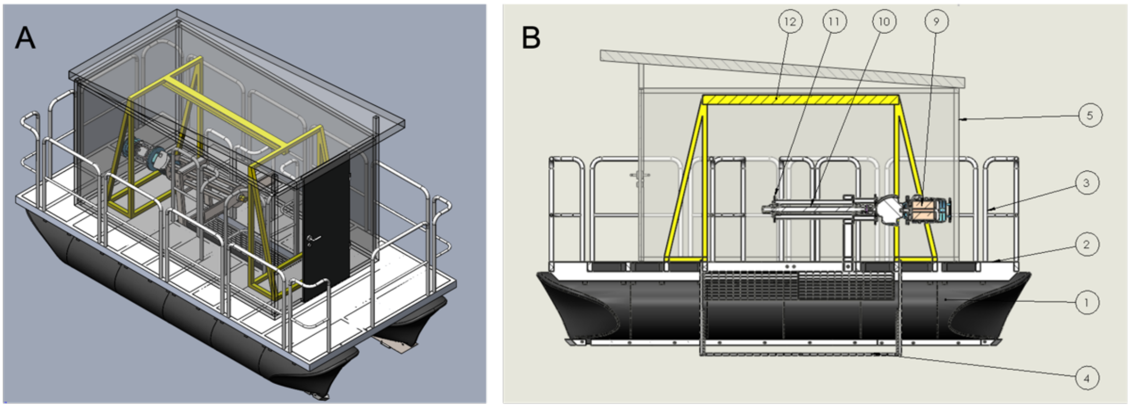

Figure 48: A: Schematic representation of the platform. B: complete detailed list of parts included in this test rig. 1) Primary hull/pontoon (consisting of pontoon floats, and structural frame) 2) Aluminium decking 3) Safety railings 4) Protective cage 5) Enclosure 6) Electrical supply and control panel 7) Light fittings 8) Mooring equipment 9) Motor and gearbox combine unit 10) Rotating assembly 11) Blades and samples 12) Gantry crane 13) Manual chain hoist (Images courtesy of the School of Mechanical & Manufacturing Engineering in DCU).

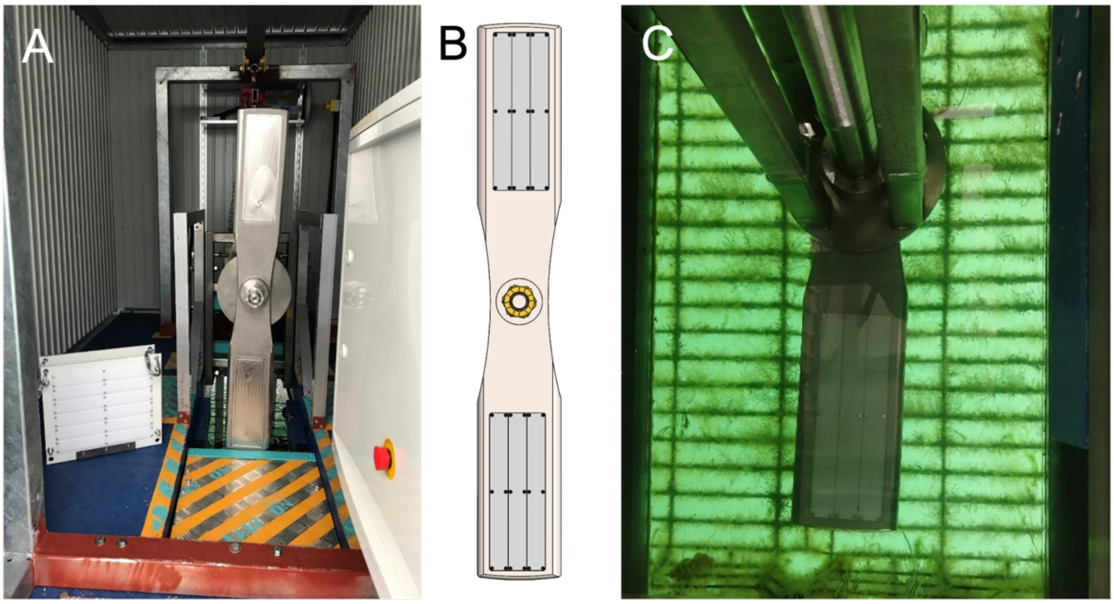

Figure 49: Blade in the raised position (A), CAD rendering of the full blade including position of six test samples located on the lower surface of the blade (B), Blade in the water (C) (Images courtesy of the School of Mechanical & Manufacturing Engineering in DCU)

5.3.2 Sample set-up for dynamic test campaing

The four coatings used in chapter 5 were selected for the dynamic test campaign are listed in Table 29. The best performing biomimetic textures identified in chapter 5 were included in the study. An image of the texture is shown in figure 50. All coatings are applied on rectangular panels made from the control composite design by INPRE Composites S.L (La Rioja; Spain). and supplied by CANOE (Paris, France).

The samples were positioned on the flat surfaces of the two-blade impeller fitted to the floating platform. The panels were arranged radially from the axis of rotation of the impeller and fitted within a shallow recess to be flush mounted over each of the four surfaces of the impeller.

Table 29 Coatings selected for long term assessment of antifouling performance.

Sample	Characteristics
Plain coated composite (Control)	200 µm thick coating made from Policor® GEL ISO NPG PA Ral 9003 gelcoat from Polynt with the Luperox® K12 G catalyst from Arkema (Paris; France)
PUD	Water-based polyurethane 1K resin
C15	Solvent-based polyurethane 2K resin
C15 + SiO_2NP	Solvent-based polyurethane 2K resin + 1% silica nanoparticles

The distribution of the sample panels made up of the different candidate coatings is detailed in Table 30 and Figure 51. The impeller is rotated at a rate of $194.8\ RPM$ for $30\ min$ every day for the full duration of the testing period, that was 24 weeks. The periodic shearing served to accelerate the growth rate of biofouling by allowing organisms to settle before subjected them to surface stresses. The duration over which shearing is applied was chosen to exceed what is typically used in detachment studies.

The samples were positioned on the flat surfaces of the two-blade impeller fitted to the floating platform. The panels are arranged radially from the axis of rotation of the impeller and fitted within a shallow recess to be flush mounted over each of the four surfaces of the impeller.

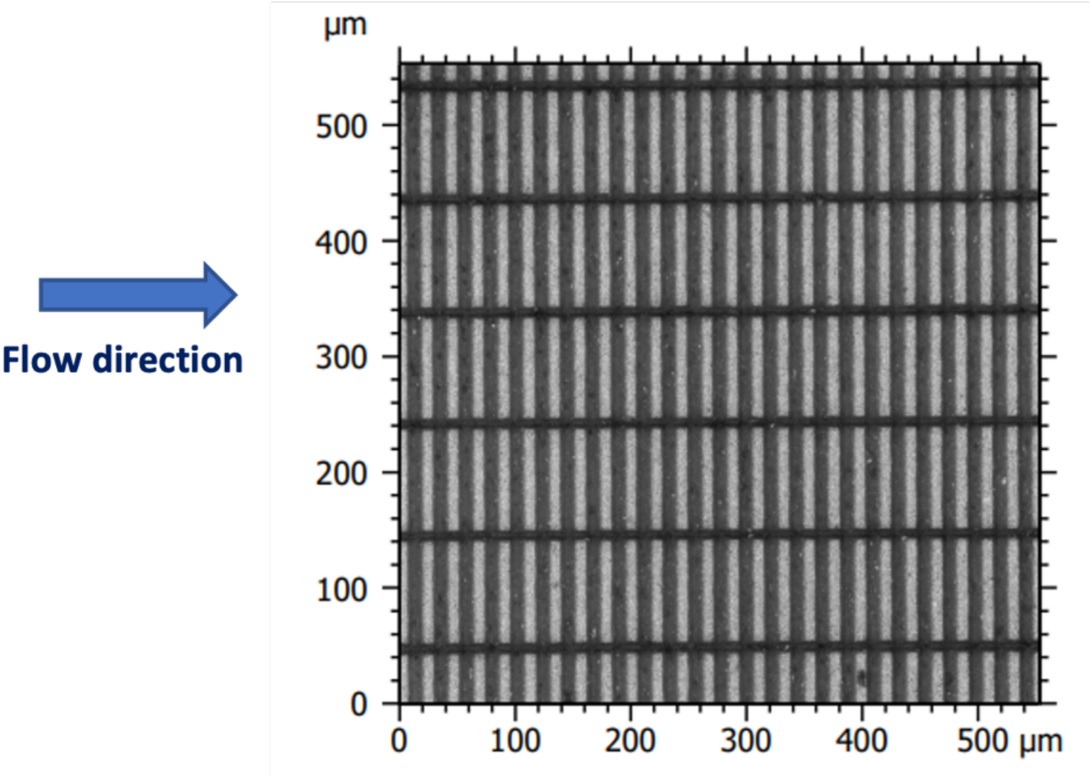

Figure 50: Diagram of the Bio-mimetic textures based on Scophthalmus rhombus and its dimensions. The arrow indicates the flow direction.

Table 30: Characteristics and position of sample materials tested

Upper surface of blades B4	
Front sample	POM-C
Middle sample	Coating 15 + SiO_2 Nanoparticles
Rear sample	Plain coated composite (control)
Upper surface of blade B3	
Front sample	Plain coated composite (control)
Middle sample	PUD
Rear sample	PUD
Lower surface of blade B2	
Front sample	Plain coated composite (control)
Middle sample	Coating 15
Rear sample	Coating 15
Lower surface of the blade B1	
Front sample	Control composite
Middle sample	Bio-mimetic textures
Rear sample	Bio-mimetic textures

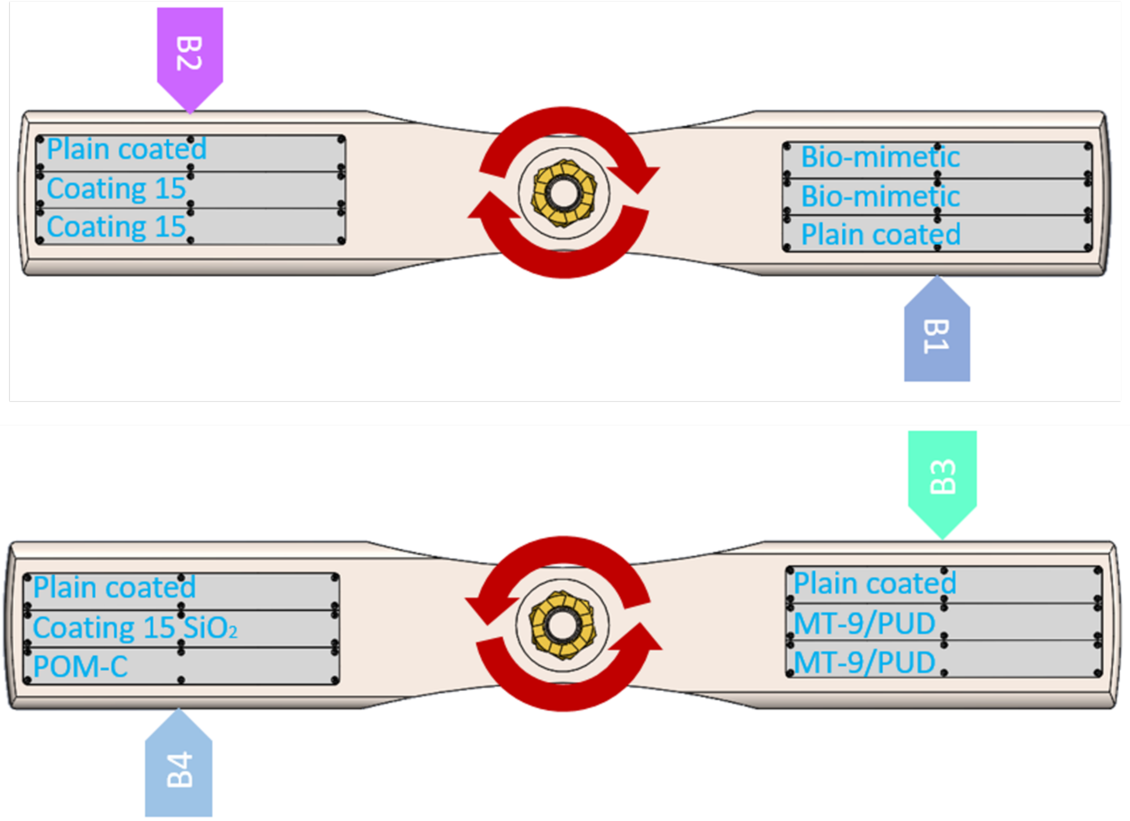

Figure 51: Top and bottom section of turbine (B1-B4) showing sample configuration.

5.3.3 Sample Analysis

The analysis has relied on periodic visual inspections of each sample over inspection windows of dimension $10\,mm$ by $10\,mm$ positioned along a sampling line parallel to the blade leading edge and centred at positions $r = \{0.255, 0.369, 0.459, 0.519, 0.569\}\,mm$. This position is defined as the projected position along a radial line which passes through the blade axis of rotation and is parallel to the blade leading edge. These inspection windows for the three samples on one side of the impeller blade are shown in Figure 52.

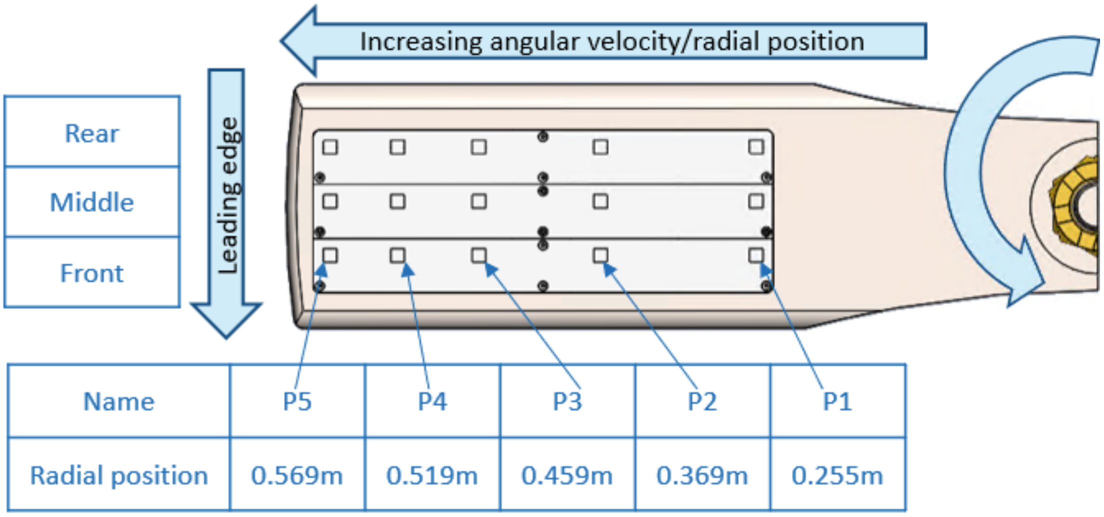

Name	P5	P4	P3	P2	P1
Radial position	0.569m	0.519m	0.459m	0.369m	0.255m

Figure 52: Explanatory turbine blade section showing the control points for the three samples at which the microscope photographs were taken for the analysis (P1-P5) and their distance in relation to the turbine's axis of rotation. The direction of rotation and the increase in angular velocity are also shown.

5.3.4 Shear stress calculation

Computational Fluid Dynamics (CFD) simulations have been used to estimate the stress distribution over the impeller surface. The simulations were conducted by Dr. Yan Delauré and PhD-student Philip Daly (School of Mechanical & Manufacturing Engineering in DCU) assuming a tidal stream velocity of 0.5 m/s, resulting in higher stresses experienced by the advancing impeller compared to the receding half. In figure 50 and table 31 is shown the instantaneous stress distributions on both the upper and lower surfaces of the impeller along the three sampling lines. These results were obtained as the impeller passed under the hull. It was anticipated that this passage would lead to flow acceleration and increased stresses. However, upon comparing the upper and lower surfaces, no noticeable effect is observed. While the front and rear sampling locations exhibit similar stresses, a predicted increase of 6-7% is observed for the middle line.

The most significant factor affecting stress levels is the radial position. As the inspection window moves from positions $P1$ to $P5$, the stress experiences an approximately four-fold increase. This indicates a strong correlation between stress levels and the radial position along the impeller (Figure 53 and Table 31)

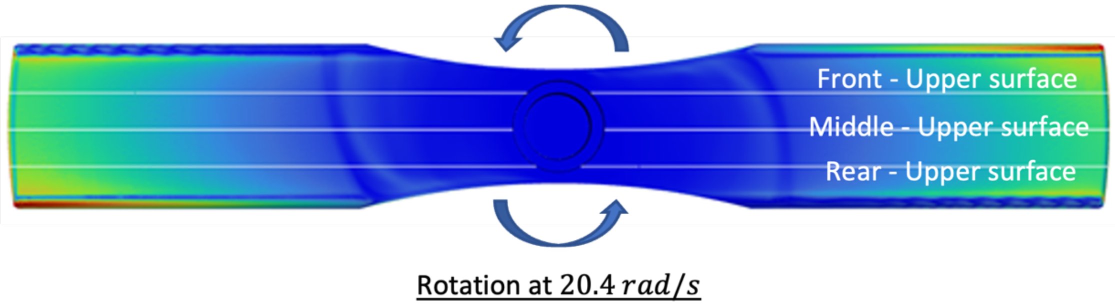

Figure 53: View of impeller lower surface showing the sampling lines. (Images courtesy of the School of Mechanical & Manufacturing Engineering in DCU)

Table 31: Minimum and maximum shear stress at sampling positions showing the minimum and maximum values.

	Maximum					**Minimum**				
Position **Front Line**	$P1$	$P2$	$P3$	$P4$	$P5$	$P1$	$P2$	$P3$	$P4$	$P5$
Stress $[N/m^2]$	72	132	191	236	276	51	104	158	199	236
Position **Middle Line**	$P1$	$P2$	$P3$	$P4$	$P5$	$P1$	$P2$	$P3$	$P4$	$P5$
Stress $[N/m^2]$	76	140	204	252	295	53	111	169	213	253
Position **Rear Line**	$P1$	$P2$	$P3$	$P4$	$P5$	$P1$	$P2$	$P3$	$P4$	$P5$
Stress $[N/m^2]$	71	131	189	233	273	51	103	159	197	234

5.3.5 Biofouling evolution from field test

Imaging of the biofouling was obtained by taking photographs of the panels in situ with the RS PRO USB microscope (Figure 54) (Radionics, Ireland) connected to Panasonic Toughbook FZ-55 for real-time monitoring and adjustments of light and exposure using Portable Capture Plus software. Photographs were taken at 30x magnification with a resolution of 12M and sRGB IEC61966-2.1 of colour profile to speed up the subsequent computing analysis. To calibrate the scale of the images, topographic textures were used which have a known length of their artefacts (10 μm between rectangles) previously checked with precision microscopic equipment in the laboratory. The methodology developed to analyse the images relies on post-processing using a supervised clustering model [94]

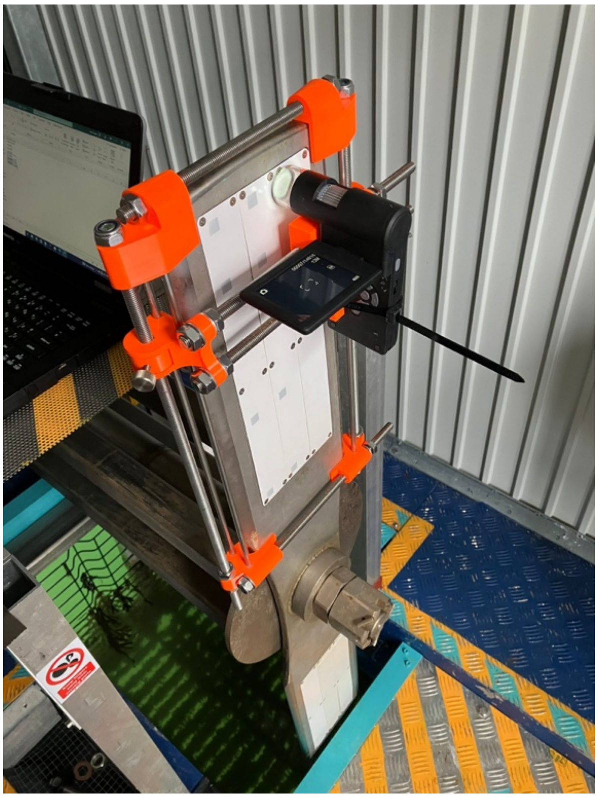

Figure 54: . Imaging setup with guides to position the microscope over the inspection windows.

The dynamic testing started on the 24th December 2022 and images were acquired at Weeks 1, 2, 6, 9, 17. Sample raw and processed images with estimated coverage percentage for the control composite, the textured composite, the Coating 15, the Coating 15 with silica nanoparticles and the PUD coating at Week 24 using the same methodology as chapter 3 and chapter 4.

To assess biofouling growth over the course of the study, a regression model was constructed in the same way as in chapter 3 in order to apply the image segmentation technique and model biofouling growth in a simple way.

To fit the graphical representations, a 4-parameter sigmoidal regression (equation 5) was applied using Sigmaplot version 11 (build 11.0.0.77) by Systat Software, Inc, based in California, United States. The default number of interactions was set to 200 in order to achieve the optimal fit. A tolerance level of $1x10^{-10}$ was utilized, and parameter standard errors in weighted regression were computed using the Chi-Square method. The normality of the data was assessed through the Shapiro-Wilk test, with a sample size limit of ≤5000 and a rejection threshold (P-Value) of 0.05. Subsequently, we focused on studying the exponential growth phase from the key function parameters (see chapter 3).

(Equation 5)

$$Y = Y_0 + \left(\frac{a}{1 + e^{-\left(\frac{x - x_0}{b}\right)}}\right)$$

5.4 Results and discussion

5.4.1 Shear stress effect on biofouling

Throughout the test campaign, two main types of biofouling were observed: slime, and barnacles. However, other biofouling organisms like green microalga like *Chlorella sp.* or Ascidia larvae (Figure 55) were also observed.

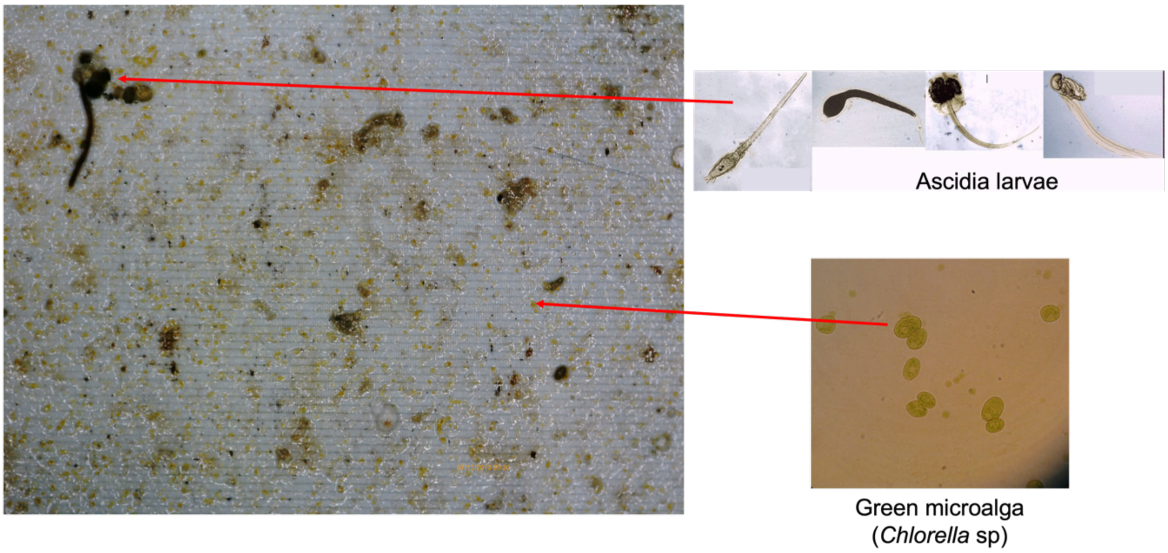

Figure 55: Characterisation of biofouling in a microscopy image taken with the RS PRO USB microscope camera-microscope at a magnification of 30x and a resolution of 12 megapixels. A larva belonging to the Ascidia group and small green spots potentially recognised as green microalgae (potentially Chlorella sp.) can be seen.

The growth of biofouling was found to be significantly influenced by the type of coating and radial position. The results at Week 24 provided valuable insights, revealing a consistent decrease in coverage as the radial position increases, in particular with barnacles. During the initial stages of barnacle development, when the barnacle exists as a mobile larva seeking a suitable surface for attachment, the shear force necessary for adhesion is relatively lower (Figure 56) [242–244]. This observation provides additional insight into the gradual colonization pattern exhibited by barnacles, whereby they tend to establish themselves first in areas characterized by lower shear stress ($P1$ and $P2$) before progressing towards locations with higher shear stress ($P4$ and $P5$).

The lower shear force requirement in the larval stage enables barnacles to initiate attachment in regions where the water flow or shear stress is comparatively mild [244]. These less turbulent environments provide a favorable condition for the larval barnacles to settle and form initial attachments. As the barnacles grow and mature, they exhibit a remarkable ability to adapt and withstand progressively higher levels of shear stress, allowing them to gradually spread to areas with greater hydrodynamic forces.

This gradual colonization behavior of barnacles is attributed to their biological strategy of optimizing their attachment strength in response to varying shear stress conditions. By strategically selecting fewer demanding environments in the early stages, barnacles can establish a stronger foothold and develop enhanced adhesion mechanisms, enabling them to thrive in areas with higher shear stress as they progress in their life cycle. So as result of this we can observe that barnacles, primarily settle and grow between positions $P1$ and $P2$, (Figure 57). In position $P1$, which is situated closer to the axis of rotation at a distance of 0.255

mm, the shear stress are comparatively lower (51.67 - 73 N/m^2) compared to positions further away. This explains the formation of barnacle clusters near positions $P1$ and $P2$ (Figure 57). In positions further away from the turbine rotation axis where the shear force is higher (for example for $P5$ is 241-281 N/m^2), the amount of barnacles was practically null and they were only found in regions such as bolts, grooves and panel joints where they can maximise the anchoring points.

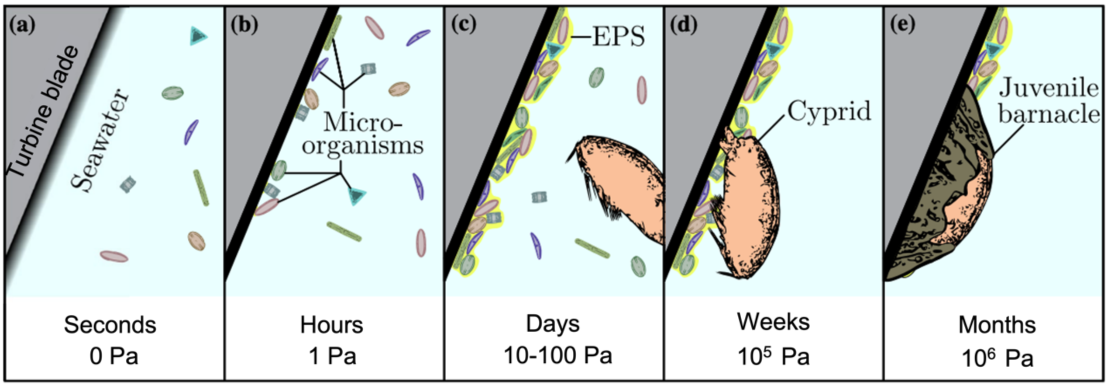

Figure 56: Schematic representation of the adhesion of the different stages of barnacles on the surface of the blade over time and the shear force required to remove them. (Modified from [245])

Furthermore, it is noteworthy that shear forces were found to be capable of removing larger barnacles even at lower radial positions and within clusters (Figure 57). This observation helps explain the significant decreases in coverage measured at certain locations as the test progressed.

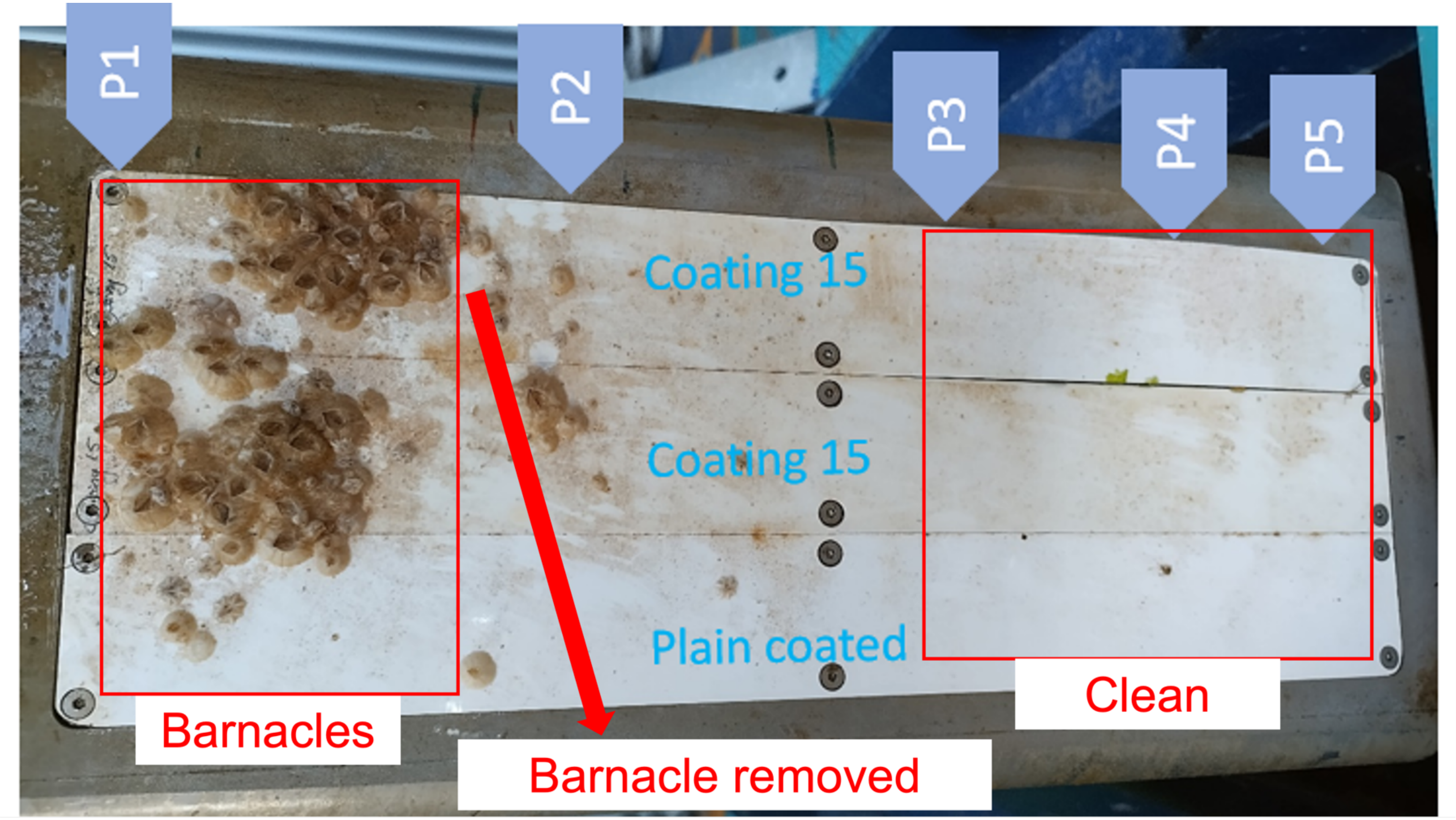

Figure 57: Longitudinal image of B1 blade in which a biofouling gradient can be observed from the more central positions with lower shear force (P1) towards the more distant positions with higher shear force (P5). White gaps are also observed near the P2 position where it is believed that the shear force has managed to remove some barnacles.

Figure 58: Sample photographic images showing B2 with the evolution of the biofouling on coating 15 middle over the duration of the testing from week 1 on the far left to week 24 on the far right.

5.4.2 Level of biofouling on different coatings

After a period of 24 weeks, it was observed variations in the extent of biofouling coverage on the surface area depending on the type of coating applied. Two coatings, PUD and Coating 15 with SiO_2 nanoparticles, demonstrated remarkable outcomes in terms of mitigating biofouling.

The favourable performance of PUD can be attributed to its gradual wear, erosion, and delamination. Although the delamination of the coating might appear counterproductive in terms of structural and material chemistry, it actually serves a beneficial purpose by aiding in the removal of adhering biofouling. The rotation of the blade generates shear forces that act upon the delaminating PUD coating (Figure 59). These shear forces, caused by the motion of the blade, exert a considerable impact on the attached biofouling organisms. As a result, the biofouling is dislodged and removed from the surface more easily compared to other coatings that do not undergo delamination. This dynamic behavior, coupled with the shear force generated during rotation, promotes the continuous removal of biofouling organisms. Consequently, the surface area covered by biofouling is reduced, leading to improved performance and efficiency of the PUD-coated surface. Some research has demonstrated the properties of self-laminating coatings to combat biofouling with very good results [246]. Nevertheless, despite the commendable outcomes demonstrated by PUD coating in combating biofouling through its self-peeling mechanism, its suitability for application in tidal turbines is questionable. The substantial shear forces generated by the rotational motion pose a significant risk of frequent detachment of this material, potentially undermining the long-term durability of turbine blades.

The limited coverage observed with Coating 15 + SiO_2 nanoparticles compared with the rest of coatings (Figure 60) can be attributed to several factors. Firstly, the low surface energy of SiO_2 surfaces provided by the SiO_2 components makes it challenging for microorganisms to adhere to the material [247,248]. This reduces the likelihood of fouling and biofilm formation. Studies have demonstrated that silica nanoparticles have the ability to enhance the presence of lysozyme on bacterial surfaces, which exhibits potent antibacterial activity and can effectively inhibit the growth of bacteria, particularly *E. coli*, for an extended period of up to 3 days [226].

Moreover, SiO_2 coatings often create a smooth surface that hinders the attachment of microorganisms and particles, facilitating easy cleaning. This feature enables the maintenance of antifouling properties by removing any accumulated particles or organisms, potentially leading to more cells being eliminated during the rinsing process after staining with acridine orange in our laboratory adhesion test showed in chapter 4.

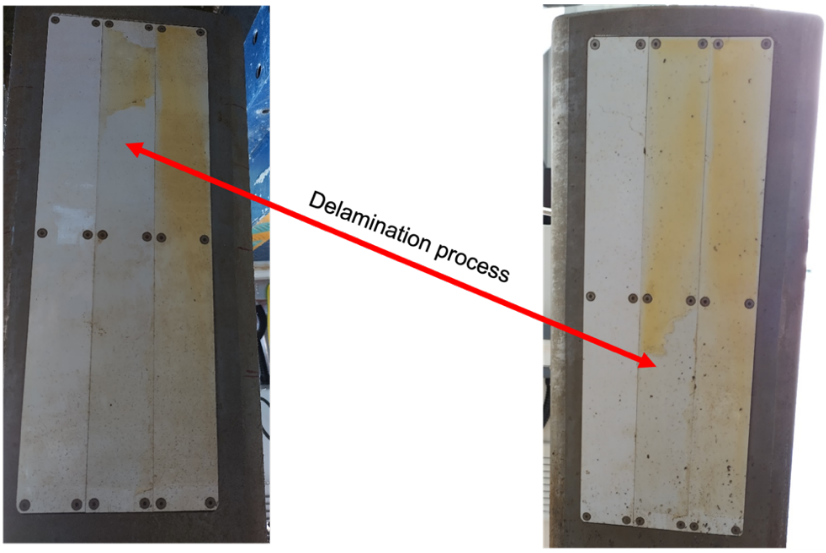

Figure 59: Images showing the PUD coating delaminating after 15 weeks of immersion. A change in colouring can also be observed, yellowing.

However, it is important to note that SiO_2 is applied in nanoparticulate form at a 1% concentration, and its small size raises concerns about potential absorption by organisms, which could result in cellular damage or other adverse consequences. Some studies have reported increased IL-6 levels in humans, DNA damage, and apoptosis associated with SiO_2 particles [227–229]. The toxicity of SiO_2 nanoparticles remains an active area of investigation, with potential risks influenced by factors such as size, shape, and surface characteristics. These results shown in a real marine environment are also in line with the results shown in the laboratory in chapter 5 where the SiO_2 particles also performed well under laboratory conditions using *N. Ovalis.*

As for the rest of the coatings, no notable differences were observed between them or even compared to the control sample. The biomimetic textures did not show a noticeable difference compared to the coating 15, or the control.

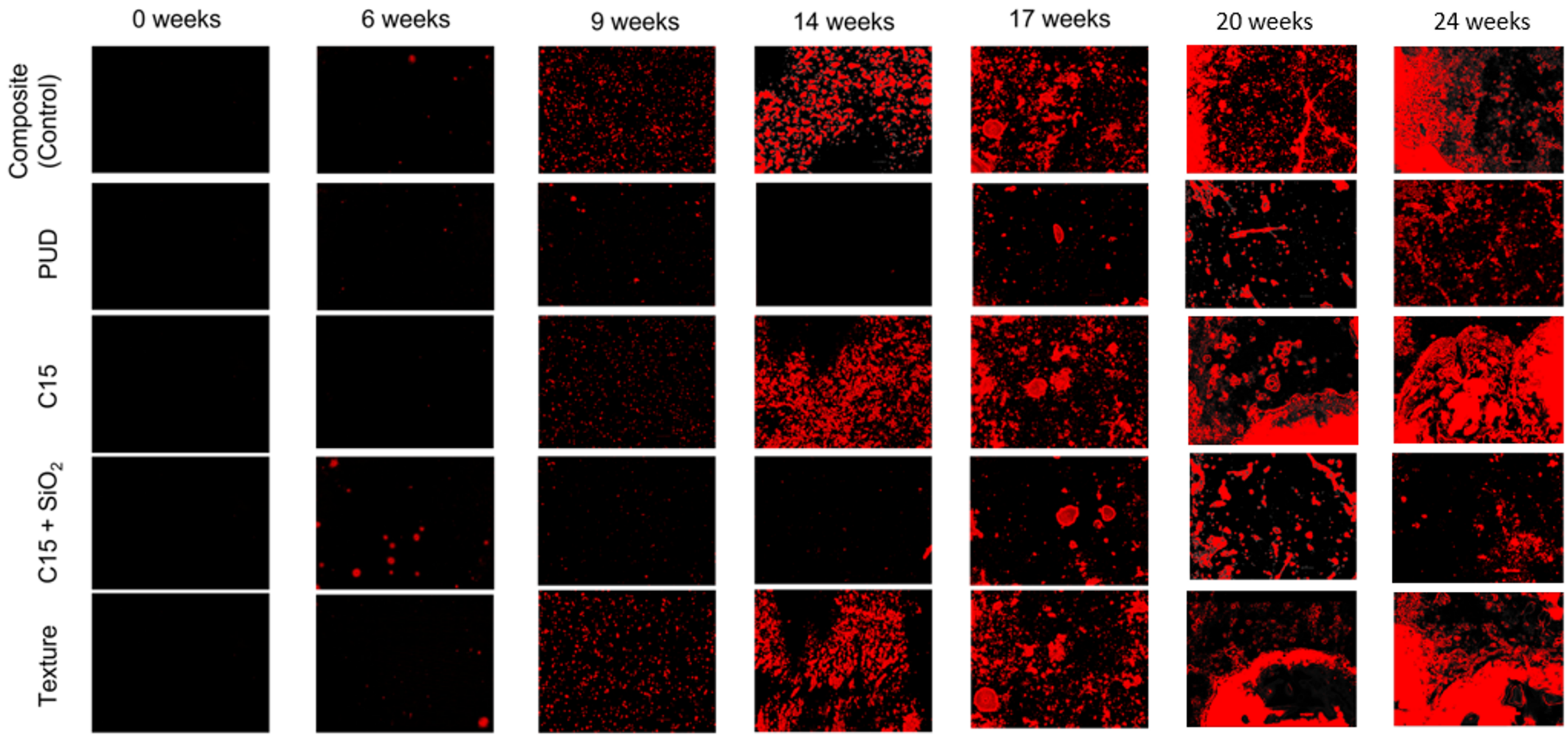

Figure 60: Processed images from visualisation with x30 magnification for all materials and position P1 along the blades. The red pixels show the biofouling cover while the black is the background without any biofouling.

5.4.3 Biofouling Growth Model

Results from three sample materials are presented here. These include a solvent based polyurethane resin with silica nano-particles (C15 SiO_2), a control composite made with the coating used on the original Magallanes hydro-turbine blade (Control) and a water based polyurethane resin (PUD). The data was acquired at three radial positions on the test turbine ($P1$, $P2$ and $P3$) where hydrodynamic surface stresses were estimated to be approximately $60\ Pa$, $230\ Pa$ and $270\ Pa$ respectively and results are shown in Figure 61, Figure 62 and Figure 63.

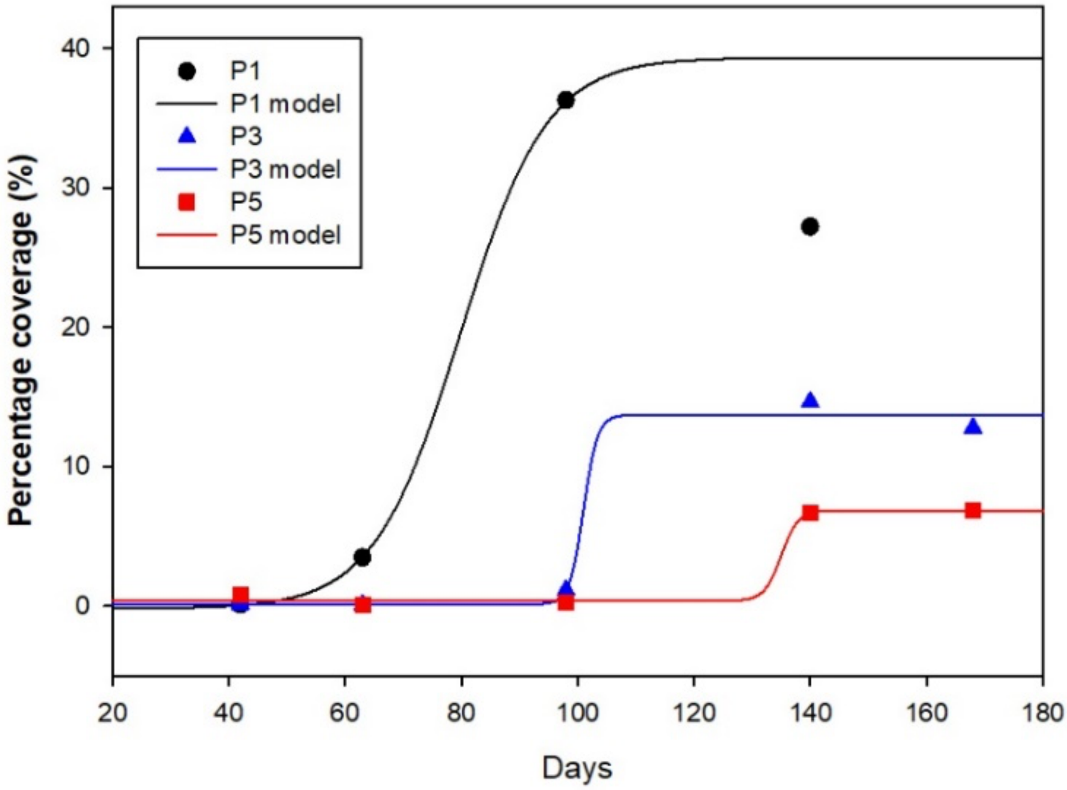

Figure 61: Evolution of biofouling coverage for C15 SiO_2 coating from 24 week test campaign and measurements at location $P1$, $P2$ and $P3$. The continuous lines represent the fitted sigmoid curves.

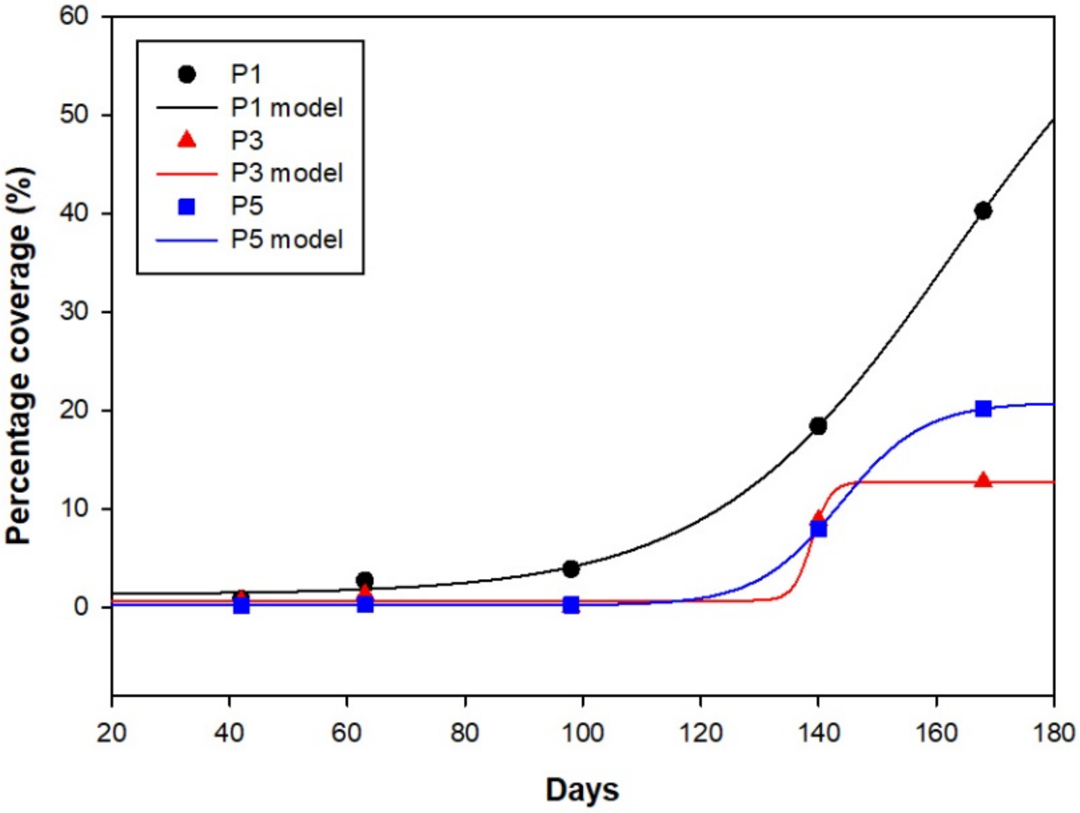

Figure 62: Evolution of biofouling coverage for Control coating from 24 week test campaign and measurements at location $P1$, $P2$ and $P3$. The continuous lines represent the fitted sigmoid curves.

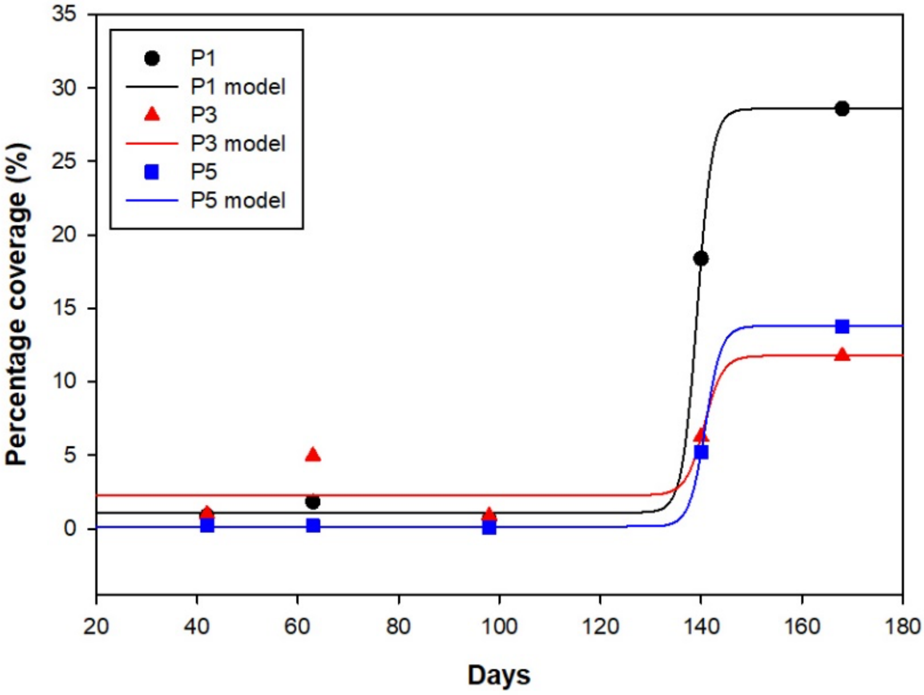

Figure 63: Evolution of biofouling coverage for PUD coating from 24 week test campaign and measurements at location $P1$, $P2$ and $P3$. The continuous lines represent the fitted sigmoid curves.

The model parameters are compared in table 32 and clearly show that the increases in surface stresses between $P1$ and $P3$ consistently reduces the asymptotic cover for all materials. Beyond $P3$ to $P5$ the change is not as as consistent. While the asymptotic cover decreases with C15 SiO_2 the opposite is observed with PUD and the control coating. In all cases however the change is small and biofouling at both $P3$ and $P5$ is exclusively from biofilm rather than the mix of biofilm and hard shell macro fouling seen at $P1$. From the data shown here, the C15 SiO_2 outperforms other coating where surface stresses are higher. It is also interesting to note that the material is also shown to have the capacity to generally delay the exponential growth phase.

Table 32: Sigmoid parameters for different sample coatings and hydrodynamic stresses

		Y_0 Initial cover	a Asymptotic cover	x_0 Latency delay	b Rate of relaxation
C15 SiO_2	$P1$	0	39.5	80	0.13
	$P3$	0	13.6	101	0.8
	$P5$	0.4	6.5	135	0.7
Control	$P1$	1.3	69.1	163	0.05
	$P3$	0.7	12.1	139	0.6
	$P5$	0.2	20.6	144	0.14
PUD	$P1$	1.1	27.5	139	0.6
	$P3$	2.3	9.5	140	0.5
	$P5$	0.1	13.6	140	0.6

5.5 Conclusion

This is the first study of novel textures and modified composites in a dynamic deployment environment to assess biofouling behaviour related to sheer stress. In this study, a variety of coatings were subjected to hydrodynamic stresses ranging from 70 Pa to 250 Pa by rotating the samples immersed in the sea at Malahide marina. These stresses were applied daily for a duration of 30 minutes.

The results indicated that, with the exception of the PUD material, none of the samples experienced significant wear or degradation. Among the tested coatings, the Coating 15 with silica nanoparticles demonstrated the best performance as an antifouling coating.

In relation of the colonization and the shear stress, barnacles are primarily observed between positions $P1$ and $P2$, where the surface shear stresses do not exceed 140 Pa. These barnacles settle in a small recess at the leading edge of the samples and tend to form clusters. Interestingly, there is evidence of barnacles being removed, likely due to shear forces, including at the lower radial position of $P1$. Moving further away from the root of the blade, biofouling takes the form of a thin biofilm. These observations are consistent with findings from a full-scale turbine after one year of operation. These findings emphasize the importance of considering the effects of shear stress on biofouling when designing and optimizing rotating systems such as blades. By understanding the relationship between these factors and biofouling distribution, researchers can develop strategies to mitigate and manage biofouling more effectively, leading to improved performance and efficiency in various applications, including marine propulsion and energy generation. The results herein contribute greatly to knowledge of marine energy studies to better understand the impact of operating in the marine environment. While the deployment site has specific characteristics, it is representative of a marine environment where biofilm growth can be monitored from early stages to establishment. These results can inform further studies on marine blade design and operation, as well as presenting standard test methods for such devices.

Chapter 6

Conclusions and future work

Over the past few years, the importance of preventing biofouling in marine environment and the development of environmentally friendly antifouling methods have been steadily increasing. This is especially notable in fields like sensor technology and materials research within the maritime sector. In order to advance antifouling technology, it is crucial to thoroughly assess the interaction between cells and surfaces to effectively hinder cell adhesion at both the microfouling and macrofouling levels. Nowadays there are different methods of analysis of biofouling such as the use of molecular markers like 18S RNA which provide us with information on the biodiversity of organisms on different materials and coatings allowing us to choose those that best resist the problem of biofouling and reduce maintenance periods. However, its high cost, as well as its great complexity or more importantly, the preservation of the biofilm when extracting the sample, makes it a complex method to apply so that alternatives such as the quantification of biofouling using basic techniques of computer image segmentation can establish a new way to evaluate biofouling in a fast, simple and effective way.

The objective of this thesis was to establish a method to efficiently and accurately evaluate biofilm growth in surfaces. To this end the use of image segmentation techniques on different materials used in the construction of sensors was studied. A growth model was developed for different materials based on the observation of biofouling both for the manufacture of sensors and for the improvement of the antifouling properties by using polyurethane based coatings, biocides using nanoparticles as well as bioinspired methods in nature such as the topography of *S. rhombus* under controlled laboratory conditions but also applied in a real marine turbine in the sea.

Chapter 2 investigates different biofilms formed on different materials used in the construction of sensors as well as attempts to establish new techniques for biofilm evaluation such as computer image segmentation or manual barnacle counting, which allows us to understand how these techniques work and then be applied in the different chapters.

In Chapter 3, all the lessons learned in Chapter 2 are collected and an attempt is made to create a very simple sigmoidal regression model for different materials placed in the sea to explain their growth pattern, as well as to continue investigating the capabilities of image classification using computer segmentation techniques.

In chapter 4 investigates how different coatings and topographies bioinspired in *S. rhombus* respond to the adhesion of the diatom used in the laboratory *Nitzschia ovalis* using image segmentation techniques developed in the last two chapters and gives useful information about the performance of these materials and coatings to be applied in a real scenario in chapter 5.

Chapter 5, takes all the learning from the previous chapters and applies it to a real-life situation where biofouling represents a major challenge, the energy sector with the deployment of a small-scale turbine in Malahide Marina. This chapter lays the groundwork for the development of methods to quantify biofouling in a fast, cheap and simple way by exploiting image segmentation techniques aided by machine learning algorithms.

6.1 Future Work

Based on the outcomes of this research there is potential for further research. Future work should focus on advancing the capabilities and applicability of image segmentation analysis for biofouling mitigation, with an emphasis on real-time monitoring, autonomous cleaning systems, environmentally friendly solutions, and a deeper understanding of biofouling dynamics in changing marine environments. Such research efforts have the potential to revolutionize biofouling management practices, enabling more efficient and sustainable operation of marine water sensors and tidal energy systems.

Some future work in the field of biofouling mitigation for marine water sensors and tidal energy systems using image segmentation analysis can focus on several key areas:

1. Refining and optimizing image segmentation algorithms: Continued research is needed to develop more accurate and efficient image segmentation algorithms specifically tailored for biofouling analysis. This involves exploring new techniques such as semantic segmentation, instance segmentation, and multi-modal imaging to improve the detection and classification of fouling organisms.
2. Building comprehensive biofouling databases: Creating large-scale, annotated databases of biofouling images will facilitate the training and validation of image segmentation models. These databases should encompass a wide range of biofouling species and growth stages, along with variations in environmental conditions, to ensure robust and reliable performance of the algorithms.
3. Integration with real-time monitoring systems: The integration of image segmentation analysis with real-time monitoring systems will enable continuous biofouling surveillance and early detection of fouling events.

Developing algorithms that can process and analyze images in real-time will allow for timely intervention and decision-making, minimizing the negative impact of biofouling on system performance.

4. Designing automated cleaning and maintenance systems: Future research should explore the development of autonomous or semi-autonomous cleaning systems based on the insights provided by image segmentation analysis. These systems could utilize robotic or mechanical devices to remove fouling organisms from sensors or energy system components, reducing the need for human intervention and improving operational efficiency.
5. Investigating environmentally friendly antifouling strategies: With the increasing societal demand for sustainable and environmentally friendly solutions, future work should focus on exploring non-toxic or eco-friendly antifouling coatings and materials. Image segmentation analysis can aid in evaluating the efficacy of these alternatives and their potential to reduce biofouling attachment.
6. Understanding biofouling dynamics in changing environments: As marine environments undergo environmental changes, including warming temperatures and ocean acidification, future research should investigate how these factors influence biofouling dynamics. Image segmentation analysis can provide valuable data on the response of fouling communities to changing conditions, contributing to a better understanding of ecological interactions and the potential impacts on marine ecosystems.

7. Scaling up and field validation studies: To validate the effectiveness of image segmentation analysis for biofouling management, large-scale field studies in real-world marine environments are necessary. These studies should involve long-term monitoring of sensors and energy systems, comparing the performance of image-based biofouling management strategies with traditional methods, and assessing the practical feasibility and cost-effectiveness of implementing such approaches on a larger scale.

This study has not only advanced our understanding of how biofouling impacts tidal turbines and marine sensors but has also contributed significantly to the development of an effective system for assessing biofouling on various materials in real conditions. Furthermore, the proposal of a low-cost and automated method for biofouling classification, employing conventional cameras and segmented pixel-based analysis, represents a groundbreaking step towards efficient monitoring and mitigation strategies. As we look to the future, the potential applications of this research are vast, promising advancements in the optimization of tidal energy systems and the development of eco-friendly antifouling solutions for water sensors and other marine technologies. Future work may explore the scalability of the proposed methods for real-world applications and delve into the broader ecological implications, fostering a sustainable future for tidal energy generation.

References

1. Scardino, A.; De Nys, R.; Ison, O.; O'Connor, W.; Steinberg, P. Microtopography and Antifouling Properties of the Shell Surface of the Bivalve Molluscs Mytilus Galloprovincialis and Pinctada Imbricata. *http://dx.doi.org/10.1080/0892701021000057882* **2010**, *19*, 221–230, doi:10.1080/0892701021000057882.

2. Whelan, A.; Regan, F. Antifouling Strategies for Marine and Riverine Sensors. *Journal of Environmental Monitoring* **2006**, *8*, 880–886, doi:10.1039/B603289C.

3. Hellio, C.; De La Broise, D.; Dufossé, L.; Le Gal, Y.; Bourgougnon, N. Inhibition of Marine Bacteria by Extracts of Macroalgae: Potential Use for Environmentally Friendly Antifouling Paints. *Mar Environ Res* **2001**, *52*, 231–247, doi:10.1016/S0141-1136(01)00092-7.

4. Sullivan, T.; McGuinness, K.; O'Connor, N.E.; Regan, F. Characterization and Anti-Settlement Aspects of Surface Micro-Structures from Cancer Pagurus. *Bioinspir Biomim* **2014**, *9*, 046003, doi:10.1088/1748-3182/9/4/046003.

5. Bers, A.V.; Wahl, M. The Influence of Natural Surface Microtopographies on Fouling. *https://doi.org/10.1080/08927010410001655533* **2007**, *20*, 43–51, doi:10.1080/08927010410001655533.

6. Characklis, W.G. Bioengineering Report: Fouling Biofilm Development: A Process Analysis. *Biotechnol Bioeng* **1981**, *23*, 1923–1960, doi:10.1002/bit.260230902.

7. Railkin, A.I. *Marine Biofouling: Colonization Processes and Defenses*; CRC press, 2003;

8. Delgado, A.; Briciu-Burghina, C.; Regan, F. Antifouling Strategies for Sensors Used in Water Monitoring: Review and Future Perspectives. *Sensors* **2021**, *21*, 389, doi:10.3390/s21020389.

9. Nurioglu, A.G.; Esteves, A.C.C.; de With, G. Non-Toxic, Non-Biocide-Release Antifouling Coatings Based on Molecular Structure Design for Marine Applications. *J Mater Chem B* **2015**, *3*, 6547–6570, doi:10.1039/C5TB00232J.

10. Salta, M.; Wharton, J.A.; Stoodley, P.; Dennington, S.P.; Goodes, L.R.; Werwinski, S.; Mart, U.; Wood, R.J.K.; Stokes, K.R. Designing Biomimetic Antifouling Surfaces. *Philosophical Transactions of the Royal Society A: Mathematical, Physical and Engineering Sciences* **2010**, *368*, 4729–4754, doi:10.1098/rsta.2010.0195.

11. Little, B.J.; Wagner, P.A. *Succession in Microfouling*; 1997;

12. Afroz, F.; Lang, A.; Habegger, M.L. Bristled Shark Skin: A Microgeometry for Boundary Layer Control? Related Content Experimental Study of Laminar and Turbulent Boundary Layer Separation Control of Shark Skin. *Bioinspir Biomim* **2008**, *3*, doi:10.1088/1748-3182/3/4/046005.

13. Zobell, C.E.; Allen, E.C. The Significance of Marine Bacteria in the Fouling of Submerged Surfaces. *J Bacteriol* **1935**, *29*, 239–251.

14. Zobell, C.E.; Rittenberg, S.C. The Occurrence and Characteristics of Chitinoclastic Bacteria in the Sea. *J Bacteriol* **1938**, *35*, 275–287.

15. Busscher, H.J.; Bos, R.; Van Der Mei, H.C. *Hypothesis Initial Microbial Adhesion Is a Determinant for the Strength of Biofilm Adhesion*; 1995; Vol. 128;.

16. Jain, A.; Bhosle, N.B. Biochemical Composition of the Marine Conditioning Film: Implications for Bacterial Adhesion. *Biofouling* **2009**, *25*, 13–19, doi:10.1080/08927010802411969.

17. Roberts, D.; Rittschof, D.; Holm, E.; Schmidt, A. Factors Influencing Initial Larval Settlement: Temporal, Spatial and Surface Molecular Components. *J Exp Mar Biol Ecol* **1991**, *150*, 203–221, doi:https://doi.org/10.1016/0022-0981(91)90068-8.

18. Chambers, L.D.; Stokes, K.R.; Walsh, F.C.; Wood, R.J.K. Modern Approaches to Marine Antifouling Coatings. *Surf Coat Technol* **2006**, *201*, 3642–3652, doi:10.1016/j.surfcoat.2006.08.129.

19. Nazar C, J. Biofilms Bacterianos. *Revista de otorrinolaringología y cirugía de cabeza y cuello* **2007**, *67*, 61–72, doi:10.4067/S0718-48162007000100011.

20. Donlan, R.M. Biofilms: Microbial Life on Surfaces. *Emerg Infect Dis* **2002**, *8*, 881–890, doi:10.3201/eid0809.020063.

21. Chloe, R.A.; Faddis, B.T. Anatomical Evidence of Microbial Biofilms in Tonsillar Tissues: A Possible Mechanism to Explain Chronicity. *Arch Otolaryngol Head Neck Surg* **2002**, *129*, 634–636.

22. Salta, M.; Wharton, J.A.; Blache, Y.; Stokes, K.R.; Briand, J.F. Marine Biofilms on Artificial Surfaces: Structure and Dynamics. *Environ Microbiol* **2013**, *15*, 2879–2893, doi:10.1111/1462-2920.12186.

23. Post, J.C.; Stoodley, P.; Hall–Stoodley, L.; Ehrlich, G.D. The Role of Biofilms in Otolaryngologic Infections. *Curr Opin Otolaryngol Head Neck Surg* **2004**, *12*, 185–190.

24. Butterfield, P.W.; Camper, A.K.; Biederman, J.A.; Bargmeyer, A.M. Minimizing Biofilm in the Presence of Iron Oxides and Humic Substances. *Water Res* **2002**, *36*, 3898–3910, doi:10.1016/S0043-1354(02)00088-X.

25. Sutherland, I.W. MINI-REVIEW Biofilm Exopolysaccharides : A Strong and Sticky Framework. *Microbiology (N Y)* **2001**, *147*, 3–9.

26. Flemming, H.-C. Biodeterioration of Synthetic Materials - A Brief Review. *Materials and Corrosion* **2010**, *61*, 986–992, doi:10.1002/maco.201005837.

27. Flemming, R.G.; Proctor, R.A.; Cooper, S.L. Bacterial Adhesion to Functionalized Polyurethanes. *J Biomater Sci Polym Ed* **1999**, *10*, 679–697, doi:10.1163/156856299X00874.

28. Mayer, C.; Moritz, R.; Kirschner, C.; Borchard, W.; Maibaum, R.; Wingender, J.; Flemming, H.-C. The Role of Intermolecular Interactions:

Studies on Model Systems for Bacterial Biofilms. *Int J Biol Macromol* **1999**, *26*, 3–16, doi:10.1016/S0141-8130(99)00057-4.

29. Atkins, P.; De Paula, J.; Keeler, J. *Atkins' Physical Chemistry*; 2014; ISBN 978-0-19-969740-3.

30. Robinson, D.M. The Chaotropic and Taxigenic Properties of Zwitterionic PH Buffers. *Naturwissenschaften* **1978**, *65*, 438–439, doi:10.1007/BF00405374.

31. Fux, C.A.; Costerton, J.W.; Stewart, P.S.; Stoodley, P. Survival Strategies of Infectious Biofilms. *Trends Microbiol* **2005**, *13*, 34–40, doi:10.1016/j.tim.2004.11.010.

32. Azevedo, N.F.; Pacheco, A.P.; Keevil, C.W.; Vieira, M.J. Adhesion of Water Stressed Helicobacter Pylori to Abiotic Surfaces. *J Appl Microbiol* **2006**, *101*, 718–724, doi:10.1111/j.1365-2672.2006.03029.x.

33. Antizar-Ladislao, B. Environmental Levels, Toxicity and Human Exposure to Tributyltin (TBT)-Contaminated Marine Environment. A Review. *Environ Int* **2008**, *34*, 292–308, doi:10.1016/J.ENVINT.2007.09.005.

34. Swain, Geoffrey. Biofouling Control: A Critical Component of Drag Reduction. In Proceedings of the Proceedings of the International Symposium on Sea Water Drag Reduction; 1998; pp. 155–161.

35. Alzieu, C. Tributyltin: Case Study of a Chronic Contaminant in the Coastal Environment. *Ocean Coast Manag* **1998**, *40*, 23–36.

36. McGinnis, C.L.; Crivello, J.F. Elucidating the Mechanism of Action of Tributyltin (TBT) in Zebrafish. *Aquatic Toxicology* **2011**, *103*, 25–31.

37. Turner, A.; Singh, N.; Richards, J.P. Bioaccessibility of Metals in Soils and Dusts Contaminated by Marine Antifouling Paint Particles. *Environmental Pollution* **2009**, *157*, 1526–1532.

38. Sarikaya, M.; Tamerler, C.; Jen, A.K.-Y.; Schulten, K.; Baneyx, F. Molecular Biomimetics: Nanotechnology through Biology. *Nat Mater* **2003**, *2*, 577–585, doi:10.1038/nmat964.

39. Ralston, E.; Swain, G. Bioinspiration—the Solution for Biofouling Control? *Bioinspir Biomim* **2009**, *4*, 015007, doi:10.1088/1748-3182/4/1/015007.

40. Davis, A.R.; Targett, N.M.; McConnell, O.J.; Young, C.M. Epibiosis of Marine Algae and Benthic Invertebrates: Natural Products Chemistry and Other Mechanisms Inhibiting Settlement and Overgrowth. In; Springer, Berlin, Heidelberg, 1989; pp. 85–114.

41. Bi, H.; Zhong, W.; Meng, S.; Kong, J.; Yang, P.; Liu, B. Construction of a Biomimetic Surface on Microfluidic Chips for Biofouling Resistance. *Anal Chem* **2006**, *78*, 3399–3405, doi:10.1021/ac0522963.

42. Richards, C.; Barrett, A.; Maguire, I.; Kwiatkowska, S.; Regan, F. Marine Inspired Textured Materials for Reduction of Biofouling on Surfaces. In Proceedings of the OCEANS 2019 - Marseille; IEEE, June 1 2019; Vol. 2019-June, pp. 1–8.

43. Richards, C.; Slaimi, A.; O'Connor, N.E.; Barrett, A.; Kwiatkowska, S.; Regan, F. Bio-Inspired Surface Texture Modification as a Viable Feature of Future Aquatic Antifouling Strategies: A Review. *Int J Mol Sci* **2020**, *21*, 5063, doi:10.3390/ijms21145063.

44. Hills, J.M.; Thomason, J.C.; Muhl, J. A Precise and Accurate Technique for the Manufacture of Complex Three - Dimensional Surfaces. *Biofouling* **2009**, *13*, 37–41, doi:10.1080/08927019809378376.

45. Sullivan, T.; McGuinness, K.; O' Connor, NE.; Regan, F. Characterization and Anti-Settlement Aspects of Surface Micro-Structures from Cancer Pagurus. *Bioinspir Biomim* **2014**, *9*, 1–11, doi:10.1088/1748-3182/9/4/046003.

46. Munther, M.; Palma, T.; Angeron, I.A.; Salari, S.; Ghassemi, H.; Vasefi, M.; Beheshti, A.; Davami, K. Microfabricated Biomimetic Placoid Scale-Inspired Surfaces for Antifouling Applications. *Appl Surf Sci* **2018**, *453*, 166–172, doi:10.1016/j.apsusc.2018.05.030.

47. Curtis, A.; Wilkinson, C. Nantotechniques and Approaches in Biotechnology. *Trends Biotechnol* **2001**, *19*, 97–101, doi:10.1016/S0167-7799(00)01536-5.

48. Richards, C.; Barrett, A.; Maguire, I.; Kwiatkowska, S.; Regan, F. Marine Inspired Textured Materials for Reduction of Biofouling on Surfaces. In Proceedings of the OCEANS 2019 - Marseille; IEEE, June 1 2019; Vol. 2019-June, pp. 1–8.

49. Vrolijk, N.H.; Targett, N.M.; Baier, R.E.; Meyer, A.E. Surface Characterisation of Two Gorgonian Coral Species: Implications for a Natural Antifouling Defence. *Biofouling* **1990**, *2*, 39–54, doi:10.1080/08927019009378128.

50. Bers, A.V.; Prendergast, G.S.; Zürn, C.M.; Hansson, L.; Head, R.M.; Thomason, J.C. A Comparative Study of the Anti-Settlement Properties of Mytilid Shells. *Biol Lett* **2006**, *2*, 88–91, doi:10.1098/rsbl.2005.0389.

51. Guenther, J.; De Nys, R. Surface Microtopographies of Tropical Sea Stars: Lack of an Efficient Physical Defence Mechanism against Fouling. *Biofouling* **2007**, *23*, 419–429, doi:10.1080/08927010701570071.

52. Long, C.J.; Schumacher, J.F.; Robinson, P.A.C.; Finlay, J.A.; Callow, M.E.; Callow, J.A.; Brennan, A.B. A Model That Predicts the Attachment Behavior of Ulva Linza Zoospores on Surface Topography. *Biofouling* **2010**, *26*, 411–419, doi:10.1080/08927011003628849.

53. Chung, K.K.; Schumacher, J.F.; Sampson, E.M.; Burne, R.A.; Antonelli, P.J.; Brennan, A.B. Impact of Engineered Surface Microtopography on Biofilm Formation of *Staphylococcus Aureus*. *Biointerphases* **2007**, *2*, 89–94, doi:10.1116/1.2751405.

54. Carman, M.L.; Estes, T.G.; Feinberg, A.W.; Schumacher, J.F.; Wilkerson, W.; Wilson, L.H.; Callow, M.E.; Callow, J.A.; Brennan, A.B. Engineered Antifouling Microtopographies – Correlating Wettability with Cell Attachment. *Biofouling* **2006**, *22*, 11–21, doi:10.1080/08927010500484854.

55. Bai, X.Q.; Xie, G.T.; Fan, H.; Peng, Z.X.; Yuan, C.Q.; Yan, X.P. Study on Biomimetic Preparation of Shell Surface Microstructure for Ship Antifouling. *Wear* **2013**, *306*, 285–295, doi:10.1016/j.wear.2012.11.020.

56. Haynes, C.L. The Emerging Field of Nanotoxicology. *Anal Bioanal Chem* **2010**, *398*, 587–588, doi:10.1007/s00216-010-3972-5.

57. Shinde, S.; Grampurohit, N.; Gaikwad, D.; Jadhav, S.; Gadhave, M.; Shelke, P. Toxicity Induced by Nanoparticles. *Asian Pac J Trop Dis* **2012**, *2*, 331–334, doi:10.1016/S2222-1808(12)60072-3.

58. Manov, D. V; Chang, G.C.; Dickey, T.D. Methods for Reducing Biofouling of Moored Optical Sensors. *J Atmos Ocean Technol* **2004**, *21*, 958–968.

59. Whelan, A.; Regan, F. Antifouling Strategies for Marine and Riverine Sensors. *Journal of Environmental Monitoring* **2006**.

60. Whitt, C.; Pearlman, J.; Polagye, B.; Caimi, F.; Muller-Karger, F.; Copping, A.; Spence, H.; Madhusudhana, S.; Kirkwood, W.; Grosjean, L.; et al. Future Vision for Autonomous Ocean Observations. *Front Mar Sci* **2020**, *7*, 697, doi:10.3389/fmars.2020.00697.

61. Delauney, L.; Compère, C.; Lehaitre, M.; Compare, C.; Lehaitre, M.; Compère, C.; Lehaitre, M. Biofouling Protection for Marine Environmental Sensors. *Ocean Science* **2010**, *6*, 503–511, doi:10.5194/os-6-503-2010.

62. Alliance for Coastal Technologies Biofouling Prevention Technologies for Coastal Sensors / Sensor Platforms. In Proceedings of the University of Maryland Center of Environmental Science, Workshop Proceedings; Solomons, Maryland, 2003; p. 23.

63. Lobe, H. Recent Advances in Biofouling Protection for Oceanographic Instrumentation. *OCEANS 2015 - MTS/IEEE Washington* **2016**, doi:10.23919/oceans.2015.7401854.

64. Manov, D. V.; Chang, G.C.; Dickey, T.D. Methods for Reducing Biofouling of Moored Optical Sensors. *J Atmos Ocean Technol* **2004**, *21*, 958–968, doi:10.1175/1520-0426(2004)021<0958:MFRBOM>2.0.CO;2.

65. Banerjee, I.; Pangule, R.C.; Kane, R.S.; Banerjee, I.; Pangule, R.C.R.S.; Kane, H.P. Antifouling Coatings: Recent Developments in the Design of Surfaces That Prevent Fouling by Proteins, Bacteria, and Marine Organisms. *Advanced Materials* **2011**, *23*, 690–718, doi:10.1002/ADMA.201001215.

66. Lizotte, M. *Fighting Fouling; Extending Sonde Deployment Times with EXO´s Wiped (C/T) Sensor*; Yellow Springs, OH, 2015;

67. Magagna, D.; Uihlein, A. Ocean Energy Development in Europe: Current Status and Future Perspectives. *International Journal of Marine Energy* **2015**, *11*, 84–104, doi:10.1016/j.ijome.2015.05.001.

68. Decaix, J.; Alligne, S.; Müller, A.; Nicolet, C.; Münch, C.; Avellan, F. Identification of 1-D Cavitation Model Parameters by Means of Computational Fluid Dynamics. *https://doi.org/10.1080/00221686.2021.1944922* **2021**, *60*, 271–282, doi:10.1080/00221686.2021.1944922.

69. Kumar, P.; Saini, R.P. Study of Cavitation in Hydro Turbines—A Review. *Renewable and Sustainable Energy Reviews* **2010**, *14*, 374–383, doi:10.1016/J.RSER.2009.07.024.

70. Kassanos, I.; Anagnostopoulos, I. Cavitation in Hydraulic Turbines. *Cavitation and Bubble Dynamics: Fundamentals and Applications* **2021**, 173–209, doi:10.1016/B978-0-12-823388-7.00001-1.

71. Dowson, D.; Taylor, C.M. Cavitation in Bearings. *Annu Rev Fluid Mech* **1979**, *11*, 35–65, doi:10.1146/annurev.fl.11.010179.000343.

72. Bayoudh, S.; Othmane, A.; Bettaieb, F.; Bakhrouf, A.; Ouada, H. Ben; Ponsonnet, L. Quantification of the Adhesion Free Energy between Bacteria and Hydrophobic and Hydrophilic Substrata. *Materials Science and Engineering: C* **2006**, *26*, 300–305, doi:10.1016/j.msec.2005.10.045.

73. Kung, C.H.; Sow, P.K.; Zahiri, B.; Mérida, W. Assessment and Interpretation of Surface Wettability Based on Sessile Droplet Contact Angle Measurement: Challenges and Opportunities. *Adv Mater Interfaces* **2019**, *6*, 1900839, doi:10.1002/admi.201900839.

74. Pogorzelski, S.J.; Mazurek, A.Z.; Szczepanska, A. In-Situ Surface Wettability Parameters of Submerged in Brackish Water Surfaces Derived from Captive Bubble Contact Angle Studies as Indicators of Surface Condition Level. *Journal of Marine Systems* **2013**, *119–120*, 50–60, doi:10.1016/j.jmarsys.2013.03.011.

75. Khajavian, E.; Attar, M.R.; Mohammadi Zahrani, E.; Liu, W.; Davoodi, A.; Hosseinpour, S. Tuning Surface Wettability of Aluminum Surface and Its Correlation with Short and Long Term Corrosion Resistance in Saline Solutions. *Surf Coat Technol* **2022**, *429*, 127950, doi:10.1016/j.surfcoat.2021.127950.

76. Chapman, J.; Lawlor, A.; Weir, E.; Quilty, B.; Regan, F. Phthalate Doped PVC Membranes for the Inhibition of Fouling. *J Memb Sci* **2010**, *365*, 180–187, doi:10.1016/J.MEMSCI.2010.09.003.

77. Chapman, J.; Weir, E.; Regan, F. Period Four Metal Nanoparticles on the Inhibition of Biofouling. *Colloids Surf B Biointerfaces* **2010**, *78*, 208–216, doi:10.1016/J.COLSURFB.2010.03.002.

78. PERCIVAL, S.L.; KNAPP, J.S.; EDYVEAN, R.; WALES, D.S. BIOFILM DEVELOPMENT ON STAINLESS STEEL IN MAINS WATER. *Water Res* **1998**, *32*, 243–253, doi:10.1016/S0043-1354(97)00132-2.

79. Inglis, T.J.; Millar, M.R.; Jones, J.G.; Robinson, D.A. Tracheal Tube Biofilm as a Source of Bacterial Colonization of the Lung. *J Clin Microbiol* **1989**, *27*, 2014–2018, doi:10.1128/jcm.27.9.2014-2018.1989.

80. Ikada, E. Electron Microscope Observation of Biodegradation of Polymers. *Journal of environmental polymer degradation 1999 7:4* **1999**, *7*, 197–201, doi:10.1023/A:1022882732403.

81. Holt, K.B.; Bard, A.J. Interaction of Silver(I) Ions with the Respiratory Chain of Escherichia Coli: An Electrochemical and Scanning Electrochemical Microscopy Study of the Antimicrobial Mechanism of Micromolar Ag. *Biochemistry* **2005**, *44*, 13214–13223, doi:10.1021/BI0508542/ASSET/IMAGES/LARGE/BI0508542F00006.JPEG.

82. Dempsey, M.J. Colonisation of Antifouling Paints by Marine Bacteria. *Botanica Marina* **1981**, *24*, 185–192, doi:10.1515/BOTM.1981.24.4.185/MACHINEREADABLECITATION/RIS.

83. Callow, J.A.; Osborne, M.P.; Callow, M.E.; Baker, F.; Donald, A.M. Use of Environmental Scanning Electron Microscopy to Image the Spore Adhesive of the Marine Alga Enteromorpha in Its Natural Hydrated State.

Colloids Surf B Biointerfaces **2003**, *27*, 315–321, doi:10.1016/S0927-7765(02)00094-2.

84. Little, B.; Wagner, P.; Ray, R.; Pope, R.; Scheetz, R. Biofilms: An ESEM Evaluation of Artifacts Introduced during SEM Preparation. *J Ind Microbiol* **1991**, *8*, 213–221, doi:10.1007/BF01576058.
85. Lee, W.-F.; Tsao, K.-T. Preparation and Properties of Nanocomposite Hydrogels Containing Silver Nanoparticles by Ex Situ Polymerization. *J Appl Polym Sci* **2006**, *100*, 3653–3661, doi:10.1002/app.23171.
86. Stewart, P.S.; Murga, R.; Srinivasan, R.; de Beer, D. Biofilm Structural Heterogeneity Visualized by Three Microscopic Methods. *Water Res* **1995**, *29*, 2006–2009, doi:10.1016/0043-1354(94)00339-9.
87. Beech, I.B.; Smith, J.R.; Steele, A.A.; Penegar, I.; Campbell, S.A. The Use of Atomic Force Microscopy for Studying Interactions of Bacterial Biofilms with Surfaces. *Colloids Surf B Biointerfaces* **2002**, *23*, 231–247, doi:10.1016/S0927-7765(01)00233-8.
88. Tow, E.W.; Rad, B.; Kostecki, R. Biofouling of Filtration Membranes in Wastewater Reuse: In Situ Visualization with Confocal Laser Scanning Microscopy. *J Memb Sci* **2022**, *644*, 120019, doi:10.1016/j.memsci.2021.120019.
89. Dobretsov, S.; Thomason, J.C.; Williams, D.N. *Biofouling Methods*; Dobretsov, S., Thomason, J.C., Williams, D.N., Eds.; Wiley, 2014; ISBN 9780470659854.

90. Chen, M.-Y.; Lee, D.-J.; Yang, Z.; Peng, X.F.; Lai, J.Y. Fluorecent Staining for Study of Extracellular Polymeric Substances in Membrane Biofouling Layers. *Environ Sci Technol* **2006**, *40*, 6642–6646, doi:10.1021/es0612955.

91. Sathe, P.; Laxman, K.; Myint, M.T.Z.; Dobretsov, S.; Richter, J.; Dutta, J. Bioinspired Nanocoatings for Biofouling Prevention by Photocatalytic Redox Reactions. *Sci Rep* **2017**, *7*, 3624, doi:10.1038/s41598-017-03636-6.

92. Azevedo, J.; Antunes, J.T.; Machado, A.M.; Vasconcelos, V.; Leão, P.N.; Froufe, E. Monitoring of Biofouling Communities in a Portuguese Port Using a Combined Morphological and Metabarcoding Approach. **123AD**, doi:10.1038/s41598-020-70307-4.

93. Richards, C.; O'Connor, N.; Jose, D.; Barrett, A.; Regan, F. Selection and Optimization of Protein and Carbohydrate Assays for the Characterization of Marine Biofouling. *Analytical Methods* **2020**, *12*, 2228–2236, doi:10.1039/D0AY00272K.

94. Delgado, A.; Power, S.; Richards, C.; Daly, P.; Briciu-Burghina, C.; Delauré, Y.; Regan, F. Establishment of an Antifouling Performance Index Derived from the Assessment of Biofouling on Typical Marine Sensor Materials. *Science of The Total Environment* **2023**, 164059, doi:10.1016/j.scitotenv.2023.164059.

95. First Scott C Riley Kazi Aminul Islam, M.R.; Hill, V.; Li, J. Rapid Quantification of Biofouling With an Inexpensive, Rapid Quantification of Biofouling With an Inexpensive, Underwater Camera and Image Analysis

Underwater Camera and Image Analysis Original Publication Citation Original Publication Citation., doi:10.3391/mbi.2021.12.3.06.

96. Berg, S.; Kutra, D.; Kroeger, T.; Straehle, C.N.; Kausler, B.X.; Haubold, C.; Schiegg, M.; Ales, J.; Beier, T.; Rudy, M.; et al. Ilastik: Interactive Machine Learning for (Bio)Image Analysis. *Nat Methods* **2019**, *16*, 1226–1232, doi:10.1038/s41592-019-0582-9.

97. Arganda-Carreras, I.; Kaynig, V.; Schindelin, J.; Cardona, A.; Sebastian Seung, H. Trainable Weka Segmentation: A Machine Learning Tool for Microscopy Image Segmentation. **2014**.

98. Dafforn, K.A.; Lewis, J.A.; Johnston, E.L. Antifouling Strategies: History and Regulation, Ecological Impacts and Mitigation. *Mar Pollut Bull* **2011**, *62*, 453–465, doi:10.1016/j.marpolbul.2011.01.012.

99. Briciu-Burghina, C.; Power, S.; Delgado, A.; Regan, F. Sensors for Coastal and Ocean Monitoring. *https://doi.org/10.1146/annurev-anchem-091922-085746* **2023**, *16*, 451–469, doi:10.1146/ANNUREV-ANCHEM-091922-085746.

100. Delrin® Plastic | Acetal Plastic Available online: https://www.dupont.com/products/delrin.html (accessed on 31 December 2020).

101. Solvay's Ryton® PPS Used for Flexible, Lightweight Coolant Lines, Brackets and Connectors Advances Complex Automotive Thermal Management Assembly Systems | Solvay Available online: https://www.solvay.com/en/article/solvays-ryton-pps-used-flexible-

lightweight-coolant-lines-brackets-and-connectors-advances (accessed on 31 December 2020).

102. Delgado, A.; Richards, C.; Daly, P.; Power, S.; Briciu-Burghina, C.; Delauré, Y.; Regan, F. Assessment of Biofouling on Typical Marine Sensors Materials. In Proceedings of the OCEANS 2023 - Limerick; IEEE, June 5 2023; pp. 1–8.

103. Arganda-Carreras, I.; Kaynig, V.; … C.R.-; 2017, undefined Trainable Weka Segmentation: A Machine Learning Tool for Microscopy Pixel Classification. *academic.oup.com*.

104. Briand, J.-F.; Pochon, X.; Wood, S.A.; Bressy, C.; Garnier, C.; Réhel, K.; Urvois, F.; Culioli, G.; Zaiko, A. Metabarcoding and Metabolomics Offer Complementarity in Deciphering Marine Eukaryotic Biofouling Community Shifts. *Biofouling* **2018**, *34*, 657–672, doi:10.1080/08927014.2018.1480757.

105. Bolyen, E.; Rideout, J.R.; Dillon, M.R.; Bokulich, N.A.; Abnet, C.C.; Al-Ghalith, G.A.; Alexander, H.; Alm, E.J.; Arumugam, M.; Asnicar, F.; et al. Reproducible, Interactive, Scalable and Extensible Microbiome Data Science Using QIIME 2. *Nat Biotechnol* **2019**, *37*, 852–857, doi:10.1038/s41587-019-0209-9.

106. de Nys R; Guenther J *The Battle against Marine Biofouling: A Historical Review*; Claire Hellio; Diego Yebra, Ed.; Woodshead Publishing: Cambridge, 2009; ISBN 9781845696313.

107. Braithwaite, R.A.; McEvoy, L.A. Marine Biofouling on Fish Farms and Its Remediation. *Adv Mar Biol* **2005**, *47*, 215–252, doi:10.1016/S0065-2881(04)47003-5.

108. Bertness, M.; Gaines, S.; … E.S.-J. of E.; 1992, undefined Components of Recruitment in Populations of the Acorn Barnacle Semibalanus Balanoides (Linnaeus). *Elsevier*.

109. Young, C.M.; Gotelli, N.J. Larval Predation by Barnacles: Effects on Patch Colonization in a Shallow Subtidal Community. *Ecology* **1988**, *69*, 624–634, doi:10.2307/1941011.

110. Hart S *Report on Marine Biofouling Consequences Seasonally, Spatially and with Depth, Exploration and Production: The Oil and gas Review.*; 2005;

111. Barthelmes, D. M. C. M. Beveridge: Cage Aquaculture.—352 Pp., 151 Figs. Farnham, Surrey: Fishings News Books Ltd. 1987. ISBN 0 85238 148 4. Ł 21.00. *Internationale Revue der gesamten Hydrobiologie und Hydrographie* **1989**, *74*, 231–231, doi:10.1002/iroh.19890740219.

112. Pratt, J.R.; Mochan, D.; Xu, Z. Rapid Toxicity Estimation Using Soil Ciliates: Sensitivity and Bioavailability. *Bull Environ Contam Toxicol* **1997**, *58*, 387–393, doi:10.1007/S001289900346.

113. Díaz, S.; Martín-González, A.; international, J.G.-E.; 2006, undefined Evaluation of Heavy Metal Acute Toxicity and Bioaccumulation in Soil Ciliated Protozoa. *Elsevier*.

114. Campbell, C.; Warren, A.; Cameron, C.; Chemosphere, S.H.-; 1997, undefined Direct Toxicity Assessment of Two Soils Amended with Sewage Sludge Contaminated with Heavy Metals Using a Protozoan (Colpoda Steinii) Bioassay. *Elsevier*.

115. Bowers, N.; Pratt, J.R.; Beeson, D.; Lewis, M. Comparative Evaluation of Soil Toxicity Using Lettuce Seeds and Soil Ciliates. *Environ Toxicol Chem* **1997**, *16*, 207–213, doi:10.1002/ETC.5620160216.

116. Luu, H.; Esteban, G.; Butt, A.; Protist, I.G.-; 2022, undefined Effects of Copper and the Insecticide Cypermethrin on a Soil Ciliate (Protozoa: Ciliophora) Community. *Elsevier*.

117. Krawczynska, W.; Pivovarova, N.; protozoologica, A.S.-A.; 1989, undefined Effects of Cadmium on Growth, Ultrastructure and Content of Chemical Elements in Tetrahymena Pyriformis and Acanthamoeba Castellanii. *agro.icm.edu.pl*.

118. Dunlop, S.; Chapman, G. Detoxication of Zinc and Cadmium by the Freshwater Protozoan Tetrahymena Pyriformis. *Environ Res* **1981**, *24*, 264–274, doi:10.1016/0013-9351(81)90156-0.

119. Stauber, J.L.; Florence, T.M. Mechanism of Toxicity of Ionic Copper and Copper Complexes to Algae. *Mar Biol* **1987**, *94*, 511–519, doi:10.1007/BF00431397.

120. Breur, H. Fouling and Bioprotection of Metals: Monitoring and Control of Deposition Processes in Aqueous Environments. Ph.D. Thesis, TNO Industrial Technology, 2001, 2003.

121. Drach, A.; Tsukrov, I.; DeCew, J.; Aufrecht, J.; Grohbauer, A.; Hofmann, U. Field Studies of Corrosion Behaviour of Copper Alloys in Natural Seawater. *Corros Sci* **2013**, *76*, 453–464, doi:10.1016/j.corsci.2013.07.019.

122. Garnier, C.; Briand, J.-F.; Aude Barani, &; Réhel, K.; Urvois, F.; Lepoupon, C.; Bouchez, A.; Debroas, D.; Bressy, C. Spatio-Temporal Variations of Marine Biofilm Communities Colonizing Artificial Substrata Including Antifouling Coatings in Contrasted French Coastal Environments. *Springer* **2017**, *74*, 585–598, doi:10.1007/s00248-017-0966-2.

123. Muthukrishnan, T.; Abed, R.M.M.; Dobretsov, S.; Kidd, B.; Finnie, A.A. Long-Term Microfouling on Commercial Biocidal Fouling Control Coatings. *Biofouling* **2014**, *30*, 1155–1164, doi:10.1080/08927014.2014.972951.

124. Camps, M.; Barani, A.; Gregori, G.; Bouchez, A.; Le Berre, B.; Bressy, C.; Blache, Y.; Briand, J.-F. Antifouling Coatings Influence Both Abundance and Community Structure of Colonizing Biofilms: A Case Study in the Northwestern Mediterranean Sea. *Appl Environ Microbiol* **2014**, *80*, 4821–4831, doi:10.1128/AEM.00948-14.

125. McNamara, C.; Lee, K.; Russell, M.; … L.M.-J. of cultural; 2009, undefined Analysis of Bacterial Community Composition in Concretions Formed on the USS Arizona, Pearl Harbor, HI. *Elsevier*.

126. Almeida, E.; Diamantino, T.; Coatings, O. de S.-P. in O.; 2007, undefined Marine Paints: The Particular Case of Antifouling Paints. *Elsevier*.

127. Almeida, E.; Diamantino, T.C.; de Sousa, O. Marine Paints: The Particular Case of Antifouling Paints. *Prog Org Coat* **2007**, *59*, 2–20, doi:10.1016/j.porgcoat.2007.01.017.

128. Yebra, D.M.; Kiil, S.; Dam-Johansen, K. Antifouling Technology—Past, Present and Future Steps towards Efficient and Environmentally Friendly Antifouling Coatings. *Prog Org Coat* **2004**, *50*, 75–104, doi:10.1016/j.porgcoat.2003.06.001.

129. Cassé, F.; Swain, G.W. The Development of Microfouling on Four Commercial Antifouling Coatings under Static and Dynamic Immersion. *Int Biodeterior Biodegradation* **2006**, *57*, 179–185, doi:10.1016/j.ibiod.2006.02.008.

130. Yeates, G.W.; Percival, H.J.; Parshotam, A. Soil Nematode Responses to Year-to-Year Variation of Low Levels of Heavy Metals. *Soil Research* **2003**, *41*, 613–625, doi:10.1071/SR02113.

131. Lejars, M.; Margaillan, A.; Bressy, C. Fouling Release Coatings: A Nontoxic Alternative to Biocidal Antifouling Coatings. *Chem Rev* **2012**, *112*, 4347–4390, doi:10.1021/cr200350v.

132. B. Todd *Materials Selection for High Reliability Copper Alloy Seawater System. The Application of Copper–Nickel Alloys in Marine Systems. Technical Report-1919, Copper Development Association (CDA), 1991*; Greenwich, CT, 1991;

133. J.R. Hunt; M.D. Bellware Proceedings of the Third Annual Marine Technology Society, Marine Technology Society. In Proceedings of the

Ocean Engineering Hardware Requires Copper–Nickel Alloys; 1967; pp. 243–275.

134. Zoolfakar, M.R.; Zahari, M.Z.; Azaim, F.Z.Z. Natural Superhydrophobic Material as Alternative Substance in Antifouling Paint. In *Advanced Structured Materials*; Springer Science and Business Media Deutschland GmbH, 2022; Vol. 162, pp. 71–83.

135. Bixler, G.D.; Bhushan, B. Biofouling: Lessons from Nature. *Philosophical Transactions of the Royal Society A: Mathematical, Physical and Engineering Sciences* **2012**, *370*, 2381–2417, doi:10.1098/rsta.2011.0502.

136. Railkin, A.I. *Marine Biofouling*; CRC Press, 2003; ISBN 9780203503232.

137. Hellio, C.; Yebra, D. *Advances in Marine Antifouling Coatings and Technologies*; 2009;

138. Jung, Y.C.; Bhushan, B. Wetting Behavior of Water and Oil Droplets in Three-Phase Interfaces for Hydrophobicity/Philicity and Oleophobicity/Philicity. *Langmuir* **2009**, *25*, 14165–14173, doi:10.1021/la901906h.

139. Greer, S.P.; Iken, K.B.; McClintock, J.B.; Amsler, C.D. Individual and Coupled Effects of Echinoderm Extracts and Surface Hydrophobicity on Spore Settlement and Germination in the Brown Alga *Hincksia Irregularis*. *Biofouling* **2003**, *19*, 315–326, doi:10.1080/08927010310001612306.

140. Costerton, J. The Biofilm Primer. **2007**.

141. O'Connor, N.; and, D.R.-J. of experimental marine biology; 1996, undefined Effects of Bacterial Films on Attachment of Barnacle (Balanus Improvisus Darwin) Larvae: Laboratory and Field Studies. *Elsevier*.

142. Gerhart, D.J.; Rittschof, D.; Hooper, I.R.; Eisenman, K.; Meyer, A.E.; Baier, R.E.; Young, C. Rapid and Inexpensive Quantification of the Combined Polar Components of Surface Wettability: Application to Biofouling. *Biofouling* **1992**, *5*, 251–259, doi:10.1080/08927019209378246.

143. Rittschof, D.; Costlow, J.D. Bryozoan and Barnacle Settlement in Relation to Initial Surface Wettability: A Comparison of Laboratory and Field Studies. *Proceedings of the 22nd European Marine Biology Symposium* **1989**, *53*, 411–416.

144. Kavanagh, C.J.; Quinn, R.D.; Swain, G.W. Observations of Barnacle Detachment from Silicones Using High-Speed Video. *J Adhes* **2005**, *81*, 843–868, doi:10.1080/00218460500189331.

145. Dahlström, M.; Jonsson, H.; … P.J.-J. of experimental; 2004, undefined Surface Wettability as a Determinant in the Settlement of the Barnacle Balanus Improvisus (Darwin). *Elsevier*.

146. Maki, J.S.; Yule, A.B.; Rittschof, D.; Mitchell, R. The Effect of Bacterial Films on the Temporary Adhesion and Permanent Fixation of Cypris Larvae, Balanus Amphitrite Darwin. *Biofouling* **1994**, *8*, 121–131, doi:10.1080/08927019409378267.

147. Dahlström, M.; Jonsson, H.; Jonsson, P.R.; Elwing, H. Surface Wettability as a Determinant in the Settlement of the Barnacle Balanus Improvisus

(DARWIN). *J Exp Mar Biol Ecol* **2004**, *305*, 223–232, doi:10.1016/j.jembe.2003.12.013.

148. Maki, J.S.; Yule, A.B.; Rittschof, D.; Mitchell, R. The Effect of Bacterial Films on the Temporary Adhesion and Permanent Fixation of Cypris Larvae, Balanus Amphitrite Darwin. *Biofouling* **1994**, *8*, 121–131, doi:10.1080/08927019409378267.

149. Resnik, M.; Benčina, M.; Levičnik, E.; Rawat, N.; Iglič, A.; Junkar, I. Strategies for Improving Antimicrobial Properties of Stainless Steel. *Materials 2020, Vol. 13, Page 2944* **2020**, *13*, 2944, doi:10.3390/MA13132944.

150. Nan, L.; Yang, K.; Ren, G. Anti-Biofilm Formation of a Novel Stainless Steel against Staphylococcus Aureus. *Mater Sci Eng C Mater Biol Appl* **2015**, *51*, 356–361, doi:10.1016/J.MSEC.2015.03.012.

151. Cowling, M.; Hodgkiess, T.; Parr, A.; … M.S.-S. of the total; 2000, undefined An Alternative Approach to Antifouling Based on Analogues of Natural Processes. *Elsevier*.

152. Thomsen, P.; conservation, E.W.-B.; 2015, undefined Environmental DNA–An Emerging Tool in Conservation for Monitoring Past and Present Biodiversity. *Elsevier*.

153. Thomsen, P.F.; Kielgast, J.; Iversen, L.L.; Møller, P.R.; Rasmussen, M.; Willerslev, E. Detection of a Diverse Marine Fish Fauna Using Environmental DNA from Seawater Samples. *PLoS One* **2012**, *7*, doi:10.1371/JOURNAL.PONE.0041732.

154. TABERLET, P.; PRUD'HOMME, S.M.; CAMPIONE, E.; ROY, J.; MIQUEL, C.; SHEHZAD, W.; GIELLY, L.; RIOUX, D.; CHOLER, P.; CLÉMENT, J.-C.; et al. Soil Sampling and Isolation of Extracellular DNA from Large Amount of Starting Material Suitable for Metabarcoding Studies. *Mol Ecol* **2012**, *21*, 1816–1820, doi:10.1111/j.1365-294X.2011.05317.x.

155. Cowan, M.M.; Warren, T.M.; Fletcher, M. Mixed-species Colonization of Solid Surfaces in Laboratory Biofilms. *Biofouling* **1991**, *3*, 23–34, doi:10.1080/08927019109378159.

156. Fletcher, M. Attachment of Pseudomonas Fluorescens to Glass and Influence of Electrolytes on Bacterium-Substratum Separation Distance. *J Bacteriol* **1988**, *170*, 2027–2030, doi:10.1128/jb.170.5.2027-2030.1988.

157. Fera, P.; Siebel, M.A.; Characklis, W.G.; Prieur, D. Seasonal Variations in Bacterial Colonisation of Stainless Steel, Aluminium and Polycarbonate Surfaces in a Sea Water Flow System. *http://dx.doi.org/10.1080/08927018909378112* **2009**, *1*, 251–261, doi:10.1080/08927018909378112.

158. Donlan, R.M.; Pipes, W.O.; Yohe, T.L. Biofilm Formation on Cast Iron Substrata in Water Distribution Systems. *Water Res* **1994**, *28*, 1497–1503, doi:10.1016/0043-1354(94)90318-2.

159. Schultz, M.P. Effects of Coating Roughness and Biofouling on Ship Resistance and Powering. *https://doi.org/10.1080/08927010701461974* **2007**, *23*, 331–341, doi:10.1080/08927010701461974.

160. Schultz, M.P.; Bendick, J.A.; Holm, E.R.; Hertel, W.M. Economic Impact of Biofouling on a Naval Surface Ship.

https://doi.org/10.1080/08927014.2010.542809 **2010**, *27*, 87–98, doi:10.1080/08927014.2010.542809.

161. Townsin, R.L. The Ship Hull Fouling Penalty. *http://dx.doi.org/10.1080/0892701031000088535* **2010**, *19*, 9–15, doi:10.1080/0892701031000088535.
162. Song, S.; Shi, W.; Demirel, Y.K.; Atlar, M. The Effect of Biofouling on the Tidal Turbine Performance. **2019**.
163. Visscher, J. Nature and Extent of Fouling of Ships' Bottoms. **1928**.
164. Hewitt, C.L.; Gollasch, S.; Minchin, D. The Vessel as a Vector – Biofouling, Ballast Water and Sediments. **2009**, 117–131, doi:10.1007/978-3-540-79236-9_6.
165. Callow, J.A.; Callow, M.E. Trends in the Development of Environmentally Friendly Fouling-Resistant Marine Coatings. *Nature Communications 2011 2:1* **2011**, *2*, 1–10, doi:10.1038/ncomms1251.
166. Münch, A.S.; Wölk, M.; Malanin, M.; Eichhorn, K.-J.; Simon, F.; Uhlmann, P. Smart Functional Polymer Coatings for Paper with Anti-Fouling Properties. *J Mater Chem B* **2018**, *6*, 830–843, doi:10.1039/C7TB02886E.
167. Yang, J.; Xue, B.; Zhou, Y.; Qin, M.; Wang, W.; Cao, Y. Spray-Painted Hydrogel Coating for Marine Antifouling. *Adv Mater Technol* **2021**, *6*, 2000911, doi:10.1002/admt.202000911.
168. Lu, G.; Tian, S.; Li, J.; Xu, Y.; Liu, S.; Pu, J. Fabrication of Bio-Based Amphiphilic Hydrogel Coating with Excellent Antifouling and Mechanical

Properties. *Chemical Engineering Journal* **2021**, *409*, 128134, doi:10.1016/j.cej.2020.128134.

169. Luoma, E.; Laurila-Pant, M.; Altarriba, E.; Nevalainen, L.; Helle, I.; Granhag, L.; Lehtiniemi, M.; Srėbalienė, G.; Olenin, S.; Lehikoinen, A. A Multi-Criteria Decision Analysis Model for Ship Biofouling Management in the Baltic Sea. *Science of The Total Environment* **2022**, *852*, 158316, doi:10.1016/j.scitotenv.2022.158316.

170. Crispim, C.A.; Gaylarde, P.M.; Gaylarde, C.C. Algal and Cyanobacterial Biofilms on Calcareous Historic Buildings. *Curr Microbiol* **2003**, *46*, 79–82, doi:10.1007/S00284-002-3815-5.

171. Ariño, X.; Gomez-Bolea, A.; Saiz-Jimenez, C. Lichens on Ancient Mortars. *Int Biodeterior Biodegradation* **1997**, *40*, 217–224, doi:10.1016/S0964-8305(97)00036-X.

172. John; D.M Algal Growth on Buildings: A General Review and Methods of Treatment. *Int Biodeterior Biodegradation* **1988**, *2*, 81–102.

173. Ortega-Calvo, J.J.; Ariño, X.; Hernandez-Marine, M.; Saiz-Jimenez, C. Factors Affecting the Weathering and Colonization of Monuments by Phototrophic Microorganisms. *Science of The Total Environment* **1995**, *167*, 329–341, doi:10.1016/0048-9697(95)04593-P.

174. Tomaselli, L.; Lamenti, G.; Bosco, M.; Tiano, P. Biodiversity of Photosynthetic Micro-Organisms Dwelling on Stone Monuments. *Int Biodeterior Biodegradation* **2000**, *46*, 251–258, doi:10.1016/S0964-8305(00)00078-0.

175. Tran, T.H.; Govin, A.; Guyonnet, R.; Grosseau, P.; Lors, C.; Garcia-Diaz, E.; Damidot, D.; Devès, O.; Ruot, B. Influence of the Intrinsic Characteristics of Mortars on Biofouling by Klebsormidium Flaccidum. *Int Biodeterior Biodegradation* **2012**, *70*, 31–39, doi:10.1016/J.IBIOD.2011.10.017.

176. Chen-Charpentier, B. Numerical Simulation of Biofilm Growth in Porous Media. *J Comput Appl Math* **1999**, *103*, 55–66, doi:10.1016/S0377-0427(98)00240-4.

177. Tran, T.H.; Govin, A.; Guyonnet, R.; Grosseau, P.; Lors, C.; Damidot, D.; Devès, O.; Ruot, B. Avrami's Law Based Kinetic Modeling of Colonization of Mortar Surface by Alga Klebsormidium Flaccidum. *Int Biodeterior Biodegradation* **2013**, *79*, 73–80, doi:10.1016/j.ibiod.2012.12.012.

178. Barberousse, H.; Ruot, B.; Yéprémian, C.; Boulon, G. An Assessment of Façade Coatings against Colonisation by Aerial Algae and Cyanobacteria. *Build Environ* **2007**, *42*, 2555–2561, doi:10.1016/J.BUILDENV.2006.07.031.

179. Avrami, M. Kinetics of Phase Change. I General Theory. *J Chem Phys* **2004**, *7*, 1103, doi:10.1063/1.1750380.

180. Avrami, M. Kinetics of Phase Change. II Transformation-Time Relations for Random Distribution of Nuclei. *J Chem Phys* **2004**, *8*, 212, doi:10.1063/1.1750631.

181. Avrami, M. Granulation, Phase Change, and Microstructure Kinetics of Phase Change. III. *J Chem Phys* **2004**, *9*, 177, doi:10.1063/1.1750872.

182. William A. Johnson; Robert F. Mehl Reaction Kinetics in Processes of Nucleation and Growth. *American Institute of Mining and Metallurgical Engineers. Technical Publication* **1939**, *135*, 416.

183. Khawam, A.; Flanagan, D.R. Solid-State Kinetic Models: Basics and Mathematical Fundamentals. *J Phys Chem B* **2006**, *110*, 17315–17328, doi:10.1021/jp062746a.

184. Fanfoni, M.; Tomellini, M. The Johnson-Mehl- Avrami-Kohnogorov Model: A Brief Review. *Il Nuovo Cimento D 1998 20:7* **1998**, *20*, 1171–1182, doi:10.1007/BF03185527.

185. Slováček, M. Application of Numerical Simulation of Heat Treatment in Industry. *Journal de Physique IV* **2004**, *120*, 753–760, doi:10.1051/jp4:2004120087.

186. Hay, J.N. Application of the Modified Avrami Equations to Polymer Crystallisation Kinetics. *British Polymer Journal* **1971**, *3*, 74–82, doi:10.1002/pi.4980030205.

187. Butler, A.J.; Canning-Clode, J.; Coutts, A.D.M.; Cowie, P.R.; Dobretsov, S.; Dürr, S.; Faimali, M.; Lewis, J.A.; Page, H.M.; Pratten, J.; et al. Techniques for the Quantification of Biofouling. *Biofouling* **2010**, 319–332, doi:10.1002/9781444315462.CH22.

188. *ASTM D6990, Standard Practice for Evaluating Biofouling Resistance and Physical Performance of Marine Coating Systems*; 2020;

189. Taylor, L.; Nickelsen, E. Ireland’s Seashore: A Field Guide. **2018**.

190. Sage, D.; Unser, M. Easy Java Programming for Teaching Image-Processing. In Proceedings of the Proceedings 2001 International Conference on Image Processing (Cat. No.01CH37205); IEEE, 2001; Vol. 2, pp. 298–301.

191. Oguslu, E.; Islam, K.; Perez, D.; Hill, V.J.; Bissett, W.P.; Zimmerman, R.C.; Li, J. Detection of Seagrass Scars Using Sparse Coding and Morphological Filter. *Remote Sens Environ* **2018**, *213*, 92–103, doi:10.1016/j.rse.2018.05.009.

192. Thornton, A.; Weinhart, T.; Bokhove, O.; Zhang, B.; D.M. Sar, van der; Kumar, K.; Pisarenco, M.; Rudnaya, M.; Savcenco, V.; Rademacher, J.D.M.; et al. *Modeling and Optimization of Algae Growth*; Technische Universiteit Eindhoven, 2010; Vol. 1059;.

193. Cirés, S.; Delgado, A.; González-Pleiter, M.; Quesada, A. Temperature Influences the Production and Transport of Saxitoxin and the Expression of Sxt Genes in the Cyanobacterium Aphanizomenon Gracile. *Toxins (Basel)* **2017**, *9*, 322, doi:10.3390/toxins9100322.

194. Silva, E.R.; Ferreira, O.; Ramalho, P.A.; Azevedo, N.F.; Bayón, R.; Igartua, A.; Bordado, J.C.; Calhorda, M.J. Eco-Friendly Non-Biocide-Release Coatings for Marine Biofouling Prevention. *Science of The Total Environment* **2019**, *650*, 2499–2511, doi:10.1016/j.scitotenv.2018.10.010.

195. Lopez, J.S.; Lee, L.; Mackey, K.R.M. The Toxicity of Copper to Crocosphaera Watsonii and Other Marine Phytoplankton: A Systematic Review. *Front Mar Sci* **2019**, *6*, 511, doi:10.3389/FMARS.2018.00511/BIBTEX.

196. Nosonovsky, M.; Bhushan, B. Multiscale Dissipative Mechanisms and Hierarchical Surfaces: Friction, Superhydrophobicity, and Biomimetics. **2008**.

197. Lopez, J.S.; Lee, L.; Mackey, K.R.M. The Toxicity of Copper to Crocosphaera Watsonii and Other Marine Phytoplankton: A Systematic Review. *Front Mar Sci* **2019**, *5*, doi:10.3389/fmars.2018.00511.

198. Schultz, M.P.; Bendick, J.A.; Holm, E.R.; Hertel, W.M. Economic Impact of Biofouling on a Naval Surface Ship. *https://doi.org/10.1080/08927014.2010.542809* **2010**, *27*, 87–98, doi:10.1080/08927014.2010.542809.

199. Thomas, K. V.; Brooks, S. The Environmental Fate and Effects of Antifouling Paint Biocides. *https://doi.org/10.1080/08927010903216564* **2009**, *26*, 73–88, doi:10.1080/08927010903216564.

200. Finnie, A.A.; Williams, D.N. Chapter. *Biofouling* **2010**, 185–206, doi:10.1002/9781444315462.CH13.

201. Beigbeder, A.; Degee, P.; Conlan, S.L.; Mutton, R.J.; Clare, A.S.; Pettitt, M.E.; Callow, M.E.; Callow, J.A.; Dubois, P. Preparation and Characterisation of Silicone-Based Coatings Filled with Carbon Nanotubes and Natural Sepiolite and Their Application as Marine Fouling-Release Coatings. *http://dx.doi.org/10.1080/08927010802162885* **2011**, *24*, 291–302, doi:10.1080/08927010802162885.

202. Sommer, S.; Ekin, A.; Webster, D.C.; Stafslien, S.J.; Daniels, J.; VanderWal, L.J.; Thompson, S.E.M.; Callow, M.E.; Callow, J.A. A Preliminary Study on the Properties and Fouling-Release Performance of

Siloxane–Polyurethane Coatings Prepared from Poly(Dimethylsiloxane) (PDMS) Macromers. *https://doi.org/10.1080/08927014.2010.531272* **2010**, *26*, 961–972, doi:10.1080/08927014.2010.531272.

203. Magin, C.M.; Long, C.J.; Cooper, S.P.; Ista, L.K.; López, G.P.; Brennan, A.B. Engineered Antifouling Microtopographies: The Role of Reynolds Number in a Model That Predicts Attachment of Zoospores of Ulva and Cells of Cobetia Marina. *https://doi.org/10.1080/08927014.2010.511198* **2010**, *26*, 719–727, doi:10.1080/08927014.2010.511198.

204. Schumacher, J.F.; Aldred, N.; Callow, M.E.; Finlay, J.A.; Callow, J.A.; Clare, A.S.; Brennan, A.B. Species-Specific Engineered Antifouling Topographies: Correlations between the Settlement of Algal Zoospores and Barnacle Cyprids. *Biofouling* **2007**, *23*, 307–317, doi:10.1080/08927010701393276.

205. Schumacher, J.F.; Carman, M.L.; Estes, T.G.; Feinberg, A.W.; Wilson, L.H.; Callow, M.E.; Callow, J.A.; Finlay, J.A.; Brennan, A.B. Engineered Antifouling Microtopographies – Effect of Feature Size, Geometry, and Roughness on Settlement of Zoospores of the Green Alga Ulva. *http://dx.doi.org/10.1080/08927010601136957* **2007**, *23*, 55–62, doi:10.1080/08927010601136957.

206. Wang, Y.; Finlay, J.A.; Betts, D.E.; Merkel, T.J.; Luft, J.C.; Callow, M.E.; Callow, J.A.; Desimone, J.M. Amphiphilic Co-Networks with Moisture-Induced Surface Segregation for High-Performance Nonfouling Coatings. *Langmuir* **2011**, *27*, 10365–10369, doi:10.1021/LA202427Z/SUPPL_FILE/LA202427Z_SI_001.PDF.

207. Cho, Y.; Sundaram, H.S.; Weinman, C.J.; Paik, M.Y.; Dimitriou, M.D.; Finlay, J.A.; Callow, M.E.; Callow, J.A.; Kramer, E.J.; Ober, C.K. Triblock Copolymers with Grafted Fluorine-Free, Amphiphilic, Non-Ionic Side Chains for Antifouling and Fouling-Release Applications. *Macromolecules* **2011**, *44*, 4783–4792, doi:10.1021/MA200269S.

208. Krishnan, S.; Ayothi, R.; Hexemer, A.; Finlay, J.A.; Sohn, K.E.; Perry, R.; Ober, C.K.; Kramer, E.J.; Callow, M.E.; Callow, J.A.; et al. Anti-Biofouling Properties of Comblike Block Copolymers with Amphiphilic Side Chains. *Langmuir* **2006**, *22*, 5075–5086, doi:10.1021/LA052978L/ASSET/IMAGES/MEDIUM/LA052978LE00007.GIF.

209. Krishnan, S.; Weinman, C.J.; Ober, C.K. Advances in Polymers for Anti-Biofouling Surfaces. *J Mater Chem* **2008**, *18*, 3405–3413, doi:10.1039/B801491D.

210. Aldred, N.; Phang, I.Y.; Conlan, S.L.; Clare, A.S.; Vancso, G.J. The Effects of a Serine Protease, Alcalase®, on the Adhesives of Barnacle Cyprids (Balanus Amphitrite). *http://dx.doi.org/10.1080/08927010801885908* **2011**, *24*, 97–107, doi:10.1080/08927010801885908.

211. Olsen, S.M.; Pedersen, L.T.; Laursen, M.H.; Kiil, S.; Dam-Johansen, K. Enzyme-Based Antifouling Coatings: A Review. *https://doi.org/10.1080/08927010701566384* **2007**, *23*, 369–383, doi:10.1080/08927010701566384.

212. Qian, P.Y.; Xu, Y.; Fusetani, N. Natural Products as Antifouling Compounds: Recent Progress and Future Perspectives.

https://doi.org/10.1080/08927010903470815 **2009**, *26*, 223–234, doi:10.1080/08927010903470815.

213. Feng, D.Q.; Ke, C.H.; Lu, C.Y.; Li, S.J. Herbal Plants as a Promising Source of Natural Antifoulants: Evidence from Barnacle Settlement Inhibition. *https://doi.org/10.1080/08927010802669210* **2009**, *25*, 181–190, doi:10.1080/08927010802669210.

214. CRISP, D.J. The Behaviour of Barnacle Cyprids in Relation to Water Movement over a Surface. *Journal of Experimental Biology* **1955**, *32*, 569–590, doi:10.1242/jeb.32.3.569.

215. Chapman, J.; Hellio, C.; Sullivan, T.; Brown, R.; Russell, S.; Kiterringham, E.; Le Nor, L.; Regan, F. Bioinspired Synthetic Macroalgae: Examples from Nature for Antifouling Applications. *Int Biodeterior Biodegradation* **2014**, *86*, 6–13, doi:10.1016/J.IBIOD.2013.03.036.

216. Scardino, A.J.; de Nys, R. Mini Review: Biomimetic Models and Bioinspired Surfaces for Fouling Control. *Biofouling* 2011, *27*, 73–86.

217. Walsh, T.R.; Knecht, M.R. Biointerface Structural Effects on the Properties and Applications of Bioinspired Peptide-Based Nanomaterials. *Chem Rev* 2017, *117*, 12641–12704.

218. Chapman, J.; Le Nor, L.; Brown, R.; Kitteringham, E.; Russell, S.; Sullivan, T.; Regan, F. Antifouling Performances of Macro- to Micro- to Nano-Copper Materials for the Inhibition of Biofouling in Its Early Stages. *J Mater Chem B* **2013**, *1*, 6194, doi:10.1039/c3tb21285h.

219. Magin, C.M.; Cooper, S.P.; Brennan, A.B. Non-Toxic Antifouling Strategies. *Materials Today* **2010**, *13*, 36–44, doi:10.1016/S1369-7021(10)70058-4.

220. Richards, C.; Delgado Ollero, A.; Mercader, C.; Eitan, A.; Delauré, Y.; Regan, F.; Muñoz, D.; Agustin, C.; Berriozabal, G. NEMMO Biomimetic and Multi-Material Solutions. D3.4.

221. Marker, A.F.; N.E.A.; R.H.; R.B. The Measurement of Photosynthetic Pigments in Freshwaters and Standardization of Methods: Conclusions and Recommendations. *Arch. Hydrobiol* **1980**, *14*, 91–106.

222. Caruana, R.; Niculescu-Mizil, A. An Empirical Comparison of Supervised Learning Algorithms. In Proceedings of the ICML 2006 - Proceedings of the 23rd International Conference on Machine Learning; 2006; Vol. 1, pp. 161–168.

223. Scardino, A.J.; Harvey, E.; De Nys, R. Testing Attachment Point Theory: Diatom Attachment on Microtextured Polyimide Biomimics. *http://dx.doi.org/10.1080/08927010500506094* **2007**, *22*, 55–60, doi:10.1080/08927010500506094.

224. Honarkar, H. Waterborne Polyurethanes: A Review. *J Dispers Sci Technol* **2018**, *39*, 507–516, doi:10.1080/01932691.2017.1327818.

225. Papaj, E.A.; Mills, D.J.; Jamali, S.S. Effect of Hardener Variation on Protective Properties of Polyurethane Coating. *Prog Org Coat* **2014**, *77*, 2086–2090, doi:10.1016/J.PORGCOAT.2014.08.013.

226. Song, H.; Ahmad Nor, Y.; Yu, M.; Yang, Y.; Zhang, J.; Zhang, H.; Xu, C.; Mitter, N.; Yu, C. Silica Nanopollens Enhance Adhesion for Long-Term Bacterial Inhibition. *J Am Chem Soc* **2016**, *138*, 6455–6462, doi:10.1021/JACS.6B00243/ASSET/IMAGES/LARGE/JA-2016-002437_0002.JPEG.

227. Yang, X.; Liu, J.; He, H.; Zhou, L.; Gong, C.; Wang, X.; Yang, L.; Yuan, J.; Huang, H.; He, L.; et al. SiO2nanoparticles Induce Cytotoxicity and Protein Expression Alteration in HaCaT Cells. *Part Fibre Toxicol* **2010**, *7*, 1–12, doi:10.1186/1743-8977-7-1/FIGURES/9.

228. Chen, M.; Von Mikecz, A. Formation of Nucleoplasmic Protein Aggregates Impairs Nuclear Function in Response to SiO2 Nanoparticles. *Exp Cell Res* **2005**, *305*, 51–62, doi:10.1016/J.YEXCR.2004.12.021.

229. Veranth, J.M.; Kaser, E.G.; Veranth, M.M.; Koch, M.; Yost, G.S. Cytokine Responses of Human Lung Cells (BEAS-2B) Treated with Micron-Sized and Nanoparticles of Metal Oxides Compared to Soil Dusts. *Part Fibre Toxicol* **2007**, *4*, 1–18, doi:10.1186/1743-8977-4-2/TABLES/3.

230. O Rourke, F.; Boyle, F.; Reynolds, A. Tidal Energy Update 2009. *Appl Energy* **2010**, *87*, 398–409, doi:10.1016/j.apenergy.2009.08.014.

231. O'Doherty, T.; O'Doherty, D.M.; Mason-Jones, A. Tidal Energy Technology. In *Wave and Tidal Energy*; John Wiley & Sons, Ltd: Chichester, UK, 2018; pp. 105–150.

232. Uihlein, A.; Magagna, D. Wave and Tidal Current Energy – A Review of the Current State of Research beyond Technology. *Renewable and*

Sustainable Energy Reviews **2016**, *58*, 1070–1081, doi:10.1016/j.rser.2015.12.284.

233. Denny, E. The Economics of Tidal Energy. *Energy Policy* **2009**, *37*, 1914–1924, doi:10.1016/j.enpol.2009.01.009.

234. Chowdhury, M.S.; Rahman, K.S.; Selvanathan, V.; Nuthammachot, N.; Suklueng, M.; Mostafaeipour, A.; Habib, A.; Akhtaruzzaman, Md.; Amin, N.; Techato, K. Current Trends and Prospects of Tidal Energy Technology. *Environ Dev Sustain* **2021**, *23*, 8179–8194, doi:10.1007/s10668-020-01013-4.

235. Johnstone, C.M.; Pratt, D.; Clarke, J.A.; Grant, A.D. A Techno-Economic Analysis of Tidal Energy Technology. *Renew Energy* **2013**, *49*, 101–106, doi:10.1016/j.renene.2012.01.054.

236. Segura, E.; Morales, R.; Somolinos, J.A. Increasing the Competitiveness of Tidal Systems by Means of the Improvement of Installation and Maintenance Maneuvers in First Generation Tidal Energy Converters—An Economic Argumentation. *Energies (Basel)* **2019**, *12*, 2464, doi:10.3390/en12132464.

237. Cfd Simulation of Cavitation over Water Turbine Hydrofoils. *Czasopismo Techniczne* **2017**, *9*, doi:10.4467/2353737XCT.17.156.7168.

238. Peyvastehnejad, A.; Regan, F.; Richards, C.; Delgado, A.; Daly, P.; Grande, J.; Delauré, Y.M.C. The Impact of Bio-Inspired Micro-Textures on Turbulence and Implications for Bio-Fouling Settlement. *Ocean Engineering* **2023**, *285*, 115223, doi:10.1016/j.oceaneng.2023.115223.

239. Bloecher, N.; Frank, K.; Bondø, M.; Ribicic, D.; Endresen, P.C.; Su, B.; Floerl, O. Testing of Novel Net Cleaning Technologies for Finfish Aquaculture. *Biofouling* **2019**, *35*, 805–817, doi:10.1080/08927014.2019.1663413.

240. Vyas, N.; Wang, Q.X.; Manmi, K.A.; Sammons, R.L.; Kuehne, S.A.; Walmsley, A.D. How Does Ultrasonic Cavitation Remove Dental Bacterial Biofilm? *Ultrason Sonochem* **2020**, *67*, 105112, doi:10.1016/j.ultsonch.2020.105112.

241. Catão, E.C.P.; Pollet, T.; Misson, B.; Garnier, C.; Ghiglione, J.-F.; Barry-Martinet, R.; Maintenay, M.; Bressy, C.; Briand, J.-F. Shear Stress as a Major Driver of Marine Biofilm Communities in the NW Mediterranean Sea. *Front Microbiol* **2019**, *10*, 462628, doi:10.3389/FMICB.2019.01768.

242. Liang, C.; Strickland, J.; Ye, Z.; Wu, W.; Hu, B.; Rittschof, D. Biochemistry of Barnacle Adhesion: An Updated Review. *Front Mar Sci* **2019**, *6*, 468324, doi:10.3389/FMARS.2019.00565/BIBTEX.

243. Kamino, K. Mini-Review: Barnacle Adhesives and Adhesion. *http://dx.doi.org/10.1080/08927014.2013.800863* **2013**, *29*, 735–749, doi:10.1080/08927014.2013.800863.

244. Schultz, M.P.; Kavanagh, C.J.; Swain, G.W. Hydrodynamic Forces on Barnacles: Implications on Detachment from Fouling-release Surfaces. *http://dx.doi.org/10.1080/08927019909378388* **2009**, *13*, 323–335, doi:10.1080/08927019909378388.

245. Menesses, M.; Belden, J.; Dickenson, N.; Bird, J. Measuring a Critical Stress for Continuous Prevention of Marine Biofouling Accumulation with

Aeration. *Biofouling* **2017**, *33*, 703–711, doi:10.1080/08927014.2017.1359574.

246. Hong, F.; Xie, L.; He, C.; Liu, J.; Zhang, G.; Wu, C. Novel Hybrid Anti-Biofouling Coatings with a Self-Peeling and Self-Generated Micro-Structured Soft and Dynamic Surface. *J Mater Chem B* **2013**, *1*, 2048–2055, doi:10.1039/C3TB00031A.

247. Chen, M.; Qu, Y.; Yang, L.; Gao, H. Structures and Antifouling Properties of Low Surface Energy Non-Toxic Antifouling Coatings Modified by Nano-SiO2 Powder. *Sci China B Chem* **2008**, *51*, 848–852, doi:10.1007/s11426-008-0069-5.

248. Akesso, L.; Pettitt, M.E.; Callow, J.A.; Callow, M.E.; Stallard, J.; Teer, D.; Liu, C.; Wang, S.; Zhao, Q.; D’Souza, F.; et al. The Potential of Nano-Structured Silicon Oxide Type Coatings Deposited by PACVD for Control of Aquatic Biofouling. *Biofouling* **2009**, *25*, 55–67, doi:10.1080/08927010802444275.

249. Flemming, H.-C. Why Microorganisms Live in Biofilms and the Problem of Biofouling. In; Springer, Berlin, Heidelberg, 2008; pp. 1–10.